Approaches to Understanding Antiretroviral Pharmacology in Difficult-to-access Tissues for HIV Treatment and Prevention

A DISSERTATION

SUBMITTED TO THE FACULTY OF THE GRADUATE SCHOOL

OF THE UNIVERSITY OF MINNESOTA

BY

Fan Wang

IN PARTIAL FULFILLMENT OF THE REQUIREMENTS

FOR THE DEGREE OF

DOCTOR OF PHILOSOPHY

Advisor: Melanie R. Nicol

Co-advisor: Angela K. Birnbaum

April 2023

Acknowledgements

I would never finish this journey without the support of so many people. I want to take this opportunity to thank them, although I am afraid my limited vocabulary will not express even one percent of my gratitude and appreciation.

I would like to extend my deepest gratitude to my advisor Dr. Melanie Nicol, who has always guided me with great patience, offered me the best resources and given me freedom to explore what I was interested in. She taught me how to ask scientific questions and how to answer them step-by-step. Her enthusiasm in scientific research and education of next generation of scientists is the inspiration lighting up my future path.
I am also grateful for the opportunity to learn from other brilliant scientists and faculty of the Experimental and Clinical Pharmacology (ECP) department and other department at the University of Minnesota. My co-advisor Dr. Angela Birnbaum has given me constant help throughout my PhD in various aspects and always encouraged me to upgrade my work and writing to a higher level. Dr. Richard Brundage was the one who opened the door to the world of pharmacometrics for me. He is one of the most knowledgeable and humblest people I have ever met. I enjoyed each of his thought-stimulating classes in which he made pharmacometrics so interesting and fascinating. Dr. Lisa Coles has shared excellent ideas in my modeling and simulation project and provided helpful suggestions in writing of the thesis. Dr. Weihua Guan and Dr. Julian Wolfson were instructors of some of my biostatistics courses. They make statistics interesting and accessible for non-statistics majors like me.

I wish to express my appreciation to the participants and their next-of-kin of the Uganda postmortem study. The postmortem research presented in this thesis was made possible through extensive international and national collaborations with other scientists. I would like to thank members of the Uganda study team - Dr. Robert Lukande, Olivie Namuju (Carol), Dr. David Meya, and Dr. Kizito Abdusalaamu - as well as members of the Minnesota meningitis study team - Dr. David Boulware and Dr. Katelyn Pastick. I also extend my gratitude to Dr. MaryPeace McRae and Kara Rademeyer, who diligently conducted the animal postmortem experiments.

I would like to give a special thank you to the Center for Orphan Drug Research and one of their experienced analytical scientist Usha Mishra, who generously shared their LC/MS with me, and helped develop and validate the LC/MS assays for some of my postmortem samples.

I would like to acknowledge my dissertation committee members - Dr. Lisa Coles, Dr. Angela Birnbaum, Dr. Weihua Guan and Dr. Melanie Nicol, for their help in formulating the results of my research into a finished product.

I also want to express my gratitude to ECP staff Susan and Becky, who kept proactively communicating with me and made my life as a graduate student much easier.

I would like to thank the former and current ECP graduate students Kyle, Mutaz, Ya-Feng, Sam, Irene, Ashwin, Abhishek and Abdelrahman, for offering help in my study and research; and Siddhee, Ibrahim, Rui, Mei-Chi, Lusi, Yingbo, Charul, Chenxu and Jessica, for keeping me company and being willingly to offer help at any time. Their support helped me get through the unprecedented time of pandemic.

I wish to acknowledge Dr. Islam Younis, Dr. Ganesh Cherala and Dr. Izna Ali, who were my internship mentors and role models as professional clinical pharmacologists.

I am fortunate to have my partner, Kevin, who always gives me selfless support and cheers me up whenever I doubt myself. His love is the pillar that makes me strong and fearless.

Last but not least, I would like to thank my dearest parents, who give me endless love throughout my life. They have always respected my decisions and encouraged me to chase my dream. I do realize receiving education, especially at a graduate level, is a privilege. I could not have come this far without standing on their shoulders.

Dedication

This thesis is dedicated to my parents and partner for their unconditional love and support

Abstract

The persistence of Human Immunodeficiency Virus (HIV) in tissue reservoirs, such as the central nervous system (CNS) and genital tissues, presents a challenge for HIV treatment and prevention. Antiretroviral drugs can achieve viral suppression in the circulatory system, but their suboptimal distribution and exposure in tissues may contribute to viral persistence. This dissertation investigated the distribution of antiretroviral drugs in difficult-to-access tissues, such as the brain and female genital tissues, and predicts exposure of tenofovir in both circulatory system and female genital tissue with a physiologically based pharmacokinetic (PBPK) modeling approach.

The study analyzed postmortem tissues collected from decedents with HIV who were on antiretroviral therapy. In chapter 2, the concentration and tissue-to-plasma penetration ratios of four antiretroviral drugs in 13 brain regions were analyzed, revealing statistically significant regional differences. In chapter 3, the concentration and tissue-to-plasma penetration ratios of four drugs in upper and lower female genital tissues were assessed, with higher penetration observed in the vagina tissue compared to the commonly used representative for the entire female genital tract, the cervix. These findings provide insights into viral compartmentalization mechanisms.

The potential confounding effects of postmortem redistribution on antiretroviral drug analysis were investigated in chapter 4, revealing different trends of redistribution depending on the drug, tissue, and postmortem time. Rapid autopsy is emphasized as a valuable tool for future pharmacological study based on postmortem analysis.

PBPK modeling was used in chapter 5 to predict drug exposure in tissues, with the development of tenofovir models integrated with a female genital compartment and validated with clinical data. Nonadherence behavior patterns were evaluated, with an interesting finding that taking “drug vacation” intermittently instead of consecutively could increase the protection of oral tenofovir, a component of preexposure prophylaxis for HIV.

Overall, this dissertation highlights the importance of understanding drug distribution in tissues for HIV treatment and prevention efforts. The findings provide valuable insights into the pharmacology of antiretroviral drugs in the brain and female genital tissues and pave the way for future studies to identify viral compartmentalization mechanisms and optimize drug exposure in tissues.

Table of contents

List of tables

List of figures

CHAPTER 1 Introduction

1.1 HIV and antiretroviral therapy

Human immunodeficiency virus (HIV) was a leading cause of death globally in the last three decades [1, 2] and remained one of the top ten causes of death for low-income countries by 2019 [3]. According to the World Health Organization (WHO), there were an estimated 1.5 million new infections and 38.4 million people living with HIV worldwide in 2021 [4]. The HIV epidemic is diverse and differs by country and region. In Sub-Sahara Africa, home to 67% of the total global population living with HIV, the dominant mode of HIV transmission is through unprotected heterosexual intercourse and perinatal transmission; while in other regions of the world, HIV prevalence is also high among men who have sex with men (MSM) and injection drug users [5].

HIV is an enveloped lentivirus that targets a variety of cells, most commonly infecting CD4+ T cells–vital cells in immune system. The infection caused by HIV is characterized by two phases: the acute phase with intensive viral replication, and the following chronic, asymptomatic phase with progressive immune activation and a low-level viral replication [6, 7]. If no interventions occur, an advanced phase marked with depletion of CD4+ cells will emerge and eventually lead to acquired immune deficiency syndrome (AIDS) [8]. People living with HIV with compromised immunity or AIDS are susceptible to various opportunistic infections (e.g. tuberculosis, cryptococcosis, toxoplasmosis, progressive multifocal leukoencephalopathy, Cytomegalovirus infection,

etc.) [9, 10] and malignancies (e.g., Kaposi sarcoma, non-Hodgkin lymphoma, cervical carcinoma, anal carcinoma, etc.) [11, 12] that lead to high rate of morbidity and mortality.

Largely due to the development and wide use of antiretroviral drugs, by 2022, HIV-associated death cases declined to one third of its peak in 2004, and new infections dropped 41% compared to 2000 [13]. There are now several classes of antiretrovirals that defend uninfected cells from HIV infection by targeting different phases in the virus's life cycle: from the viral entry of the host cell, reverse transcription of the viral RNA to DNA, integration of viral DNA into the host's nucleus, to maturation and budding of the virus from the host cell. The antiretroviral classes corresponding to each stage listed above are the fusion/entry inhibitors, reverse transcriptase inhibitors, integrase inhibitors, and protease inhibitors, respectively [14-17].

Antiretroviral drugs play an essential role in both treatment and prevention of HIV. First, antiretroviral therapy is chronic treatment for viral suppression for people living with HIV, people on antiretroviral therapy usually take a combination of three antiretrovirals from at least two antiretroviral classes, consisting of two nucleotide reverse transcriptase inhibitors (a NRTI backbone) plus an integrase strand transfer inhibitor (INSTI), protease inhibitor, or entry inhibitor. The choice of particular drugs is based on age, pregnancy/perinatal status, antiretroviral therapy experience, variant type of drug-resistance, etc. [18-21] Second, people living with HIV maintaining viral suppression via antiretroviral therapy also prevents HIV transmission to their HIV-negative sex partners, fetus and newborns (treatment as prevention). Furthermore, pre-exposure prophylaxis (PrEP) is a prevention regimen containing antiretrovirals given to HIV-negative individuals at risk of HIV exposure to proactively reduce the acquisition of HIV,

and it is now (by March 2023) available as two daily oral formulations of tenofovir/emtricitabine, a long-acting injectable for cabotegravir and a vaginal ring for dapivirine [18-21]. Post-exposure prophylaxis (PEP) is a regimen for people who have been exposed to potential HIV infection and is usually a 28-day regimen containing two or three antiretrovirals [21].

1.2 Obstacles in curing HIV and penetration of antiretrovirals in deep tissues

Despite the high antiviral activity of antiretroviral therapy that has greatly prolonged life expectancy and improved quality-of-life of people living with HIV, current antiretroviral therapy is not the cure for HIV due to the existence of HIV reservoirs [22]. HIV reservoirs refers to the hiding places of HIV, which can establish throughout the body after infection and serve as the hub of persistent virus [23-30]. Previous studies found HIV reservoirs in various anatomical sites, including the lymphoid tissues, gastrointestinal tract, respiratory tract, liver, genital tract, and brain/CNS [23-31]. Within each biological system, especially the deep tissues like brain/CNS, the tissue compartmentalization provides an isolating environment that favors the persistence of HIV reservoirs. Phylogenetic analysis, which is a PCR-based genomic analysis, has been applied to identify the viral compartmentalization in different tissues, characterized by significant genetic distance of the viral variants among tissues. With phylogenetic analysis, viral compartmentalization in CSF compared to plasma had been identified in at least some people living with HIV, regardless of stage in HIV infection, whether receiving the antiretroviral therapy or the timing of receiving antiretroviral therapy [32-34]. Recently, the “Last Gift” program applied phylogenetic analysis in postmortem human

tissues from different anatomical sites and provided further evidence of viral compartmentalization in the CNS with solid brain tissues and migration of HIV between CNS and other tissues [23, 30]. The exact reasons for viral compartmentalization are still undefined and several factors might be involved, including the differential penetration of antiretrovirals in those deep tissues. Optimal penetration can be substantial in minimizing and eliminating the reservoirs, and incomplete penetration may contribute to persistent HIV replication. Brain/CNS and the female genital tract (FGT) are the two focuses of interest in this thesis for brain/CNS's importance in cognitive function and FGT's role in sexual transmission.

1.2.1 Brain

Brain is a major anatomical reservoir of HIV. Despite undetectable HIV RNA in the circulatory system, HIV DNA and RNA can be detected in CSF (CSF escape) and brain tissues [23-25, 30, 35, 36]. Irrespective of the presence of replication-competent provirus, persistence of HIV in CNS is associated with neuroinflammation which contributes to neurocognitive disorders [37-39]. To effectively eliminate or suppress HIV in CNS, it is essential for the antiretrovirals to reach optimal concentrations in the brain, not only in plasma. However, antiretroviral distribution in the CNS is limited by the existence of physiological barriers – the blood-brain barrier (BBB) and the blood-cerebrospinal fluid-barrier (BCSFB), which is a common problem for CNS-targeting medications. HIV replication and compartmentalization in the CNS is associated with development of drug-resistance [40, 41], neurocognitive disorders [42, 43], and potential contributions to the viral rebound after treatment interruption [44]. As evidence showed that use of CNS-penetrating

antiretrovirals was associated with lower CSF viral load [45-47] and better neurophysiological outcomes [46, 48-50], I hypothesized that suboptimal exposures of antiretrovirals may increase the risk of persistent viral replication in CNS. Increasing antiretroviral concentration to achieve better CNS-penetrating or switching to better CNS-penetration drug may lead to better control of CNS HIV persistence. Conversely, some antiretrovirals such as efavirenz, may elicit neuropsychiatric adverse effects that are believed to be concentration-dependent [51-53]. For examples, Gutierrez et al. found higher incidence and severity of some neuropsychiatric events in the group receiving full dose of efavirenz (600 mg/day) than the group receiving stepped-dose (200 mg/day in the first week, 400 mg/day in the second week, and 600 mg/day from the third week) [52]; Mukonzo et al. found neuropsychiatric symptoms were common for people taking efavirenz, and was associated with higher efavirenz plasma concentration and certain CYP2B6 genotypes [53]; Hakkers et al. found efavirenz plasma concentrations higher than therapeutic range (> 4 mg/L) was associated with worse cognitive function at baseline, and for those people (i.e., plasma concentration > 4 mg/L), switching to a non-efavirenz based therapy resulted in more cognitive improvements than those stayed on efavirenz-based therapy [51]. It is clear that, targeting appropriate antiretroviral concentrations for brain tissues is a critical balancing act.

Measuring concentration in the brain is not as convenient as in blood, such as is routinely done with therapeutic drug monitoring (TDM). As brain tissue is not readily available from clinical routines, cerebrospinal fluid (CSF) has been widely used as a surrogate of the entire CNS for investigations of viral replication and antiretroviral distribution; however, the adequacy of CSF as a surrogate for brain has not been well

justified, and some studies found that CSF is not representative of brain tissue [54, 55]. Exposure and penetration of antiretrovirals pertaining in this dissertation (i.e., tenofovir (taken as oral tenofovir disoproxil fumarate (TDF)), dolutegravir, lamivudine and efavirenz) in the CNS measured in CSF or brain tissues are summarized in Table 1-1. Overall, designs of studies investigating antiretroviral CNS penetration are variable, however, CSF concentrations and penetration of each drug are relatively more consistent across different studies, while concentrations measured in postmortem brain tissues (including CSF) tended to be higher than the CSF from living participants. This raises the question of whether CSF could represent the entire CNS. Despite large variability, the plasma normalized CNS distribution (or penetration in Table 1-1) of the four antiretroviral drugs in an ascending order (according to the average penetration in each study) seems to be: dolutegravir < tenofovir < lamivudine < efavirenz.

Table 1-1 Summary of studies investigating CNS penetration of tenofovir, dolutegravir, efavirenz and lamivudine.

Author(s)	Bio-matrix	Dosage	Population	N	Sampling time after dose (h)	Concentration (ng/mL)	No. % > IC_{50}	Penetration (CNS/ plasma)
Tenofovir								
Calcagno, 2011 [56]	CSF	300 mg (TDF) once daily	Adults living with HIV	21	Median (IQR), 15 (13.8- 19.4)	Median (IQR), 6 (<2- 8)		Median (IQR), 0.05 (0- 0.13)
Best, 2012 [57]	CSF	300 mg (TDF) once daily	Adults living with HIV		Mean ± SD, 11 ± 7.8	Median (IQR), 5.5 (2.7- 11.3), n=77	23	Median (IQR), 0.057 (0.03- 0.1), n=38
Lahiri, 2016 [58]	CSF	300 mg (TDF) once daily	Adults living with HIV	30		Undetectable in most participants	3.4	

Van den Hof, 2018 [59]	CSF		Children living with HIV	4	Range 15-20	Median (IQR), 1 (1–3)	0	Median (IQR), 0.021 (0.020-0.024) *
Nicol, 2019 [60]	Postmortem CSF		Adult decedents lived with HIV	11		Median (IQR), 138 (77- 675)		Geometric mean (95% CI), 0.29 (0.11- 0.77)
	Postmortem brain tissue			4		Range 161- 2644		Geometric mean (95% CI), 0.36 (0.14- 1.24)
Ferrara, 2020 [61]	Postmortem brain tissue		Adult decedents lived with HIV	7		Median (IQR), 148 (81-292) ¶		
Dolutegravir								

Letendre, 2014 [62]	CSF	50 mg once daily	Adults living with HIV	12	Range 2-6	Week 2: Median (range), 18.2 (4.0–23.2)	100	Week2: Median (range) 0.0052 (0.0011-0.0066)
				12		Week 16: Median (range), 13.2 (3.7–18.3)	100	Week 16: Median (range) 0.0041 (0.003-0.02)
Gele´, 2019 [63]	CSF		Adults living with HIV	13		Median (range), 9.6 (3.6-22.8)	100	Median (range), 0.0065 (0.0019-0.051)
Calcagno, 2021 [64]	CSF		Adults living with HIV	41	Median (range), 15 (2-26)	Median (IQR), 11 (5.3-16.9)		Median (IQR), 0.0052 (0.0032-0.0075)

Efavirenz								
Tashima, 1999 [65]	CSF	600 mg once daily	People living with HIV	10	Range 9- 13	Mean (range), 11.1 (2.1- 18.7)		Mean (range), 0.0061 (0.0026-0.0112)
Antinori, 2005 [66]	CSF		People living with HIV	11	Range 1–12			Median (range), 0.0 (0.0–0.0)
Best, 2011 [67]	CSF		People living with HIV		Mean ± SD, 12.5 ± 5.4	Median (IQR), 13.9 (4.1- 21.2), n= 80	97.5	Median (IQR), 0.005 (0.0026-0.0076), n=69
Nightingale, 2016 [68]	CSF	800 mg once daily	HIV-TBM (Vietnam)	47		Geometric mean (95% CI), 60.3 (46.6- 79.4)		Median (IQR), 0.027 (0.013-0.056)

		600 mg once daily	HIV+ subjects (United Kingdom)	25		Geometric mean (95% CI), 15 (11.7- 19.7)		Median (IQR), 0.01 (0.007-0.012)
Van den Hof, 2018 [59]	CSF		Children living with HIV	12		Median (IQR), 10 (8–13)	100	Median (IQR), 0.681 (0.555-0.819) *
Nicol, 2019 [60]	Postmortem brain tissue		Adult decedents lived with HIV	4		Range 1227- 4854		Geometric mean (95% CI), 1.28 (1.089- 1.79)
Ferrara, 2020 [61]	Postmortem brain tissue		Adult decedents lived with HIV	2		Median (IQR), 36 (29-41) ¶		

Lamivudine								
Antinori, 2005 [66]	CSF		People living with HIV	55	Range 1–12			Median (range), 0.229 (0.0–4.90)
Van den Hof, 2018 [59]	CSF		Children living with HIV	17	Range 15-20	Median (IQR), 97 (51–144)	100	Median (IQR), 0.464 (0.331-0.607) *
Nicol, 2019 [60]	Postmortem CSF		Adult decedents lived with HIV	14		Median (IQR), 566 (366- 1638)		Geometric mean ratio (95% CI), 0.54 (0.27- 1.11)
	Postmortem brain tissue			4		Range 328- 784		Geometric mean ratio (95% CI), 0.37 (0.23- 0.64)
Ferrara, 2020 [61]	Postmortem brain tissue		Adult decedents	4		Median (IQR), 64 (BLQ-272) ¶		

			lived with HIV					
Delille, 2014 [69]	CSF	300 mg once daily	Adults living with HIV	13	@~24	Total: Mean (95% CI), 8.7 (7.2- 10.5)		Total: Geometric mean ratio (95% CI), 0.03 (0.02- 0.04)
						Unbound: Mean (95% CI), 0.6 (0.4- 0.9) [Θ]	0 [Θ]	Unbound: Geometric mean ratio (95% CI), 0.09 (0.06- 0.12) [Θ]

* CSF/plasma concentration ratio was corrected by plasma protein-binding.
¶ Overall median (IQR) of three brain regions. BLQ: below limit of quantification. Lower limit of quantification is 25 ng/mL.
Θ Unbound CSF and plasma concentrations are used in calculation.

1.2.2 Female Genital Tract

Worldwide, women and girls accounted for 50% of the new HIV infections in 2020, but in sub-Saharan Africa, the percentage was disproportionately higher at 63% [70]. Women acquire HIV most commonly from sexual transmission; thus, maintaining an optimal penetration of drugs used for PrEP in the entire female genital tract (i.e., ovary, uterus, cervix and vagina; in this dissertation, ovary and uterus are referred to as the upper genital tissues, and cervix and vagina are referred to as the lower genital tissues) is crucial for women among groups at higher risk for HIV infection. Clinical trials of oral PrEP have shown inconsistent effectiveness results for cisgender women [71-73], while protection for MSM and transgender women were consistently high [74, 75]. This is likely attributed to non-adherence (not taking the drug in the amount and timeframe as prescribed) [76] and the sub-optimal presence of active drug in vaginal tissue as compared to rectal tissue (the major HIV transmission site for MSM) [77, 78]. In addition, as demonstrated in a primate model, HIV viral particles could rapidly spread throughout the entire female genital tract, not just in vaginal tissue [79]. Such spread of the HIV particles necessitates a more complete understanding of drug concentrations distributed to each female genital compartment. However, in previous studies of antiretroviral pharmacology, tissue sampling was largely constrained to biopsy of lower female genital tract [77, 80-82] and more readily available as cervicovaginal fluid [78, 80, 83-85], so we have little information about the deeper solid tissues where HIV transmits and persists. Some studies have used animal models to overcome this limitation [79], but animal studies are not

fully translatable to human due to different physiology, and the fact that HIV is, by definition, a human-specific virus that does not affect other animals.

Table 1-2 summarizes the studies investigating exposure and penetration of antiretroviral drugs in the FGT. Similar to the studies investigating CNS distribution of antiretrovirals, most studies investigating FGT tended to utilize the more accessible bio-matrix, cervicovaginal fluid, while sampling for vaginal tissue, cervical tissue and upper FGT were relatively rare. The methods measuring penetration also varied by studies. Dumond et al. and Patterson et. al. used the AUC ratio (cervicovaginal fluid AUC divided by plasma AUC) as indication of penetration, however, the Dumond group measured AUC within 24 hours post dose, while Patterson et al. measured AUC for 14 days. Other studies determined penetration with concentration ratios (cervicovaginal fluid concentration divided by plasma concentration). Tenofovir concentrations in FGT tissues were only measured in two studies [77, 78] and were lower than in those measured in cervicovaginal fluid, which suggests a potential overestimation of studies using cervicovaginal fluid and insufficient exposure of tenofovir in the FGT, however, this speculation is subject to bias due to small sample size.

Table 1-2 Summary of studies investigating female genital tract penetration of tenofovir, lamivudine and efavirenz.

Author(s)	Bio-matrix	Regimen State	Population	N	Sampling time after dose (h)	Concentration (ng/mL)	Penetration (CSF/ plasma)
Tenofovir							
Kwara, 2008 [83]	cervicovaginal fluid	Steady state	Women living with HIV	16	8-12 h	Mean (95%CI), 84 (24-289)	Mean (95%CI), 5.15 (1.18-22.6)
					3-4 h	Mean (95%CI), 67 (17-275)	Mean (95%CI), 0.75 (0.16-3.49)
Dumond, 2007 [84]	cervicovaginal fluid	Steady state Steady state	Women living with HIV	10	0, 2, 4, 6, 12 and 24 h	AUC0-24h (ug*h/ml): Median (IQR), 1.75 (0.6, 3.13)	Median (IQR) AUC ratio, 0.75 (0.37, 6.45)
						Ctau (ng/mL):	

						Median (IQR) 68.4 (28.2, 112.6)	
		Single dose					Median (IQR) AUC ratio, 1.35 (0.0023, 4.47).
Patterson, 2011 [78]	cervicovaginal fluid	Single dose	Healthy females	7	1, 2, 5, 7, 10 and 14 days	AUC1-14d (ng*d/mL): Median (IQR), 251 (151-1257)	Median (IQR) AUC1-14d ratio, 2.6 (1.7-13.4)
						C24h: Median (IQR), 69 (57-586)	

	Cervical biopsy			1		AUC0-14d (ng*d/mL): 510	
						C24h (ng/g): 50	
	Vaginal biopsy			1		AUC0-14d (ng*d/mL): 50	
						C24h (ng/g): 6.8	
Rahangdale, 2015 [85]	cervicovaginal fluid	Steady state	Women living with HIV	13		Median (range): 113 (1.15, 2258)	

	Endometrial tissue			3		Median (range): 26 (21, 52)	
Louissaint, 2013 [77]	Vaginal biopsy	Single dose	Healthy females	6		C24h (day 1) Median (IQR), 4 (1, 9) ng/g	
Lamivudine							
Kwara, 2007 [83]	cervicovaginal fluid	Steady state	Women living with HIV	20	8-12 h	Mean (95%CI), 394 (135-1154)	Mean (95%CI), 3.19 (1.19–8.53)
					3-4 h	Mean (95%CI), 783 (280-2197)	Mean (95%CI), 0.97 (0.41–2.3)
Dumond, 2007 [84]	cervicovaginal fluid	Steady state	Women living with HIV	13	0, 2, 4, 6, 12 and 24 h	AUC0-24h (ug*h/ml): Median (IQR), 26.3 (1.12, 49)	Median (IQR) AUC ratio: 2.41 (1.09, 15.48)

						Ctau at SS (ng/mL): Median (IQR), 1731 (1083, 3265)	
		Single dose					Median (IQR) AUC ratio: 3.95 (1.87, 6.71)
Efavirenz							
Kwara, 2007 [83]	cervicovaginal fluid	Steady state	Women living with HIV	13	8-12 h	Mean (95%CI), 18.4 (6.95-48.73)	Mean (95%CI), 0.01 (0–0.03)
					3-4 h	Mean (95%CI), 29.8 (6.3- 142.1)	Mean (95%CI), 0.01 (0–0.05)
Dumond, 2007 [84]	cervicovaginal fluid	Steady state	Women living with HIV	6	0, 2, 4, 6, 12 and 24 h	AUC0-24h (ug*h/ml):	Median (IQR) AUC ratio, 0.005 (0.001, 0.008)

						Median (IQR), 0.15 (0.087, 0.21)	
						Ctau (ng/mL): Median (IQR), 5.6 (3.5, 9.1)	
		Single dose					Median (IQR) AUC ratio, 0.004 (0.001, 0.006)

1.3 Postmortem analysis and postmortem redistribution

Postmortem analysis is a method initially used to determine the cause/time of death in the forensic toxicology field. Recently it has been applied in HIV research to understand HIV reservoirs and antiretroviral penetration in the human body [23, 30, 60, 61]. Postmortem analysis is a promising solution to circumvent the difficulty of deep tissue sampling and the inaccurate/comprehensive estimation of HIV reservoir and the penetration of antiretroviral in the CNS and FGT of using CSF and lower FGT fluid as representative of the entire corresponding biological system. In this thesis, we used postmortem analysis to investigate the penetration of antiretrovirals in the brain/CNS and FGT.

However, biological and chemical activities do not immediately cease at death. Following the cessation of circulatory and respiratory systems and function of the brain, blood flow movements still take place for a short period of time before coagulation, and passive diffusion of chemical molecules and putrefaction occur as well; these activities drive the postmortem redistribution of drugs [86]. According to observations by forensic toxicologists, substances with volume of distribution (Vd) larger than 3 L/kg or being lipophilic drugs/organic bases are more likely subject to postmortem redistribution [86]. The central to peripheral blood concentration ratio has been used as a marker of postmortem redistribution in human cases in the forensic researches, as the peripheral blood such as femoral blood was assumed to be less affected by postmortem redistribution and could reflect the drug concentration at time of death [86, 87]. However, this did not always hold true and changes in drug concentration in femoral blood has been

observed [88-91]. As sampling in human cases are limited such that postmortem redistribution cannot be directly observed, animal-based studies have been used to investigate mechanism of postmortem redistribution regarding both temporal and spatial changes at multiple anatomical sites. In a rat-based study conducted by Gleba et al., morphine concentration in femoral blood drastically decreased from 4000 ng/mL at time of death to less than 1000 ng/mL at 16 hours post death, while concentrations in the heart blood, liver and brain were relatively invariable at the time points sampled (0, 8, 16 and 24 hours post death) [92]. In another animal-based postmortem redistribution study of alprazolam, drug concentrations at an earlier time point 2-hour post death were also measured, and rapid changes in fat, heart and lung were captured within the 2-hour window after death [93]. The imaging technology, μX-Ray Computed Tomography, was applied to directly observe postmortem redistribution of caesium ions (Cs +) from the stomach in rats over a time period of 6 days, and researchers found temperature and body position could affect the trajectory and speed of diffusion of Cs + after death [94]. Postmortem redistribution of antiretrovirals has never been studied before, but is possible since some antiretrovirals have the aforementioned properties (e.g., lamivudine has a pKa of 14.3; efavirenz has a pKa of 12.5, log P of 4.6 and Vd of 4.5 L/kg). Study of postmortem redistribution of antiretrovirals with animal model is feasible and warranted to fill the knowledge gap.

1.4 Physiologically-based pharmacokinetic (PBPK) modeling

PBPK modeling is a bottom-up mathematical modeling approach that describes the movement of a drug with detailed physiological mechanisms. With adequate

mechanistic equations of the body systems (for a full-body PBPK model, the mechanistic equation is based on physiochemical features of the drug and physiological features of the individual tissues), PBPK models simulate the process of absorption, distribution, metabolism, and excretion of the drug in the human body in order to predict its pharmacokinetic profiles and the related therapeutic effect/toxicity, and it has been vigorously applied in various stages of drug development [95]. In general, there are a few basic building blocks of a PBPK model: 1. the physiological properties of the target population, such as organ volumes, tissue composition, blood flow rates, expression levels of enzymes/transporters involved in the disposition of the drug; 2. the physicochemical properties of the drug, such as molecular weight, solubility, lipophilicity (logP/logD), pKa/pKb; 3. biological properties of the drug, such as fraction unbound in plasma (fup), partition coefficients (Kps), permeability, active processes (Km, Vmax, Kd); 4. formulation properties, such as dissolution for extra venous formulations [96, 97]. All of these information are incorporated into ordinary differential equations describing mass movement between tissue compartments [96, 97].

There has been a burst of applying PBPK modeling in the research and development of antiretroviral drugs for HIV in recent years, among which multiple PBPK models have been development for tenofovir disoproxil fumarate, one antiretroviral mostly prescribed in oral PrEP and in the initial antiretroviral therapy [21]. For example in the case of PBPK models for tenofovir, the goals of developing such models include predicting pharmacokinetics of tenofovir in special populations such as pregnant women [98, 99] and their fetus [100], and the geriatric population [101], and predicting pharmacokinetics of tenofovir under drug-drug interaction mediated by transporters [102, 103]. Besides, PBPK

modeling also has the advantage in predicting tissue exposure with reliable inputs. As nonadherence is one of the biggest issues concerning the effectiveness of oral PrEP [76] due to insufficient exposure in the transmission site and in the circulatory system, PBPK modeling could be applied to predict and evaluate effectiveness and risk of PrEP dosing under scenarios of nonadherence.

1.5 Research objectives and thesis outline

The overall objective of my thesis is to characterize penetration of multiple antiretrovirals into the HIV reservoirs of the brain/CNS and FGT to inform optimal dosing of antiretrovirals and future development of new antiretrovirals. Target populations are people living with HIV receiving antiretroviral therapy and women who are at risk of HIV infection and are taking oral tenofovir as prevention. To fulfill the overall objective, four studies were conducted with the following objectives, further details are presented in chapters 2 through 5:

1. To characterize penetration of four antiretrovirals—dolutegravir, tenofovir, lamivudine and efavirenz—in 13 different regions in brain/CNS with postmortem analysis. (Chapter 2)
2. To characterize penetration of three antiretrovirals, tenofovir, lamivudine and efavirenz, and one antifungal, fluconazole, in upper (ovary and uterus) and lower (cervix and vagina) FGT tissues. (Chapter 3)
3. To explore postmortem redistribution of antiretrovirals using a mice model. Tenofovir, lamivudine and efavirenz were used as examples. (Chapter 4)

4. To predict FGT exposure of tenofovir with PBPK modeling and to simulate pharmacokinetic profiles for different nonadherence scenarios to evaluate efficacy of PrEP under nonadherence. (Chapter 5)

CHAPTER 2 Post-mortem Analysis of Dolutegravir, Tenofovir, Lamivudine and Efavirenz Penetration in Multiple CNS Compartments

2.1 Introduction

The central nervous system (CNS) is a reservoir of HIV, which contributes to compartmentalized replication of the virus [104-107], and subsequently the development of resistance to antiretroviral therapy (ART) [108-110], viremic relapse after treatment interruption [106], and HIV-associated neurocognitive disorders (HAND) despite viral suppression in the peripheral blood [49, 111, 112]. One hypothesis of compartmentalized viral replication in the CNS is that the exposure of antiretrovirals in the CNS is insufficient to eliminate the virus and provides a favorable environment to select variants less susceptible to the current ART regimen. This hypothesis is indirectly supported by studies that show use of CNS-penetrating antiretrovirals (ARVs) is associated with lower CSF viral load [45-47] or better neurophysiological outcomes [46, 48-50]. Meanwhile, some ARVs are associated with neurotoxicity [113] and even potentially contribute to development of HAND [114]. Therefore, understanding CNS penetration of ARVs is critical to improving therapy to balance between protecting the CNS from HIV persistence and from drug-induced neurotoxicity. As brain tissue is not readily available from clinical routines, cerebrospinal fluid (CSF) has been widely used as a surrogate of the entire CNS for investigation of viral replication and ARV distribution; however, the adequacy of

considering CSF as a surrogate for brain has not been well justified, and some studies found CSF is not representative of brain tissue [54, 55].

In the current study, we used human postmortem brain tissues. These samples included multiple anatomical regions which were used to determine whether there were differences in distribution and penetration of four ARVs, dolutegravir, tenofovir, lamivudine and efavirenz, that are first-line or alternative first-line treatments in multiple guidelines [18, 21, 115]. We also examined whether demographic and clinical factors could potentially affect CSF or brain penetration. In addition, since the phenomena of post-mortem redistribution has been reported in multiple forensic toxicological studies [116], but has never been described for antiretrovirals, we used a mouse model to investigate the potential for post-mortem redistribution of three ARVs in brain tissues.

2.2 Methods

2.2.1 Human postmortem study

Decedents with HIV who were hospitalized due to advanced HIV/AIDS were enrolled with written informed consent from next-of-kin for autopsy at Mulago National Referral Hospital or Kiruddu General Hospital in Kampala, Uganda from 2017 to 2020. Medical history including HIV and opportunistic infection diagnoses, use of ART and concomitant medications, and adherence were collected from a combination of hospital records (when available) or from interviews with next-of-kin or caretakers. Autopsies were performed within 32 hours of death, during which approximately 1–2 g of brain tissue/fluid were collected from 13 regions of the CNS (i.e., CSF, frontal lobe, corpus callosum, parietal lobe, occipital lobe, globus pallidus, hippocampus, cerebellum,

midbrain/substantia nigra, pons, medulla oblongata, cervical spinal cord/meninges and choroid plexus/arachnoid) and immediately snap-frozen in liquid nitrogen. Whole blood from the femoral vein was collected into EDTA vacutainers and spun at 2400–3000 rpm at 4°C for 10 min to separate plasma. CSF was collected via cisternal puncture. Specimens were transferred via liquid nitrogen to –80°C freezers where they were stored until analysis. The study protocol was approved by the Research Ethics Review Committee at Mulago National Referral Hospital. Plasma creatinine concentrations and plasma and CSF albumin concentrations were measured by Fairview Diagnostic Laboratories (Minneapolis, Minnesota, USA) (the assays were not clinically validated since the samples were postmortem plasma and CSF).

2.2.2 Quantification of ARVs with LC-MS/MS

Quantification of dolutegravir, tenofovir, lamivudine and efavirenz in human and mouse tissue were performed with liquid chromatography with tandem mass spectrometry (LC-MS/MS) at the Clinical Pharmacology Analytical Services lab at the University of Minnesota College of Pharmacy. The method for tenofovir, lamivudine and efavirenz in human plasma, CSF, brain tissue has been previously described [60, 117]. Dolutegravir was measured in a simultaneous assay with four other antimicrobials. Dolutegravir was quantified in a separate assay. Tenofovir, lamivudine and efavirenz were quantified with fluconazole in another 4-drug simultaneous assay. However, for simplicity, we only present content related to dolutegravir, tenofovir, lamivudine and efavirenz, and omit other analytes.

Brain tissue sample preparation

An approximate weight of 0.3 g of brain tissue was combined with twice the volume of 5% BSA (Bovine Serum albumin) solution (i.e., 0.3 g of tissue + 0.6 mL of solution). The sample was homogenized using a Tissue Tearor model 985370-395 (BIOSPEC Products). The homogenate was centrifuged for 15 minutes at 15,000 x g and the top supernatant layer was removed for sample extraction.

Sample extraction for dolutegravir

For brain homogenate and CSF, a 10 µL aliquot of internal standard, dolutegravir-d5, at 5000 ng/mL was added to each sample (100 uL volume). For plasma, a 10 µL aliquot of internal standard (dolutegravir-d5) at 5000 ng/mL was added to each sample (100 µL volume). After briefly vortex-mixing, the sample proteins were precipitated with 500 uL of ice-cold acetonitrile and centrifuged for 5 minutes at 15,000 x g. The supernatant was removed and evaporated to dryness using a nitrogen evaporator (Zymark Turbo Vap LV, Hopkinton, MA) set at 37°C. The residue was reconstituted with 100 µL of 50:50 deionized (DI) water with 0.1% formic acid: DMSO.

Sample extraction for tenofovir, lamivudine and efavirenz

For brain homogenate, CSF and plasma, a 20 µL aliquot of internal standard (tenofovir-d6, lamivudine-C13, d2, and efavirenz-d4) at 500 ng/mL was added to each sample (200 µL volume). After briefly vortex- mixing, the sample proteins were precipitated with 800 µL of ice-cold acetonitrile and centrifuged for 5 minutes at 15,000 x g. The supernatant was removed and split equally into two separate tubes. The supernatant was dried for 30 minutes under nitrogen at 37C. One sample tube was reconstituted with 100 µL of mobile phase (0.1% formic acid in DI water) for tenofovir and lamivudine testing, and the remaining sample tube was reconstituted with 100 µL of

mobile phase consisting of (25:75) 10 mM ammonium acetate: acetonitrile for efavirenz testing. The other set of tubes were reconstituted with 100 µL of 50:50 DI water with 0.1% formic acid: DMSO for dolutegravir determination.

Sample analysis (tenofovir and lamivudine)

Detection and quantification of tenofovir and lamivudine was performed using an Acquity UPLC ultrahigh-performance liquid chromatograph (Waters, Milford MA) coupled with a Quattro Ultima triple stage quadrupole mass spectrometer (Micromass, Manchester, United Kingdom). The chromatographic separation was performed with an ACQUITY UPLC HSS T3 (2.1 x 50 mm), reversed phase column with a 1.7-micron particle size. The mobile phase used for the gradient elution consisted of (A) 0.1% formic acid in DI water (B) 0.1% formic acid in acetonitrile. The chromatographic conditions were isocratic from 0 to 1.50 min at 0% B, followed by a linear gradient at 1.5 to 2.75 min of 0% - 45% B and returning to the starting conditions (at 3.0 min) with a flow rate of 0.3 mL/min, for a total run time of 6 minutes. The column temperature was maintained at 30°C. The detector settings of the Quattro Ultima were: ESI with the stainless steel spray needle, positive polarity ionization, multiple reaction monitoring mode (MRM); spray voltage, 4000 V; cone voltage, 50V; Desolvation temperature, 400°C; Source temperature 100°C; argon collision gas.

Sample analysis (efavirenz)

Detection and quantification of efavirenz was performed using a high-performance liquid chromatograph (Agilent 1200 Series, Santa Clara CA) coupled with a TSQ Quantum triple stage quadrupole mass spectrometer (Thermo-Electron, San Jose, CA). The chromatographic separation was performed with an ACQUITY UPLC BEH

C18 (2.1 x 50 mm), reversed phase column with a 1.7-micron particle size. The mobile phase used for isocratic elution consisted of (A) 10 mM ammonium acetate in water, pH 6.8 (B) Acetonitrile. The mobile phase used was a mixture (by volume) of 10 mM ammonium acetate in water, pH 6.8 (25%) and acetonitrile (75%) with a flow rate of 0.25 ml/min and total run time of 2 minutes. The column temperature was maintained at 30°C. The detector settings of the TSQ Quantum were: ESI with the stainless steel spray needle, negative polarity ionization, selective reaction monitoring mode (SRM); spray voltage, 4500 V; capillary temperature, 400 °C; argon collision gas pressure, 1.5 mTorr; unit resolution for Q1 and Q3, 0.7 u (FWHM); and ions detected (m/z), efavirenz precursor 314, product 244 and efavirenz-d4 precursor 318, product 248. The collision energy for both efavirenz and its internal standard was set at 19eV.

Sample analysis (dolutegravir)

Detection and quantification of dolutegravir was performed using high-performance liquid chromatograph (Agilent 1100 Series, Santa Clara CA) coupled with a Sciex API4000 triple quadrupole instrument (MDS-SCIEX, Concord, Ontario, Canada). The chromatographic separation was performed with a Phenomenex Synergi Polar-RP (20 x 75 mm), reversed phase column with a 4-micron particle size. The mobile phase used for the gradient elution consisted of (A) 0.1% formic acid in DI water (B) 0.1% formic acid in acetonitrile. The chromatographic conditions were isocratic from 0 to 0.50 min at 0% B, followed by a linear gradient at 0.6 to 2.0 min of 0% - 75% B and returned to the starting conditions at 2.1 minutes, with a flow rate of 0.5 mL/min, for a total run time of 6 minutes. The column temperature was maintained at 30°C. Mass spectrometric detection was performed using MRM (multiple reaction monitoring) in positive

ionization mode. Source conditions were as follows: the turbo-gas temperature was set at 600°C, and the ion spray needle voltage was optimized at 5,000 V. The mass spectrometer was operated at unit resolution for both Q1 and Q3, with a dwell time of 25 ms per MRM channel. Gas pressures were optimized as follows: CAD, 4 psi; CUR, 20 psi; GS1 and GS2, 70 psi.

Lower limit of quantifications (LLOQs)

LLOQs of dolutegravir, tenofovir, lamivudine and efavirenz in plasma, CSF and brain tissues are shown in Table 2-1.

Table 2-1 LLOQs of dolutegravir, tenofovir, lamivudine and efavirenz in plasma, CSF and brain tissues.

	Dolutegravir	Tenofovir	Lamivudine	Efavirenz
Plasma (ng/mL)	20	10	10	10
CSF (ng/mL)	20	5	5	
Brain tissue (ng/g)	8	20	20	20

2.2.3 Data analysis

Penetration of a drug in a certain anatomical compartment was indicated by tissue penetration ratio which is the ratio of tissue concentration to plasma concentration. The tissue to plasma concentration ratio was only reported for human postmortem brain tissues when the drug concentration was quantifiable both in the plasma and the tissue compartment. Arithmetic means of concentrations and penetration ratios of 12 solid brain

regions were calculated for human samples and named as “composite brain”, in order to compare to CSF.

Summary statistics were calculated for absolute concentrations and penetration ratios. For each drug, comparison of natural log transformed concentrations and penetration ratios across all brain regions were conducted with the one-way analysis of variance (ANOVA) test, followed by a post-hoc pairwise comparison for all pairs using the paired t-test (*p*-value adjusted for multiple comparisons by the Holm method). The effect of age, sex, cryptococcus, tuberculosis, postmortem interval (time interval between death and autopsy), concomitant use of rifampin, estimated glomerular filtration rate (eGFR; estimated with the CKD-EPI equations), plasma creatinine, time since last dose, and CSF/plasma albumin ratio on the penetration of ARVs were tested by simple linear (univariate) regression. All statistical analyses were conducted at the significance level of α=0.05. The data was analyzed using R statistical software (version 4.0.3).

2.3 Results

2.3.1 Characteristics of study participants

Forty-nine participants were included in the final analysis, with clinical and demographic characteristics shown in Table 2-2. Age of decedents ranged from 18 to 79, with 75% of participants under 46 years of age. Causes of death included HIV- related opportunistic infections (i.e., cryptococcal meningitis, tuberculosis, pneumonia, and toxoplasmosis), malignancies (i.e., Kaposi sarcoma and pancreatic tumor), anemia, respiratory/cardiac/hepatic failure, etc. The most commonly prescribed ARV combinations were tenofovir disoproxil fumarate/lamivudine/efavirenz, followed by

tenofovir disoproxil fumarate/lamivudine/dolutegravir. Concomitant medications for *Cryptococcus* and tuberculosis infections included fluconazole, flucytosine, amphotericin B, isoniazid, ethambutol, rifampin and pyrazinamide.

Table 2-2 Characteristics of the postmortem study participants.

	Median (IQR) or n (%)
N	49 (100)
African	49 (100)
Age, year	40 (32, 47)
Female	23 (47)
HIV duration, day	598 (112, 2370)
CD4+ count, cells/mm^3	56 (23, 118)
HIV Viral load, copies/mL	8099 (34, 87467)
Cryptococcus	18 (37)
Tuberculosis	19 (39)
Post-mortem interval, hour	8 (5, 15)
eGFR, mL/min/1.72m^2	19 (10, 44)
CSF /serum albumin ratio	31 (12, 50)
HIV regimen*	
TDF/3TC/EFV	19 (39)
TDF/3TC/DTG	16 (33)
ABC/3TC/DTG	3 (6.1)
AZT/3TC/NVP	3 (6.1)

ABC/3TC/ATV/r	2 (4.1)
AZT/3TC/ATV/r	2 (4.1)
ABC/3TC/EFV	1 (2.0)
ABC/3TC/NVP	1 (2.0)
AZT/3TC/EFV	1 (2.0)
TDF/3TC/LPV/r	1 (2.0)
Time since last ARV dose, hour	22 (12, 46)
Duration on current ARV regimen, day	86 (34, 536)
Tuberculosis regimen	
Isoniazid/ethambutol/rifampin/pyrazinamide	16 (33)
Isoniazid/rifampin	2 (4.1)

*Detailed information of tuberculosis regimen was available from 18 participants.
Abbreviations: TDF, tenofovir disoproxil fumarate; 3TC, lamivudine; EFV, efavirenz; DTG, dolutegravir; ABC, abacavir; AZT, zidovudine; NVP, nevirapine; ATV, atazanavir; r, ritonavir; LPV, lopinavir.

2.3.2 Concentration of dolutegravir, tenofovir, lamivudine and efavirenz in plasma and brain sub-compartments

We initially assayed samples from 53 participants, then excluded records with plasma concentrations below the lower limit of quantification (BLQ) in each subset of four ARVs. There were 49 participants in the final analysis. The median and IQR of the four ARV concentrations in plasma, CSF and the 12 regions in the brain are shown in Table 2-2, as well as the number of BLQs in each brain region. Figure 2-1 displays the distribution of the concentrations in each anatomical compartment with a visual comparison to EC50 or EC90-95 documented in FDA labels [118-121]. Dolutegravir had the

highest portion of BLQ samples followed by tenofovir, while lamivudine and efavirenz were detectable in all brain samples, regardless of region (Table 2-3). Notably, the BLQ samples in brain specimens were not randomly distributed across participants as 74% of BLQ samples came from the same 2 subjects. The highest median concentration of dolutegravir, lamivudine and efavirenz in all 13 brain regions (Figure 2-1 and Table 2-3) were seen in cervical spinal cord/meninges, while the highest concentration of tenofovir was observed in the parietal lobe. The lowest median concentrations of the 13 brain regions (Figure 2-1 and Table 2-3) were: midbrain/substantia nigra for dolutegravir, corpus callosum for tenofovir, frontal lobe for lamivudine, and choroid plexus/arachnoid for efavirenz.

As for comparisons between ARV concentrations in brain regions to corresponding EC50 or EC90-95, overall, most participants attained brain concentrations above the highest EC50 for dolutegravir or EC90-95 for efavirenz. In contrast, for tenofovir and lamivudine, most participants had brain concentrations above the lower bound of EC50 but lower than the upper bound of EC50 (Figure1). ANOVA tests across all brain regions for the log10- transformed concentrations were significant for lamivudine ($p < 0.001$) and efavirenz ($p = 0.021$), but not for dolutegravir ($p = 0.117$) or tenofovir ($p = 0.073$). In the post-hoc pairwise comparisons for lamivudine, 20 pairs were significantly different, with frontal lobe concentrations being significantly less than nine other regions (Table 2-4). CSF and plasma concentration for dolutegravir (r = 0.78), tenofovir (r = 0.82) and lamivudine (r = 0.79) were highly correlated, with significant linear relationships ($p < 0.05$ for all) (Figure 2-2). Correlation between CSF and

composite brain were stronger for dolutegravir (r=0.77, p=0.044) and lamivudine (r=0.94, p<0.001) than tenofovir (r=0.5, p=0.082) (Figure 2-2).

Table 2-3 Concentrations of dolutegravir, tenofovir, lamivudine and efavirenz in plasma and various brain regions.*

	Dolutegravir			Tenofovir			Lamivudine			Efavirenz		
Anatomical compartments	Median (IQR), ng/mL or ng/g	n	BLQ	Median (IQR), ng/mL or ng/g	n	BLQ	Median (IQR), ng/mL or ng/g	n	BLQ	Median (IQR), ng/mL or ng/g	n	BLQ
Plasma	405 (128, 861)	17	0	1164 (288, 2320)	37	0	2290 (746, 4610)	46	0	1663 (766, 3070)	21	0
Brain												
Frontal lobe	18 (6, 29)	8	2	70 (47, 458)	14	1	420 (208, 770)	17	0	2060 (1716, 2850)	7	0
Parietal lobe	18 (8, 26)	8	2	216 (66, 301)	13	1	518 (363, 674)	14	0	1966 (1451, 3076)	6	0

Occipital lobe	18 (8, 22)	8	2	166 (48, 508)	14	1	468 (258, 776)	17	0	1802 (1555, 2998)	7	0
Cerebellum	18 (0, 26)	8	3	114 (40, 458)	14	1	554 (334, 1085)	15	0	1841 (1398, 2160)	5	0
Corpus callosum	16 (0, 20)	8	3	47 (25, 159)	13	2	536 (432, 839)	15	0	2320 (1956, 2913)	6	0
Medulla oblongata	18 (8, 24)	8	2	138 (65, 406)	14	1	662 (476, 1160)	17	0	2480 (1980, 3777)	7	0
Pons	21 (0, 28)	8	3	68 (57, 229)	12	1	611 (544, 1144)	14	0	2560 (1770, 2580)	5	0
Globus pallidus	17 (0, 23)	8	3	106 (52, 406)	14	1	538 (246, 1026)	17	0	2600 (1591, 3204)	7	0
Hippocampus	16 (0, 21)	8	3	101 (41, 268)	13	1	526 (410, 804)	15	0	1984 (1909, 2028)	6	0

Midbrain/substantia nigra	15 (7, 25)	8	2	82 (46, 370)	13	1	608 (416, 1004)	15	0	2520 (1760, 4307)	6	0
Cervical spinal cord/meninges	30 (21, 34)	6	0	108 (56, 245)	14	2	736 (526, 1128)	15	0	3060 (2052, 3634)	7	0
Choroid plexus/arachnoid	26 (0, 34)	8	3	176 (83, 1000)	12	1	573 (334, 1046)	16	0	1338 (1126, 2388)	6	0
CSF	27 (0, 48)	16	6	104 (58, 218)	35	0	586 (323, 1222)	44	0			
Composite brain	20 (4, 26)	8		93 (43, 389)	16		531 (355, 1004)	17		2360 (1812, 3269)	7	

* Concentration units are ng/g for solid brain tissues, or ng/mL for plasma and CSF. Summary statistics of concentrations are expressed as median (IQR), followed by total number and number of BLQ for each brain region of all available samples.

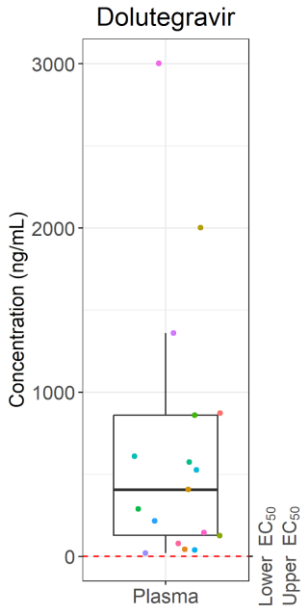
Dolutegravir
Concentration (ng/mL)
3000
2000
1000
0
Plasma
Lower EC50
Upper EC50

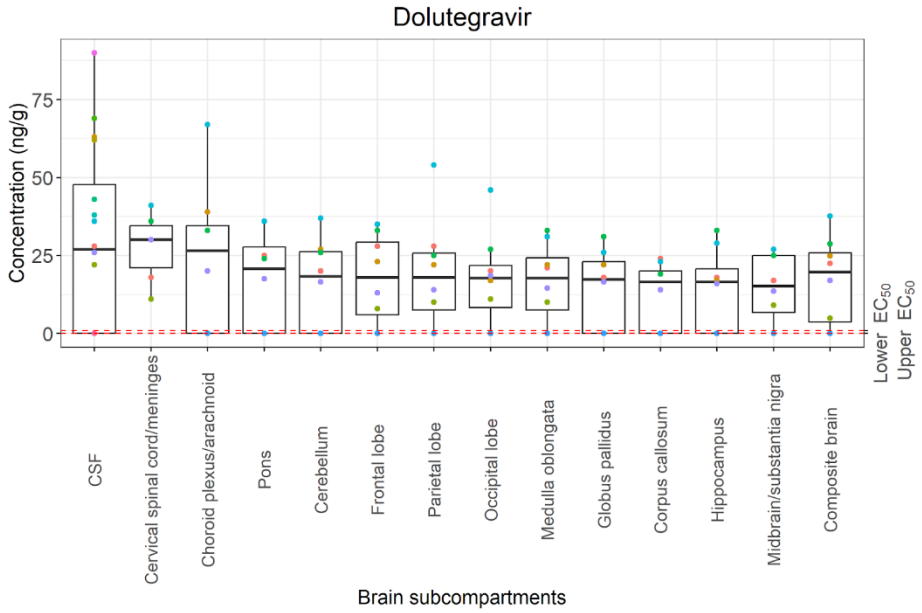
Dolutegravir
Concentration (ng/g)
75
50
25
0
CSF
Cervical spinal cord/meninges
Choroid plexus/arachnoid
Pons
Cerebellum
Frontal lobe
Parietal lobe
Occipital lobe
Medulla oblongata
Globus pallidus
Corpus callosum
Hippocampus
Midbrain/substantia nigra
Composite brain
Brain subcompartments
Lower EC50
Upper EC50

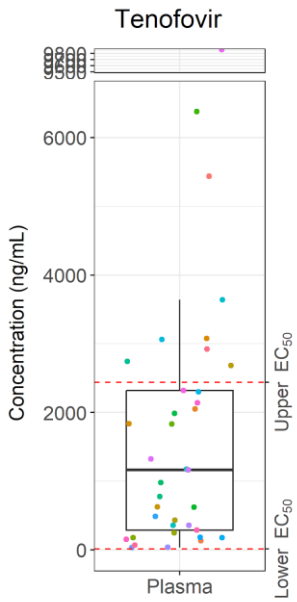
Tenofovir
Concentration (ng/mL)
6000
4000
2000
0
Upper EC50
Lower EC50
Plasma

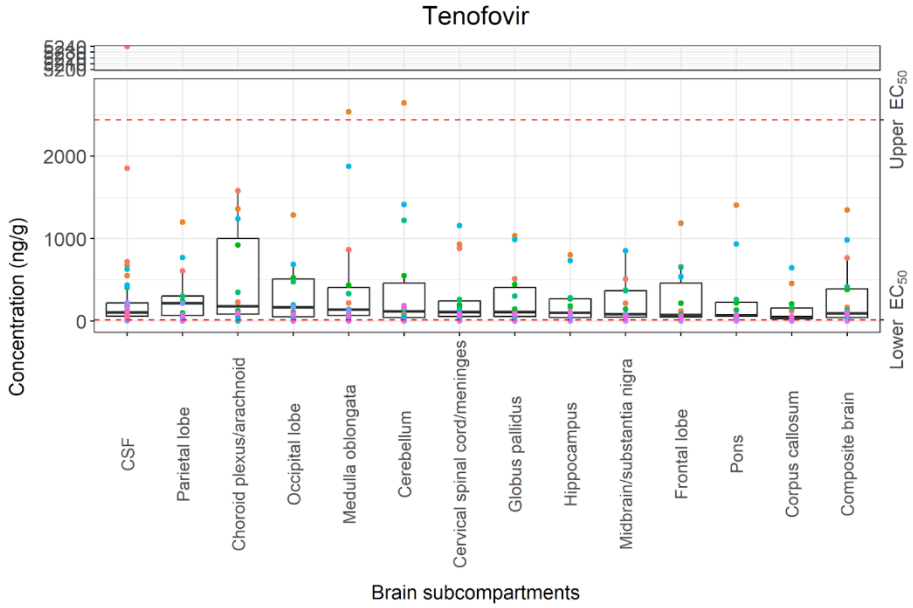
Tenofovir
Concentration (ng/g)
2000
1000
0
Upper EC50
Lower EC50
CSF
Parietal lobe
Choroid plexus/arachnoid
Occipital lobe
Medulla oblongata
Cerebellum
Cervical spinal cord/meninges
Globus pallidus
Hippocampus
Midbrain/substantia nigra
Frontal lobe
Pons
Corpus callosum
Composite brain
Brain subcompartments

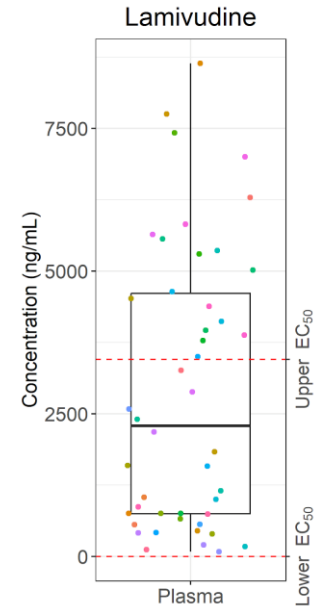
Lamivudine
Concentration (ng/mL)
7500
5000
2500
0
Plasma
Upper EC50
Lower EC50

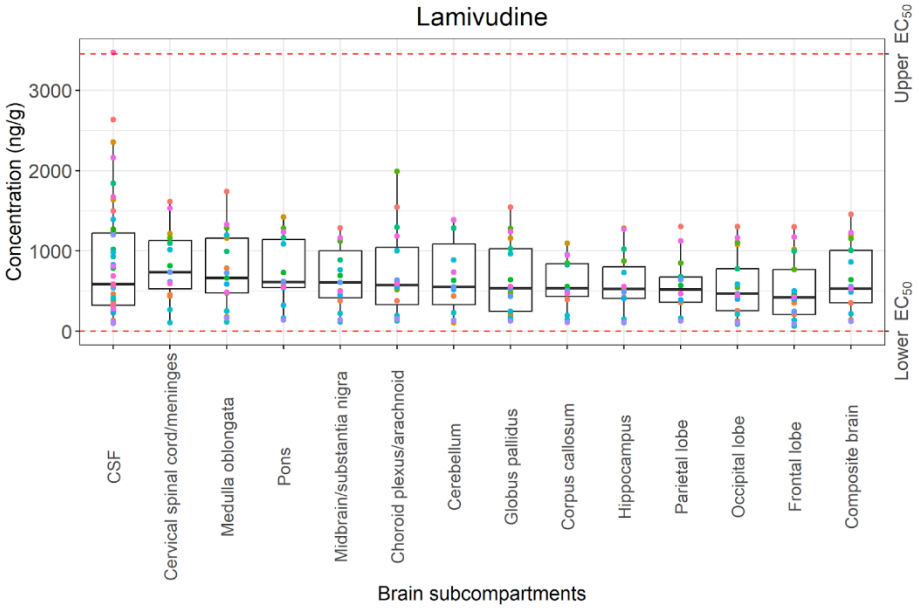
Lamivudine
Concentration (ng/g)
3000
2000
1000
0
Upper EC50
Lower EC50
CSF
Cervical spinal cord/meninges
Medulla oblongata
Pons
Midbrain/substantia nigra
Choroid plexus/arachnoid
Cerebellum
Globus pallidus
Corpus callosum
Hippocampus
Parietal lobe
Occipital lobe
Frontal lobe
Composite brain
Brain subcompartments

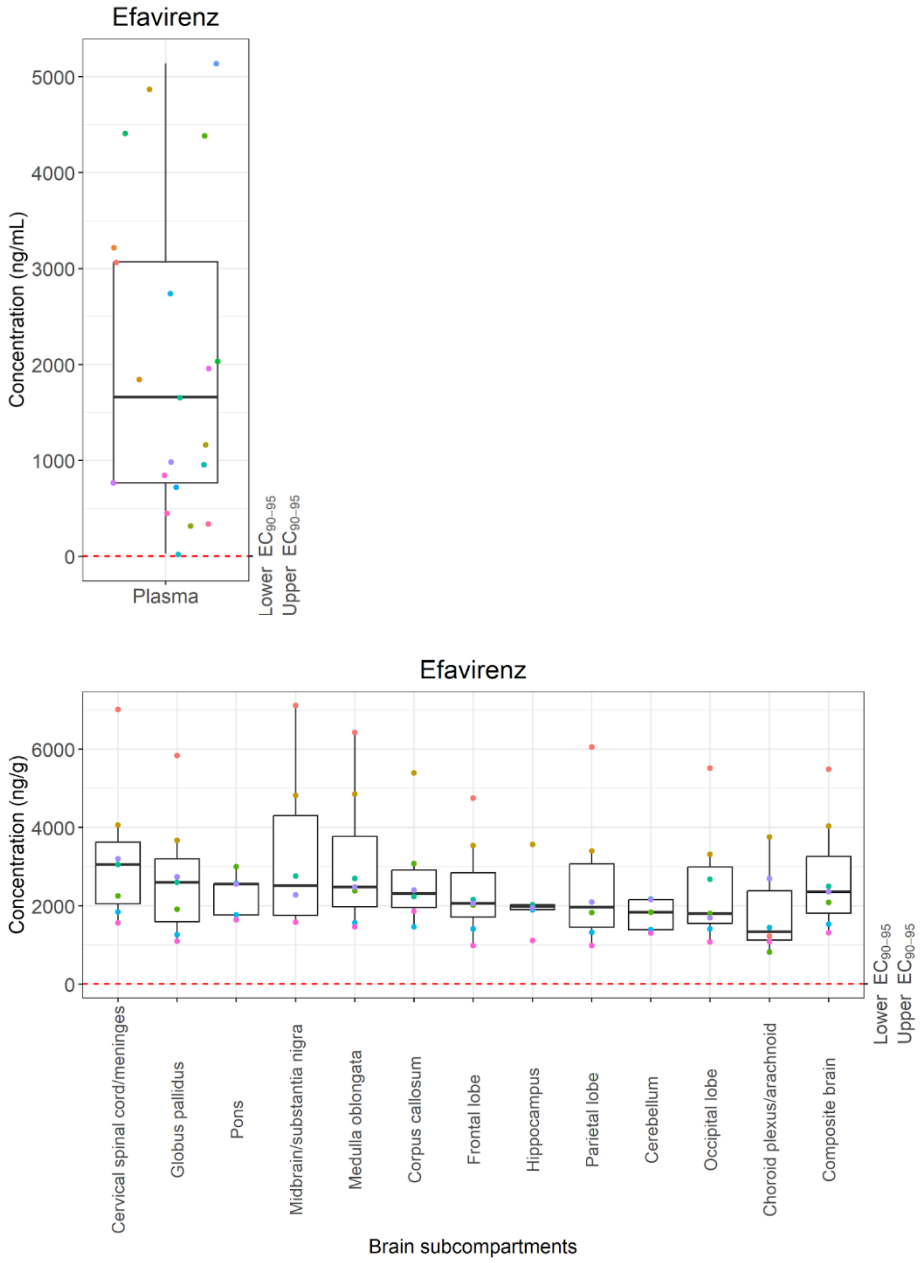

Figure 2-1 Boxplots of dolutegravir, tenofovir, lamivudine and efavirenz in plasma and brain region concentrations. Individuals are indicated by color. Boxes plots of solid brain tissues are ranked by medians from greatest to smallest (except for CSF and composite brain). Red dashed lines in the box plots represent the lower and upper boundary of *in*

vitro EC50 (dolutegravir 0.008 – 0.90 ng/mL; tenofovir 11.5 – 2439.5 ng/mL; lamivudine 0.69 – 3450 ng/mL) or EC90-95 (efavirenz 0.537 – 7.9 ng/mL).

Table 2-4 Pairwise comparisons of brain regions with significantly different concentrations or tissue-penetration-ratios. Fold difference is the geometric mean of ratios between concentration/tissue-penetration-ratio of region in the first column and the second column.

Region	**Region**	**Fold difference**	**Adjusted *p*-value (paired t-test)**
Lamivudine concentration			
Frontal lobe	Globus pallidus	0.70	0.003
	Hippocampus	0.76	0.015
	Medulla oblongata	0.62	< 0.001
	Midbrain/substantia nigra	0.73	0.041
	Pons	0.62	0.002
	CSF	0.58	< 0.001
	Cerebellum	0.67	< 0.001
	Choroid plexus/arachnoid	0.63	< 0.001

	Cervical spinal cord/meninges	0.63	< 0.001
Occipital lobe	CSF	0.70	0.041
	Choroid plexus/arachnoid	0.77	0.007
	Cervical spinal cord/meninges	0.76	0.002
	Medulla oblongata	0.75	0.004
	Pons	0.74	0.002
Parietal lobe	Cervical spinal cord/meninges	0.76	0.018
	Medulla oblongata	0.74	0.026
	Pons	0.73	0.039
Midbrain/substantia nigra	Pons	0.84	0.041
	Cervical spinal cord/meninges	0.84	0.002
Corpus callosum	Pons	0.80	0.001
Efavirenz concentration			
Frontal lobe	Medulla oblongata	0.79	0.04
Tenofovir tissue-to-plasma ratio			
Corpus callosum	Cerebellum	0.32	< 0.001

	Choroid plexus/arachnoid	0.43	< 0.001
	Globus pallidus	0.58	0.04
	Medulla oblongata	0.42	0.01
Lamivudine tissue-to-plasma ratio			
Frontal lobe	Globus pallidus	0.69	0.002
	Hippocampus	0.75	0.016
	Medulla oblongata	0.61	< 0.001
	Midbrain/substantia nigra	0.72	0.035
	Pons	0.60	0.001
	CSF	0.58	< 0.001
	Cerebellum	0.66	< 0.001
	Choroid plexus/arachnoid	0.76	< 0.001
	Cervical spinal cord/meninges	0.62	0.002
Occipital lobe	Choroid plexus/arachnoid	0.76	0.006
	Cervical spinal cord/meninges	0.76	0.005
	Medulla oblongata	0.74	0.006

	Pons	0.73	0.001
Parietal lobe	Cervical spinal cord/meninges	0.76	0.046
	Medulla oblongata	0.74	0.041
	Pons	0.72	0.045
Midbrain/substantia nigra	Cervical spinal cord/meninges	0.85	0.006
Corpus callosum	Pons	0.80	0.003
Efavirenz tissue-to-plasma ratio			
Frontal lobe	Medulla oblongata	0.79	0.04

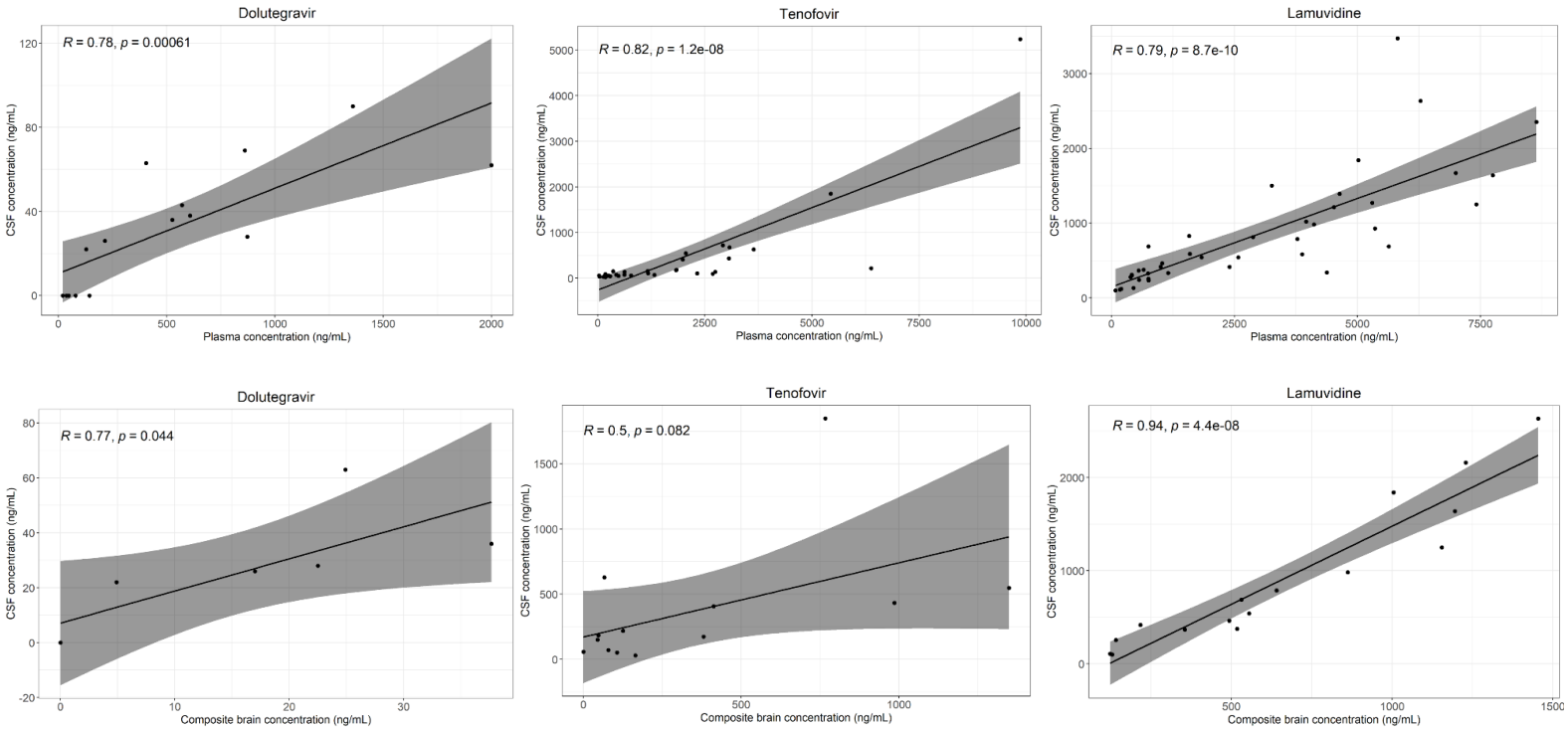

Figure 2-2 Scatterplots of correlations between CSF and plasma (upper panel) and CSF and composite brain (lower panel). R: Pearson correlation coefficient. P: p-value of linear regression.

2.3.3 Penetration of dolutegravir, tenofovir, lamivudine and efavirenz in brain regions

ARV penetration was determined by the ratios between the concentration in a certain brain region and plasma. Distribution and summary statistics are illustrated in Figure 2-3 and Table 2-5. All ANOVA tests of penetration ratios displayed significance across regions (dolutegravir, $p = 0.002$; tenofovir, $p < 0.001$; lamivudine, $p < 0.001$; efavirenz, $p = 0.021$). With p-value adjustment in the post hoc pairwise comparisons, no pairs were significant for dolutegravir; 4 pairs were significantly different for tenofovir, with a lower penetration ratio in the corpus callosum compared to four other regions; 18 pairs were significantly different for lamivudine, and penetration ratio in the frontal lobe was significantly lower than 9 other regions; and 1 pair was significantly different for efavirenz with a lower penetration ratio in the frontal lobe compared to that of the medulla oblongata (Table 2-4).

Table 2-4 is color-coded by rank order of the median penetration ratios, with higher penetration ratios colored with darker shades. Regions with the highest penetration ratios were choroid plexus/arachnoid (dolutegravir and tenofovir), CSF (lamivudine), and pons (efavirenz); the lowest are corpus callosum (dolutegravir and tenofovir), frontal lobe (lamivudine), and choroid plexus/arachnoid (efavirenz).

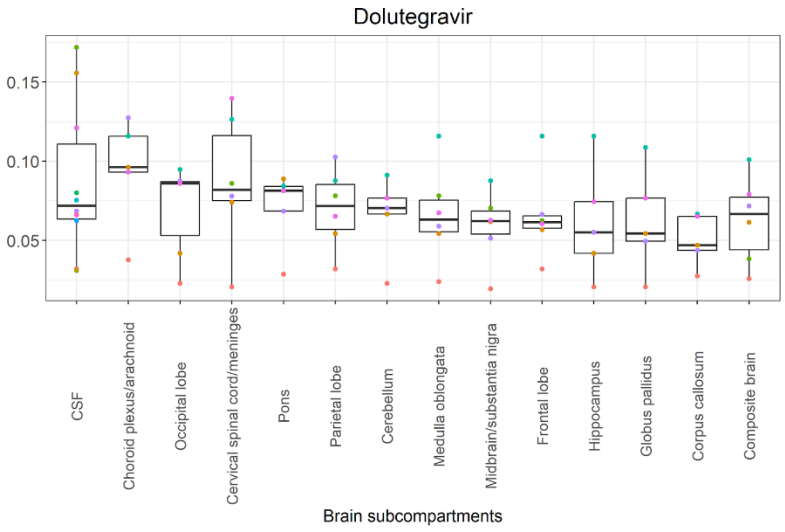
Dolutegravir
0.15
0.10
0.05
CSF
Choroid plexus/arachnoid
Occipital lobe
Cervical spinal cord/meninges
Pons
Parietal lobe
Cerebellum
Medulla oblongata
Midbrain/substantia nigra
Frontal lobe
Hippocampus
Globus pallidus
Corpus callosum
Composite brain
Brain subcompartments

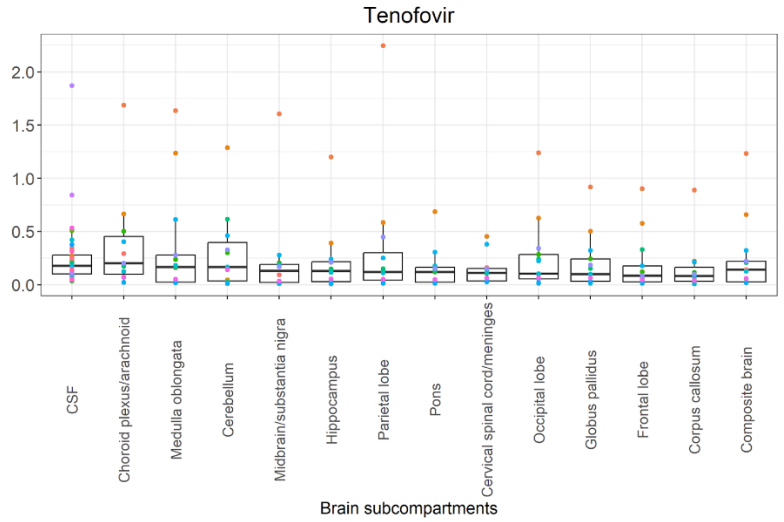
Tenofovir
2.0
1.5
1.0
0.5
0.0
CSF
Choroid plexus/arachnoid
Medulla oblongata
Cerebellum
Midbrain/substantia nigra
Hippocampus
Parietal lobe
Pons
Cervical spinal cord/meninges
Occipital lobe
Globus pallidus
Frontal lobe
Corpus callosum
Composite brain
Brain subcompartments

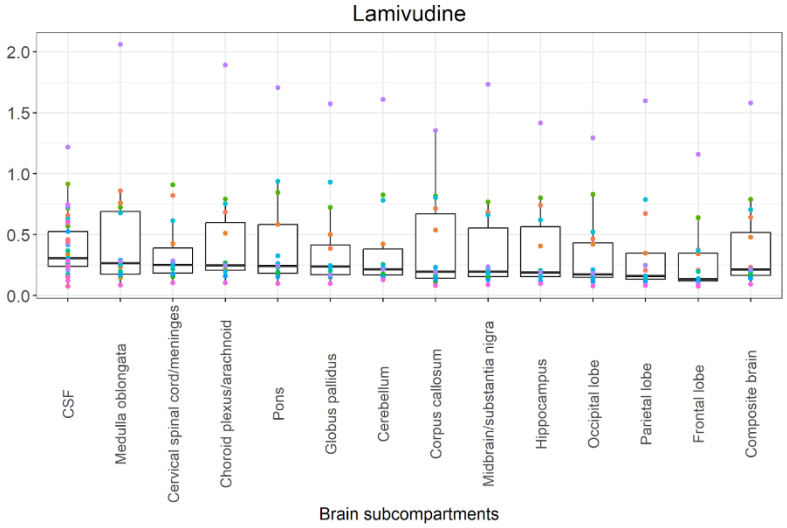
Lamivudine
2.0
1.5
1.0
0.5
0.0
CSF
Medulla oblongata
Cervical spinal cord/meninges
Choroid plexus/arachnoid
Pons
Globus pallidus
Cerebellum
Corpus callosum
Midbrain/substantia nigra
Hippocampus
Occipital lobe
Parietal lobe
Frontal lobe
Composite brain
Brain subcompartments

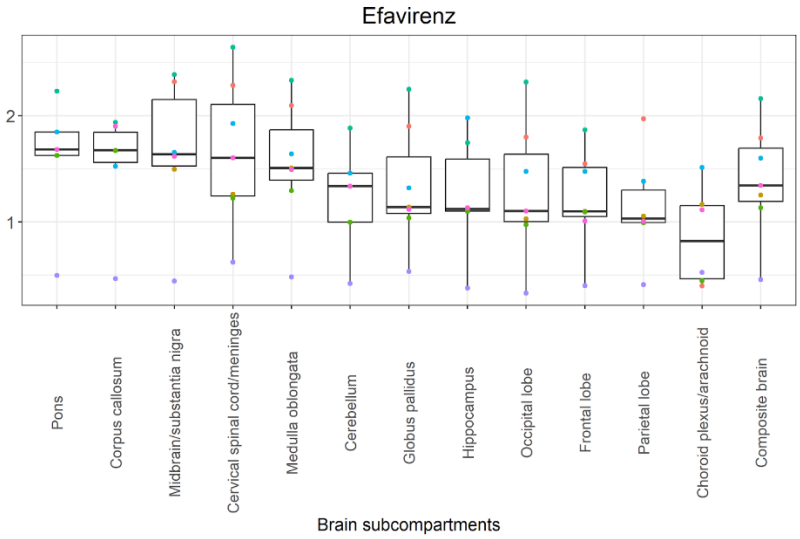

Figure 2-3 Boxplots of dolutegravir, tenofovir, lamivudine and efavirenz penetration ratios in brain sub-compartments. Different colors indicate individual participants. Boxplots of solid brain tissues are ranked by medians from highest to lowest (except for CSF and composite brain which are displayed first and last respectively). The penetration ratios are the ratios of brain region concentration and plasma concentration of each individual.

Table 2-5 Summary statistics of penetration ratios of dolutegravir, tenofovir, lamivudine and efavirenz in 13 brain regions. Within each column, cells are color coded by medians with a spectrum of shades of green, with the darkest green indicating the highest penetration ratios and the lightest green indicating the lowest penetration ratios.

Penetration Ratio	Dolutegravir		Tenofovir		Lamivudine		Efavirenz	
Compartments	n	Median (IQR)	n	Median (IQR)	n	Median (IQR)	n	Median (IQR)
Frontal lobe	6	0.061 (0.058, 0.066)	13	0.085 (0.027, 0.176)	16	0.135 (0.119, 0.349)	7	1.099 (1.052, 1.512)
Parietal lobe	6	0.072 (0.057, 0.085)	12	0.12 (0.042, 0.3)	13	0.161 (0.135, 0.348)	6	1.031 (0.997, 1.3)
Occipital lobe	6	0.086 (0.053, 0.087)	13	0.103 (0.054, 0.284)	16	0.174 (0.148, 0.432)	7	1.102 (1.003, 1.637)
Cerebellum	5	0.07 (0.067, 0.077)	11	0.165 (0.034, 0.395)	14	0.215 (0.169, 0.382)	5	1.337 (0.998, 1.459)
Corpus callosum	5	0.047 (0.044, 0.065)	11	0.08 (0.031, 0.162)	14	0.195 (0.143, 0.671)	6	1.673 (1.561, 1.843)
Medulla oblongata	6	0.063 (0.055, 0.075)	13	0.166 (0.023, 0.277)	16	0.265 (0.175, 0.69)	7	1.507 (1.394, 1.868)
Pons	5	0.081 (0.068, 0.084)	11	0.119 (0.024, 0.163)	13	0.24 (0.183, 0.583)	5	1.684 (1.627, 1.848)
Globus pallidus	5	0.054 (0.049, 0.077)	13	0.101 (0.031, 0.242)	16	0.238 (0.17, 0.416)	7	1.139 (1.079, 1.612)
Hippocampus	5	0.055 (0.042, 0.074)	12	0.128 (0.029, 0.216)	14	0.191 (0.155, 0.567)	6	1.122 (1.102, 1.593)
Midbrain/substantia nigra	6	0.062 (0.054, 0.068)	12	0.131 (0.022, 0.191)	14	0.195 (0.157, 0.555)	6	1.637 (1.527, 2.153)
Cervical spinal cord/meninges	6	0.082 (0.075, 0.116)	12	0.111 (0.035, 0.152)	14	0.252 (0.186, 0.39)	7	1.604 (1.243, 2.105)

Choroid plexus/arachnoid	5	0.096 (0.093, 0.116)	11	0.2 (0.098, 0.454)	15	0.247 (0.206, 0.597)	6	0.82 (0.465, 1.153)
CSF	10	0.072 (0.063, 0.111)	32	0.176 (0.099, 0.279)	41	0.307 (0.239, 0.525)		
Composite brain	6	0.067 (0.044, 0.077)	13	0.141 (0.026, 0.22)	16	0.212 (0.166, 0.518)	7	1.344 (1.193, 1.695)

2.3.4 Covariates on CSF and brain penetration

Results from the univariate regression between multiple demographic or clinical factors and penetration ratio in CSF or composite brain are shown in Table 2-6. Males had higher dolutegravir penetration in CSF than females (p=0.045), but no sex differences were observed for drug concentrations with the composite brain (p=0.475). Participants with cryptococcal meningitis had higher CSF penetration of lamivudine (p=0.027) and a trend towards higher CSF penetration of dolutegravir (p=0.05). The ratio of CSF and serum albumin, which reflects the permeability/integrity of the blood-brain-barrier (BBB) [122] and blood-CSF-barrier (BCSFB) [123], though not statistically significant, had a trend of CSF penetration rising with CSF/serum albumin for dolutegravir (p=0.054), tenofovir (p=0.07) and lamivudine (p=0.087). Concomitant use of rifampin was significantly associated with higher tenofovir penetration ratio in composite brain (p=0.043). Variables that were identified in univariate analysis as potentially important ($p \leq 0.05$) for penetration in CSF or composite brain are shown in Figure 2-4. Age, co-infection with TB, post-mortem interval, eGFR, serum creatinine, and time since last dose were not significant predictors of drug penetration into CSF nor brain compartments.

Table 2-6 Beta coefficients and p-values of univariate linear regression analysis of multiple factors and CSF/composite brain penetration. *P*-values < 0.05 are marked with an asterisk.

Variable	Dolutegravir		Tenofovir		Lamivudine		Efavirenz
	CSF	Composite brain	CSF	Composite brain	CSF	Composite brain	Composite brain
Age, year							
Beta	-0.0005	0.002	-0.0005	-0.0008	-0.003	-0.0005	-0.034
p	0.735	0.057	0.942	0.936	0.351	0.966	0.376
Sex (female as reference)							
Beta	-0.064	0.019	0.086	-0.064	0.035	0.100	-0.214
p	0.045 *	0.478	0.491	0.753	0.638	0.625	0.678
Cryptococcus (positive as reference)							

Beta	-0.059	-0.045	-0.200	-0.044	-0.167	-0.118	-0.182
p	0.050	0.151	0.116	0.827	0.027 *	0.575	0.724
Tuberculosis							
Beta	-0.031	0.030	0.056	0.352	0.060	0.342	-0.277
p	0.376	0.204	0.650	0.069	0.437	0.079	0.588
Post-mortem interval, hour							
Beta	0.001	-0.003	-0.002	-0.025	-0.003	-0.009	-0.092
p	0.596	0.165	0.835	0.110	0.486	0.623	0.080
Rifampin use							
Beta	0.056	-0.035	-0.095	-0.406	-0.115	-0.338	0.277
p	0.064	0.154	0.443	0.043 *	0.140	0.082	0.588
eGFR, mL/min/1.72m^2							

Beta	-0.0006	0.0006	-0.001	0.007	0.001	0.002	-0.0006
p	0.556	0.512	0.684	0.153	0.471	0.650	0.952
Serum creatinine, g/dL							
Beta	0.017	0.004	0.021	-0.012	0.007	-0.031	-0.036
p	0.486	0.851	0.399	0.782	0.609	0.462	0.687
Time since last dose, hour							
Beta	-0.0002	-0.002	-0.0003	0.0007	-0.0001	0.0002	-0.001
p	0.855	0.340	0.804	0.446	0.819	0.911	0.733
CSF/serum albumin ratio							
Beta	0.002	-0.0002	0.002	-0.003	0.003	0.0002	0.017
p	0.054	0.765	0.070	0.697	0.087	0.972	0.481

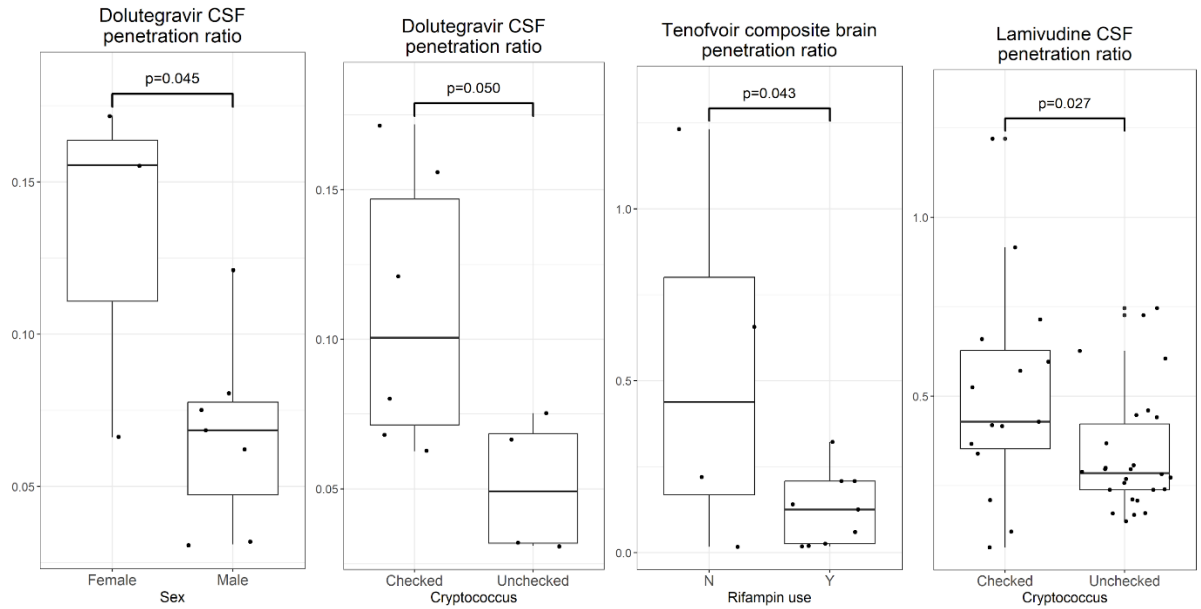

Figure 2-4 Boxplots/scatterplots of key variables ($p \leqslant 0.05$) for CSF and composite brain penetration.

2.4 Discussion

Our robust sampling approach of 12 brain regions, plasma, and CSF allows for a comprehensive analysis of antiretroviral distribution throughout the CNS, which has led to several important observations. First, for a certain participant, concentrations and penetration ratios were similar across brain regions. Second, overall in the population, there were significant reginal differences for tenofovir, lamivudine and efavirenz. Third, the rank ordering of penetration into compartments was different for each antiretroviral, likely due to their different physiochemical properties.

The majority of previous studies investigating ARV penetration have used CSF as a surrogate of the whole CNS, however how representative CSF is of brain concentrations is unknown. Dolutegravir concentrations observed in CSF in our study are slightly higher than 3 previous studies (median concentrations: 26 ng/mL, current study; 9.6 -13.2 ng/mL [62, 64, 124], while the penetration ratios (compared to plasma) are about 10 times higher (median penetration ratios: 0.072, current study; 0.0041- 0.0065 [62, 64, 124]). This discrepancy might be due to the different clearance between compartments, as CSF might have slower clearance than plasma for its slower turnover rate [125], and therefore ratios would be influenced by sampling times. Tenofovir (given as tenofovir disoproxil fumarate) concentrations and penetration ratios in the CSF measured in the current study (median concentration, 104 ng/mL; median tissue to plasma ratio, 0.18) and our previous analysis (median concentration, 137 ng/mL; geometric mean tissue to plasma ratio, 0.29) [60] were high, compared to previous studies done by others, with concentration medians ranging from undetectable to 6 ng/mL and penetration ratios between 0.021 and 0.05 [56-59].

However, the concentrations in brain tissues in the current study (median 93 ng/g) were similar to another postmortem study by Ferrara *et al* (median 148 ng/mL) [61]. Lamivudine concentrations in CSF (median 586 ng/g) was higher than measured by Van den Hof *et al* [59]. (median 97 ng/mL), and composite brain (median 531 ng/g) in the current study were higher than those measured by Ferrara *et al*. (median 63 ng/mL) [61], but the penetration ratios were within the range of same order of magnitude (median tissue to plasma ratio: 0.21, current study; 0.33, Van den Hof *et al*. [59]).

Previous studies show that efavirenz concentration in CSF was less than 1% of plasma [59, 65-68], which was expected to be near the lower limit of quantification of our bioanalytical assay; therefore, we did not measure efavirenz in CSF. Efavirenz concentration in brain tissue measured by Ferrara *et al*. in postmortem analysis (median 36 ng/mL, n = 2) [61] was lower than the current study (median in composite brain 2360 ng/mL). Efavirenz-related neuropsychiatric reactions and neurocognitive disorders are of concern in HIV treatment. As our study revealed that efavirenz had higher CNS penetration than other types of ARV, it may suggest the increased occurrence of CNS adverse effects.

Notably, regional differences were discovered, especially for lamivudine and efavirenz, and it seems that the cortical regions tend to be less penetrable than other regions. Regional differences of ARV exposure, no matter with significantly difference or not, could create a selective pressure that drives the mutation of HIV towards a certain ARV and could therefore contribute towards the creation of HIV reservoirs. In general, for ARVs with relatively low genetic barriers to resistance such as tenofovir, lamivudine and efavirenz [126], which are the ones that showed significant regional differences in our

analysis, it is better to combine them with ARVs that exhibit higher genetic barriers, such as dolutegravir [127, 128] and protease inhibitors [129], so that the combined antiretroviral therapy could prevent the development of resistance due to viral mutation. On the other hand, for ARVs that are more penetrable and are well-known to exhibit neurotoxicity (e.g., efavirenz), the regional difference flags the potentially more vulnerable regions (i.e., regions with higher penetration ratios), would warrant *in vitro* or preclinical studies to look for a cutoff concentration for toxicity and provide reference to adjust clinical dosing.

The significant difference between sexes for CSF penetration of dolutegravir has not been previously reported; however, with only 3 observations in the female group with both CSF and plasma available, our findings could be due to chance. The ratio between CSF and serum albumin indicate the integrity of BBB [122] and BCSFB [123] since more albumin leaks into CSF as the integrity of the barriers deteriorate. We saw a positive trend between CSF penetration trended with CSF/serum albumin for dolutegravir, tenofovir and lamivudine, but small sample sizes could have influenced statistical significance. The difference in CSF penetration of lamivudine with- and without *Cryptococcus* infection is consistent with our previous analysis [60] and implies that meningeal infection is likely to increase drug distribution into CSF. Although CSF/serum albumin ratio did not differ by *Cryptococcus* infection status in our study, the increased drug distribution could be mediated by the increased permeability of BBB/BCSFB.

To our knowledge, the current study is the most extensive investigation of ARV distribution and penetration in a variety of sub-anatomical brain tissues. Nonetheless, there are limitations in the current study. First, despite our large total sample size relative

to other studies, not all participants had a complete case (i.e., all 13 brain regions collected and measured) due to challenges in obtaining postmortem brain, thus some of the analysis (e.g., paired t tests that required no missing values in the paired data) were not statistically powered. Second, our participants were critically ill upon death, which might be accompanied by multiple organ dysfunction that impacts pharmacokinetics of drugs in the body, although we attempted to qualify for this by measures of kidney function such as creatinine clearance. Also, we were not able to robustly account for participants' adherence, and the adherence information were mostly from interview with caretakers since oral medications in Uganda are not administered by hospital staff but rather by caretakers. However, we used detectable plasma concentration as criteria to confirm the recent administration of ARVs so that the penetration ratios could reflect more accurate CNS penetrating property. Furthermore, most of the participants had increased BBB permeability as measured by CSF/serum albumin ratio, therefore, caution must be taken while extrapolating results to the general population.

These findings pave the way for future studies to validate the clinical significance of these regional differences. Future studies could investigate the neurological effect of efavirenz by collecting patients' antemortem neurocognitive and neuropsychiatric measurements and analyzing the correlation between neurological effect and brain distribution of efavirenz. In addition, correlation between tissue viral load and mutation/resistance and regional exposure of ARVs could also be identified. In conclusion, with postmortem analysis, we measured the penetration of dolutegravir, tenofovir, lamivudine and efavirenz in various brain regions which are rarely available in

common clinical or research settings, and significant regional differences were discovered that may inform future clinical care.

CHAPTER 3 A Post-mortem Analysis of Tenofovir, Lamivudine, Efavirenz and Fluconazole Penetration in Female Genital Tissues [1]

3.1 Introduction

The female genital tract (FGT) is a significant anatomical site of pathogen persistence and sexual transmission of infectious diseases. Optimal drug exposure in the FGT is paramount for prevention and treatment of FGT-involved infectious diseases, such as HIV and vaginal candidiasis. Although much of the focus on mucosal HIV transmission in women has been on the lower FGT (i.e., cervix and vagina), HIV infection can occur throughout the entire FGT, as demonstrated in rhesus macaques vaginal transmission model of simian immunodeficiency virus.[79] Candidiasis is an infection caused by the yeast *Candida*. While candidiasis is more commonly associated with infections in the vulvovaginal area compared to other FGT sites, it can, in rare cases, occur in the upper FGT (i.e., ovary and uterus) as well.[130] Despite this, our knowledge of FGT tissue exposure to antiretrovirals and antifungals has predominantly been obtained through sampling of the lower FGT mostly via cervicovaginal tissue and cervicovaginal fluid.[78, 83-85, 131-133] Studies related to FGT drug exposure in upper tissue tracts (i.e., ovarian and uterine tissue) in non-pregnant women is scarce due to difficulty of sampling.

[1] This chapter was taken from an article previously published. The original citation is as follows: Wang F, Namuju OC, Pastick KA, Abdusalaamu K, Mishra U, Collins L, Boulware DR, Lukande R, Meya DB, Nicol MR. A post-mortem analysis of tenofovir, lamivudine, efavirenz and fluconazole penetration in female genital tissues. J Antimicrob Chemother. 2022 Oct 28;77(11):3180-3186.

In order to fill the knowledge gap surrounding exposure of anti-infectives in four different solid tissues of the FGT including the upper and lower areas, we explored tissue penetration of three commonly prescribed antiretroviral drugs, tenofovir, lamivudine and efavirenz, in addition to an antifungal, fluconazole in postmortem FGT tissues (i.e., ovarian, uterine, cervical, and vaginal) from a population of Ugandan women living with HIV/AIDs prior to time of death.

3.2 Methods

3.2.1 Study participants and sample collection

All study participants were hospitalized patients living with HIV/AIDs who passed away at Mulago National Referral Hospital in Kampala, Uganda from 2017-2020. Written informed consent was obtained from next-of-kin for conducting an autopsy study. Antiretroviral therapy (ART) history, including recent medication adherence was extracted from medical charts and from interviews with caretakers. Autopsies were performed shortly after consent and time of death (typically within 24 hours). During autopsies, approximately 1-2 g tissue sections from various organs and anatomical sites (including vagina, cervix, uterus, and ovary) were collected and immediately snap-frozen in liquid nitrogen or dry ice/ethanol bath. Whole blood from the femoral vein was collected into EDTA vacutainers and spun at 2400-3000 rpm at 4˚C for 10 minutes to separate plasma. Tissue and plasma specimens were transferred via liquid nitrogen to -80˚C freezers prior to analysis. The study protocol was approved by the Research Ethics Review Committee at Mulago National Referral Hospital.

3.2.2 Sample processing and quantification of anti-infective concentrations

Plasma and tissue concentrations of tenofovir, lamivudine and fluconazole were quantified simultaneously, while efavirenz was quantified separately from the other three drugs due to different polarity. The following assay procedure descriptions only focuses on FGT assay, as assays for plasma samples were conducted by the Clinical Pharmacology Analytical Services (CPAS) lab (University of Minnesota, Minneapolis, USA) as described in Chapter 2 and a previously published paper [60]. The assays for the FGT samples were adapted from the plasma assay and conducted at the Center for Orphan Drug Research (CODR) (University of Minnesota, Minneapolis, USA). A three-day accuracy & precision validation was conducted to validate and establish the assay for FGT samples in the CODR lab.

The preparation of blank FGT tissue lysate, and processing of QC samples, calibration standard samples and participant samples are as follow:

Blank FGT tissue lysate: cervical and vaginal tissues used to prepare QC and calibration standard samples were collected at University of Minnesota Biological Materials Procurement Network (BioNet, Minneapolis, Minnesota, USA) from HIV negative patients undergoing gynecologic surgery. The patients did not take any of the study drugs before surgery. Tissue samples were homogenized and mixed with phosphate-buffered saline (PBS) at a 1:2 volume ratio (e.g., 0.5 g tissue + 1 mL PBS). The mixture was centrifuged at 4696 g for 15 min and supernatant collected and used for QC and calibration standard samples.

Calibration standard samples: 200 μL of the mixture of the standard stocks of tenofovir, lamivudine, fluconazole and efavirenz were spiked with 20 μL of the 4-Mix IS

and diluted with blank tissue lysate to form a series of final concentrations of 0, 50, 100, 250, 500, 1000, 2500, 5000, 10000 ng/mL. For each run batch, the calibration standard samples were run in triplicates for each concentration level.

QC samples: QC stocks were prepared from separate standard stocks from the calibration standard stocks and were in bulk amounts (at least 15 mL for each concentration level) for four concentration levels, 50, 200, 800 and 4000 ng/mL by diluting the mixed standards of tenofovir, lamivudine, fluconazole and efavirenz with blank tissue lysate. For each QC sample, 200 μL of the QC stock was spiked with 20 μL of a mixture internal standard (IS) of tenofovir-d6, lamivudine-$^{13}C_1$, d2, efavirenz-d4 and fluconazole-d4 (referred to as 4-Mix IS). For the accuracy & precision validation assay, QC samples were run in five replicates for each concentration. For the runs for study samples, each QC concentration level were run in duplicates.

Participant FGT samples: for each female genital specimen (i.e., ovarian, uterine, cervical, and vaginal tissue), 0.3 g of tissue was weighed, cut into small pieces, and homogenized in 0.6 mL phosphate buffered saline (PBS) with a portable rotor stator (Omni TH). Two hundred microliters of supernatant were collected after centrifuging the homogenate at 4696 g for 15 minutes, then spiked with 20 μL of the 4-Mix IS.

Following the preparation of the QC, calibration standard and participant samples described as above, protein was then precipitated by adding 800 μL ice-cold acetonitrile and the supernant removed after centrifugation at 15000 g for 15 minutes. The supernatant was then condensed under a nitrogen flow, followed by reconstitution with mobile phase and injection (volume of 20 μL/sample) for liquid chromatography – tandem mass spectrometry (LC-MS/MS) assay.

The simultaneous detection and quantification of tenofovir, lamivudine, and fluconazole in FGTs were performed using an Ultra Performance Liquid Chromatography (UPLC) (Thermo Scientific) coupled with a TSQ Quantum triple stage quadrupole mass spectrometer (Thermo-Electron, San Jose, CA) (LC-MS/MS). The chromatographic separation was performed with a ACQUITY UPLC HSS T3 (2.1 x 50 mm), reversed phase column with a 1.8-micron particle size. The mobile phase used for the gradient elution consisted of (A) 0.1% formic acid in DI water (B) 0.1% formic acid in acetonitrile. The chromatographic conditions were isocratic from 0 to 1.50 min at 0% B, followed by a linear gradient at 1.5 to 2.75 min of 0% - 45% B and return to the starting conditions (at 3.0 min) with a flow rate of 0.3 mL/min, for a total run time of 6 minutes. The column temperature was maintained at 30°C. The detector settings of the mass spectrometer were: ESI with the stainless-steel spray needle, positive polarity ionization, multiple reaction monitoring mode (MRM). The ion transitions were as follows: 288 to 176 for tenofovir, 230 to 112 for lamivudine, and 307 to 238 for fluconazole.

Chromatographic separation of efavirenz was performed with an ACQUITY UPLC BEH C18 (2.1 × 50 mm), reversed phase column with a 1.7-micron particle size (Waters, Milford MA), on the same LC-MS/MS system mentioned above. The mobile phase used is a mixture of 10 mM ammonium acetate in water, pH 6.8 (30%) and acetonitrile (70%) with an isocratic elution flow rate of 0.25 mL/min and total run time of 2 minutes. The column temperature is maintained at 30°C. The detector settings of the mass spectrometer were: ESI with the stainless-steel spray needle, negative polarity

ionization, selective reaction monitoring mode (SRM). The ion transition was 314 to 244 for efavirenz.

The acceptance criteria for calibration curves was: in each run, the calibrator at lower limit of quantification (LLOQ) was ± 20%, and other non-zero calibrators were ± 15% of nominal concentrations [134]. The acceptance criteria for QC samples was: ≥ 67% of QCs should be ± 15% of the nominal, and ⩾ 50% of QCs per level should be ± 15% of their nominal [134]. In the three-day accuracy & precision assay, all calibration curves had $R^2 > 0.999$ and all calibrators met the acceptance criteria; all QC samples met the acceptance criteria, except the lamivudine QCs for LLOQ in the 3rd accuracy & precision assay, for which two samples out of five were ± 20% of nominal concentration, which was considered as a minor violation of criteria but did not affect the overall assay performance. For the runs for study samples, all QC samples met the criteria; all the efavirenz calibration standard samples met the criteria, while the other three drugs had two samples of the 50 ng/mL (LLOQ) failed the ± 20% criteria on two separate runs.

3.2.3 Statistical analysis

The penetration metric was defined as the ratio between tissue and plasma concentration (tissue-to-plasma ratio, or TPR). TPR was used rather than raw concentration as there was expected variability in concentrations due to the variation in time since last dose and, in the case of fluconazole, variable dosages. Median (Interquartile Range (IQR)) were given as the summary statistics for concentrations and TPRs of tenofovir, lamivudine, efavirenz, and fluconazole in each tissue compartment. Friedman test (non-parametric analysis for repeated measures) was used for the global

comparisons of difference among the four FGT compartments and the paired Wilcoxon test was used for comparisons between other three FGT compartments with the cervical compartment, as it was the most common tissue compartment measured and has been used to broadly refer to FGT in previous studies.[78, 83-85] Pearson correlation coefficients (r) and the corresponding p-values were used to show the correlation between plasma concentration and tissue concentration. The potential of postmortem redistribution was measured with linear regression of the relationship between TPR and postmortem interval.

3.3 Results

3.3.1 Participant demographics

Postmortem tissues were sampled from 27 female Ugandan participants living with HIV/AIDs at time of death. Demographic characteristics of deceased participants can be seen in Table 3-1. The majority of study participants were young to middle-age. Twenty-two participants were receiving ART at time of death and 13 were receiving fluconazole for the treatment of cryptococcal meningitis. Of the 21 participants with available dosing history, all had received ART for at least 7 days prior to time of death and 67% were said to be adherent to their ART. The most common ART regimen prescribed was tenofovir disoproxil fumarate/lamivudine/efavirenz (44.4%). The most common causes of death are cryptococcal meningitis and TB. Other causes included various types of cancer, anemia, respiratory failure, heart failure, etc. Tissue concentrations were only reported for those with detectable corresponding plasma concentrations.

3.3.2 Exposure of anti-infective drugs in the FGT

The median concentration of tenofovir was highest in vaginal tissue across the four FGT compartments (i.e., vaginal, cervical, uterine, ovarian), and median vaginal concentrations were 64% higher than the cervical (p=0.03) (Figure 3-1A). When normalizing for plasma, the TPR of tenofovir in vaginal tissue was greater than ovarian, uterine, and cervical tissues as well (Table 3-2). More than 50% of participants attained TPR>1 in all four FGT compartments with the highest proportion of TPR > 1 being vaginal tissue (Table 3-3).

Similarly, vaginal concentrations of lamivudine were higher than the other FGT compartments and median vaginal concentrations were 50% higher than the cervical concentrations (p=0.0003) (Figure 3-1B). TPRs of lamivudine were greater in vaginal tissue when compared to the other three tissue compartments (Table 3-2). More than 50% of participants attained TPR>1 in all four FGT compartments, with vaginal tissue again having the highest proportion of participants with TPR > 1 (Table 3-3).

Median concentration of efavirenz was highest in ovarian tissue, and concentrations in ovarian, vaginal, and uterine tissues were all significantly higher than in cervical tissue by 82% (p= 0.01), 37% (p< 0.01) and 33% (p=0.03), respectively (Figure 3-1C). TPRs of efavirenz demonstrated the same relationships among the four FGTs as concentration (Table 3-2). All the four FGT compartments had less than 50% participant samples attaining TPR>1. Ovarian tissue had the highest TPR>1 proportion than the other FGTs (Table 3-3).

While the median concentration of fluconazole was highest in the ovarian tissue, only vaginal concentrations were statistically higher (22%) than cervical concentrations

(p=0.02) (Figure 3-1D). TPRs of fluconazole in the four FGT compartments were comparable, with the highest median being in vaginal tissue (Table 3-2). Vaginal TPRs were significantly higher than the cervical (p=0.02). The proportion of participants attaining TPR>1 was less than 50% in any of the four FGT compartments, with vaginal tissue having the highest proportion (Table 3-3).

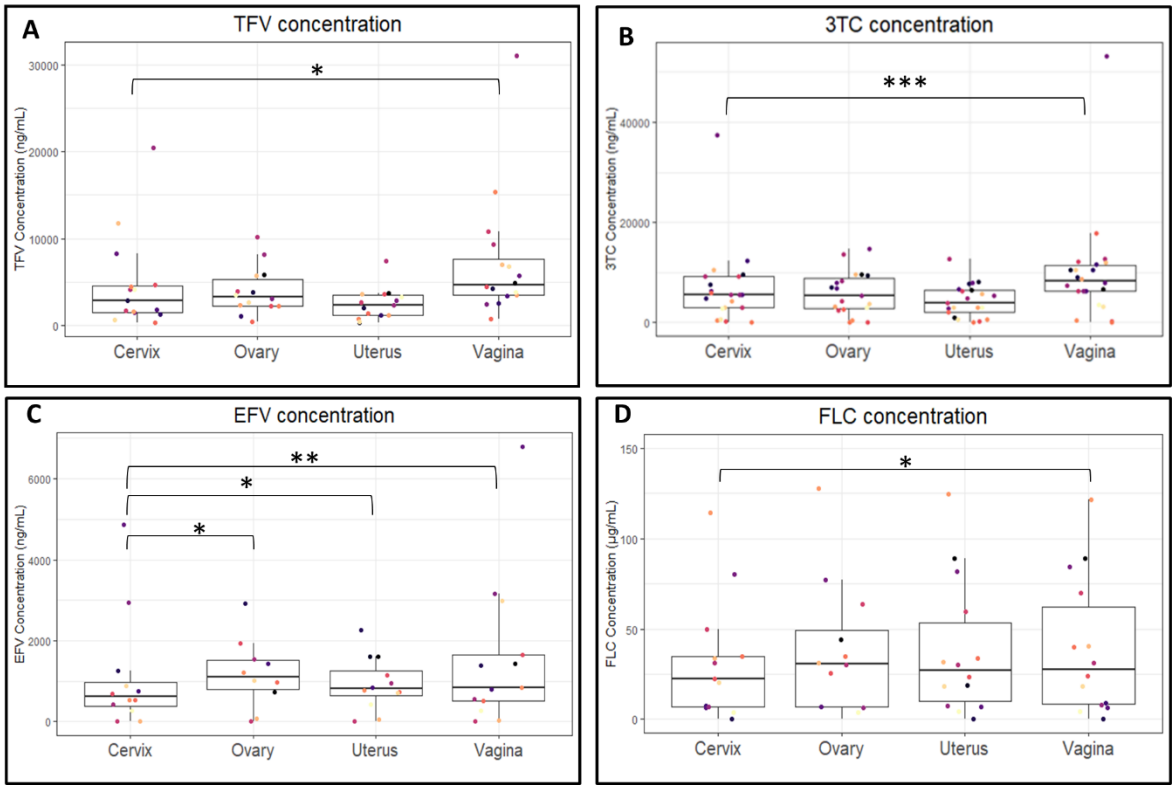

Figure 3-1 Concentrations of tenofovir (A), lamivudine (B), efavirenz (C) and fluconazole (D) in ovarian, uterine, cervical, and vaginal tissue. In each plot, points with the same color represent the same individual. Note: p<0.05-- *; p<0.01-- **; p<0.005-- ***. Abbreviations: TFV—tenofovir; 3TC—lamivudine; EFV—efavirenz; FLC—fluconazole.

Table 3-1 Demographic characteristics and medication use.

Characteristic	Median (IQR)
Age (years)	34 (26–45)
Height (cm)	161 (156–163)
Most recent CD4+ T cell count (cells/mm^3)[a]	23 (5–112)
eGFR (mL/min/1.73 m^2)	14 (9–32)
Time on current ART regimen (days)	200 (42–558)
Time on fluconazole regimen (days)	7.5 (3–15)
Most recent viral load (copies/mL)[b]	Undetectable–1,100,000
Time since last antiretroviral dose prior death (h)[c]	20.2 (13.6–42.4)
Time since last fluconazole dose prior to death (h)	18.9 (10.9–24.8)
Post-mortem interval (h)	7.5 (5.2–12.2)
Characteristic	*N*=27
Cryptococcal meningitis, *n* (%)	12 (44.4)
TB, *n* (%)	12 (44.4)
Antiretrovirals, *n* (%)	
Tenofovir disoproxil fumarate	17 (63.0)
Lamivudine	21 (77.8)
Efavirenz	11 (40.7)
Dolutegravir	7 (25.9)
Nevirapine	3 (11.1)
Abacavir	2 (7.4)

Zidovudine	2 (7.4)
Fluconazole	15 (55.6)
200 mg, *n*	3
400 mg, *n*	1
800 mg, *n*	2
1200 mg, *n*	5
Unknown, *n*	4

[a]Time interval between death and the most recent CD4+ T cell counts ranged from 2 days to 6.9 years.
[b]Most recent viral load is shown as range for seven participants. Time interval between death and the most recent viral load ranged from 11 days to 783 days.
[c]Time of last ART dose was provided by next of kin or taken from medical records.

Table 3-2 TPRs in ovarian, uterine, cervical and vaginal tissue.

Drug	Cervix TPR			Ovary TPR			Uterus TPR			Vagina TPR		
	Median (IQR)	*n*	*P*	Median (IQR)	*n*	*P*	Median (IQR)	*n*	*P*	Median (IQR)	*n*	*P*
Tenofovir	1.22 (0.77–1.96)	15	ref	1.21 (0.88–1.89)	14	0.95	1.14 (0.65–2.91)	15	0.41	1.86 (1.31–5.54)	16	**0.03**
Lamivudine	1.24 (0.98–1.67)	21	ref	1.34 (0.97–1.72)	19	0.81	1.05 (0.94–1.63)	21	0.36	1.83 (1.11–2.92)	22	**0.001**
Efavirenz	0.51 (0.22–0.82)	12	ref	0.65 (0.24–1.23)	10	**0.01**	0.51 (0.35–0.88)	12	**0.04**	0.59 (0.28–0.7)	13	**0.02**
Fluconazole	0.92 (0.90–0.96)	13	ref	0.85 (0.64–0.94)	12	1	0.89 (0.86–0.94)	14	0.69	0.94 (0.87–1.10)	14	**0.017**

Values of *n* are the sample size and *P* values are from the Wilcoxon test between the other FGT tissues and the cervical tissue (indicated as ‘ref’).

Table 3-3 The proportion of TPR greater than 1 by tissue and drug.

Tissue	Tenofovir		Lamivudine		Fluconazole		Efavirenz	
	n	TPR>1 (%)	*n*	TPR>1 (%)	*n*	TPR>1 (%)	*n*	TPR>1 (%)
Ovary	14	71	19	68	12	17	10	40
Uterus	15	60	21	57	14	14	12	8
Cervix	15	60	21	71	13	15	12	25
Vagina	16	88	22	86	14	43	13	23
% of TPR>1 in all tested tissue samples		70		71		23		23
% of participants with at least 1 tissue with TPR>1		100		91		43		29

3.3.3 Correlation between plasma and tissue concentration

Figure 3-2 shows the correlation between plasma and tissue concentration. Tenofovir concentrations in plasma were not correlated with any FGT compartment. Plasma concentration of lamivudine and efavirenz were only significantly correlated with uterine concentration ($r=0.68$, $p<0.001$ and $r=0.6$, $p=0.4$, respectively). Fluconazole plasma concentrations were significantly correlated with fluconazole in all tissue compartments (ovarian: $r=0.9$, $p<0.001$; uterine: $r=0.93$, $p<0.001$; cervical: $r=0.91$, $p=0.03$; vaginal: $r=0.91$, $p<0.001$).

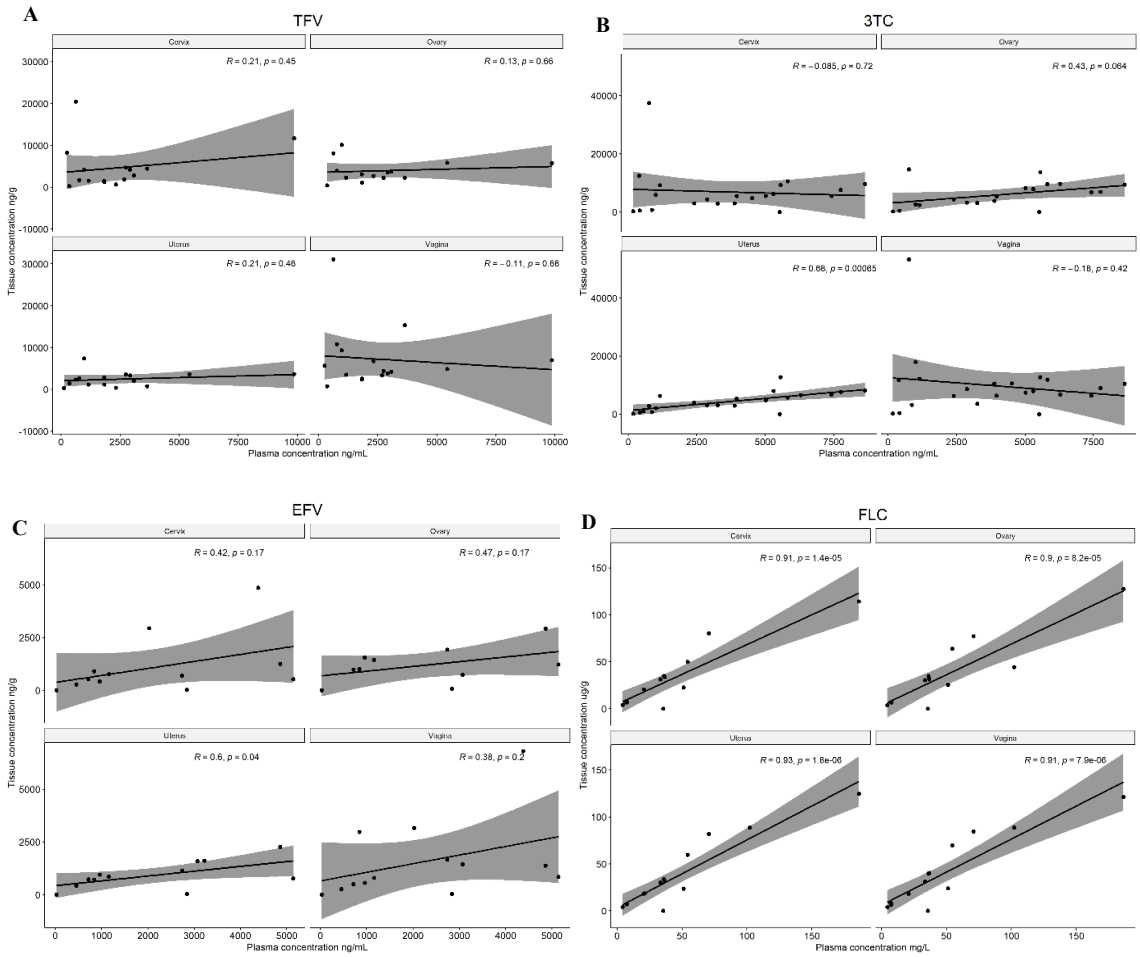

Figure 3-2 Correlations between plasma concentration and tissue concentration for tenofovir (A), lamivudine (B), efavirenz (C) and fluconazole (D) in four FGT compartments. The solid black line is the best fit line. The shaded area surrounding the best fit line is the 95% confidence interval. Pearson correlation coefficients and corresponding p-values are shown in plots. Abbreviations: TFV—tenofovir; 3TC—lamivudine; EFV—efavirenz; FLC—fluconazole.

3.3.4 Impact of postmortem redistribution

To examine the impact of postmortem redistribution, we explored the relationship between TPR and post-mortem intervals (Figure 3-3). Postmortem interval was not significant as a predictor for TPR in any of the models for tenofovir, lamivudine, efavirenz or fluconazole in any of the FGT tissue compartments ($p > 0.05$), apart from lamivudine in uterine tissue where longer time to postmortem was associated with increased TPR ($p=0.036$, slope coefficient=0.066, suggesting an 0.066 increase in TPR every hour postmortem).

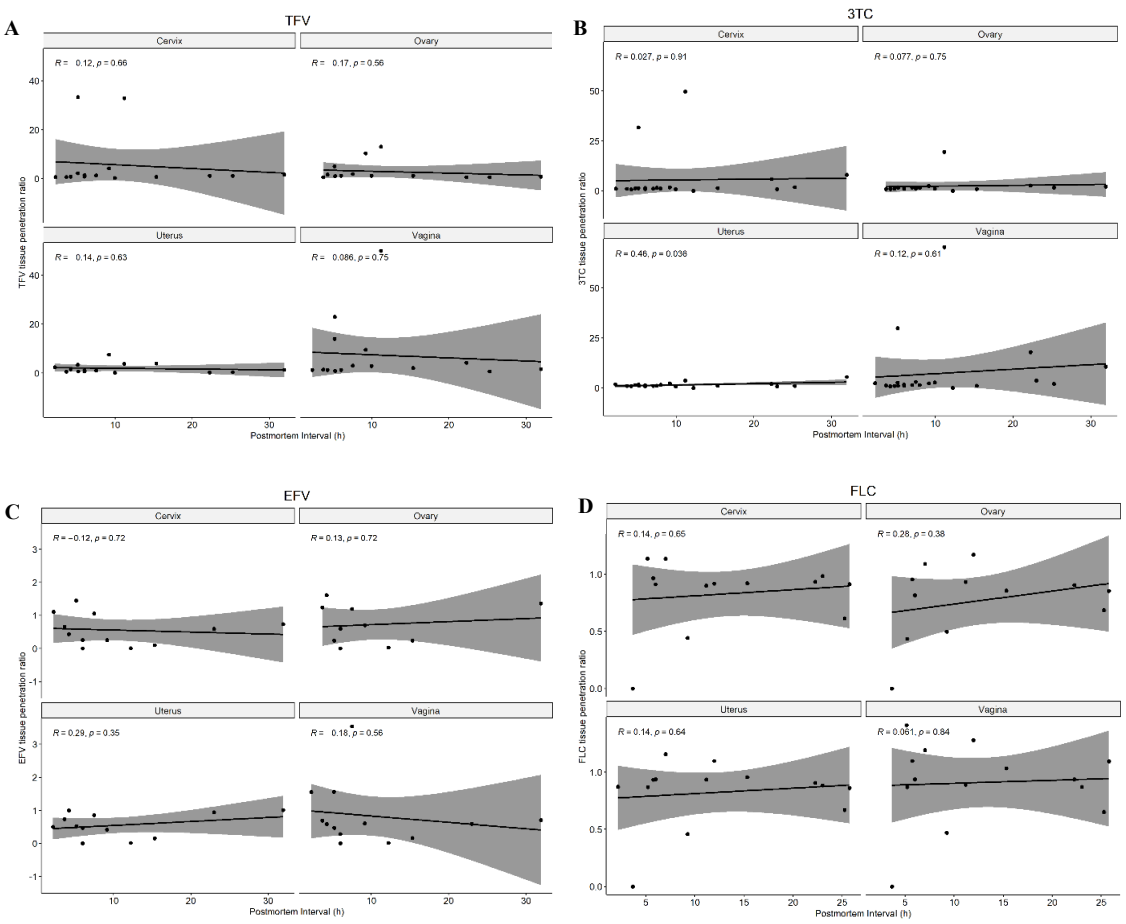

Figure 3-3 Tissue-to-plasma ratios against postmortem interval for tenofovir (A), lamivudine (B), efavirenz (C) and fluconazole (D) in four FGT compartments. The solid black line is the best fit line. The shaded area surrounding the best fit line is the 95% confidence interval. Pearson correlation coefficients and corresponding p-values are shown in plots. Abbreviations: TFV—tenofovir; 3TC—lamivudine; EFV—efavirenz; FLC—fluconazole.

3.4 Discussion

In this study, we simultaneously measured the concentration of two commonly prescribed NRTIs, tenofovir and lamivudine, and an NNRTI, efavirenz, in addition to the antifungal fluconazole, in postmortem tissues of the reproductive tracts of Ugandan women living with HIV/AIDs prior to death. We normalized data to plasma to understand the relative penetration into the FGT compartments. Our major findings were: (1) penetration ratios of the four drugs were different among the ovarian, uterine, cervical, and vaginal tissues, thus, cervical tissue may not be an adequate representative for the entire FGT; (2) penetration ratios of tenofovir and lamivudine in female genital tissues were >1 for most participants, but not for efavirenz and fluconazole.

Several studies have measured tenofovir exposure in cervical or vaginal biopsies from healthy, non-pregnant women without HIV infection, and results are very variable given different study designs.[77, 78, 81, 82] In a 2021 study conducted by Thurman and colleagues, at 24 hours after a 14-day multiple dose period, tenofovir concentrations (medians 56 ng/mL for blood, 52.8 ng/g for cervical tissue and 63.1 ng/g for vaginal tissue) were more than 50-fold less than what we measured,[81] but both are notably similar to plasma as we reported. Hendrix *et al*. measured tenofovir concentration in vaginal biopsy of HIV-uninfected women who took oral TDF daily for 6 weeks.[82] However, TFV concentration of half of the vaginal biopsy samples were lower than the lower limit of quantification of that particular assay, such that a measure of tissue penetration compared to blood is not accessible.[82] There are other studies including that which was conducted by Thurman *et al*., which measured tenofovir in cervical/vaginal biopsies after a single

oral dose of tenofovir disoproxil fumarate, but they are not discussed here or comparable to our results as our participants were considered to be at steady state.[77, 78, 81] Data on lamivudine exposure in the FGT at steady state is even more scarce. Herrera and colleagues measured exposure of lamivudine in vaginal tissues of 18 healthy, non-HIV participants during and after they took the combination of lamivudine and raltegravir for 7 days, and the average lamivudine TPR was 8, which is higher than what we found (median 1.86).[80]

So far, only two studies have measured tenofovir or lamivudine in upper reproductive tissues. Rahangdale *et al*. measured tenofovir in endometrial tissues of non-pregnant women living with HIV and reported values ~ 1% (median 26 ng/g) of what we measured in the uterine tissues (median 2356.6 ng/g).[85] In addition, Yeh *et al*. measured ART concentrations in amniotic fluid of women living with HIV during delivery however, the sample size was small (n=1 for tenofovir, n=6 for lamivudine).[135] The concentrations of tenofovir and lamivudine in amniotic fluid were one-third and one-fourth of the median tenofovir and lamivudine concentrations of uterine tissues in our study but comparisons are challenging given the small sample size in this group, and the different tissue compartment/matrix sampled.[135]

Before our current study, efavirenz concentration has only been measured in cervicovaginal fluid as representative of its exposure in FGT by Kwara *et al*. and Dumond *et al*.[83, 84] Both studies measured efavirenz concentration in paired cervicovaginal fluid and blood plasma samples at steady state of women who were living with HIV.[83, 84] In the study by Kwara *et al*., the mean of cervicovaginal fluid-to-plasma ratio was 0.01 for both samples taken at before and 3-4 hours after administration.[83]

Dumond *et al*. had more intensive sampling and derived the penetration (i.e. cervicovaginal fluid-to-plasma ratio) with AUCs of efavirenz concentration in cervicovaginal fluid and blood plasma, and the median ratio was 0.004.[84] Since different biomatrix was used in our study for FGT, the results are not directly comparable, but the relationship of FGT penetration of efavirenz compared to the NRTIs are similar (i.e., penetration of efavirenz at FGT is less than tenofovir and lamivudine).[83, 84]

Exposure of fluconazole in lower FGT from two previous studies by Mikamo *et al*. and Houang *et al*. are lower than what we reported; however, these were both single-dose studies using a dose lower than any used in our cohort.[132, 133] The two studies investigated the pharmacokinetics of fluconazole after a single oral dose of 150 mg for treatment of vaginal candidiasis, where the peak concentrations in vaginal tissue were estimated as 3.8[132] and 2.4 μg/g,[133] respectively. Meanwhile, Mikamo *et al*. is the only study published to date that has measured fluconazole exposure in the upper FGT [132] (i.e., the uterus, endometrium, oviduct and ovary), with estimated Cmax as 4, 4.1, 4.5 and 3.9 μg/g, respectively, following a 150 mg dose. The exposure of fluconazole in FGT was reported by Mikamo *et al*. to be similar as compared to the serum, which implies a tissue-to-plasma ratio of about 1, similar to our findings. Most importantly, these exposures are considered optimal as minimum inhibitory concentrations (MICs) of fluconazole for *C. albicans* are within 0.4 to 0.8 mg/L.[133]

Aside from different biologic sample matrices and varying study design, there are other possible explanations for the high drug concentrations in plasma and FGT tissues in our study. As all our participants were hospitalized and critically ill at time of death, multi-organ dysfunction would not be unexpected. Consequently, the pharmacokinetics

of drugs may have been affected as a collective result of altered absorption, distribution, elimination, and excretion under a critically ill status. For instance, change of gastrointestinal function and hypoperfusion of vital organs reduces absorption and albumin escape increases the free drug portion that is subject to greater distribution and clearance. However, it is worth noting that tenofovir, lamivudine, and fluconazole have relatively low protein binding, which implies that decreased albumin should only minimally affect their free drug portion available for elimination. Hepatic and renal failure usually results in a reduced metabolic capacity and excretion.[136] The majority of participants in our study had an eGFR less than 60 mL/min/1.73 m^3, which indicates a degree of renal impairment and is presumably a contributing factor of the high concentrations of tenofovir, lamivudine, and fluconazole, as all three are primarily renal excreted, whereas efavirenz concentrations in our study were more similar to those observed clinically. Moreover, tissue concentration after death may change due to postmortem redistribution, under mechanisms including cell death, ongoing blood movement, passive diffusion along a concentration gradient and putrefaction,[86] but the exact "necrokinetics" are still unclear. Commonly proposed properties that make a drug to be subject to postmortem redistribution include having a volume of distribution (V_d) greater than 3 L/kg and being lipophilic and basic.[86, 137] Tenofovir, lamivudine, and fluconazole have V_d of less than 3 L/kg and relatively small Log P; however, lamivudine and fluconazole are weak bases, which may lead to postmortem redistribution. On contrary, efavirenz is lipophilic and has rather high V_d. Nonetheless, for the fact that we conducted most of our autopsy within 24 hours post-death (median 7.5 hours), and all but

one TPRs were not significantly associated with postmortem interval, thus, we believe postmortem redistribution is not particularly worrisome in this case.

Optimal penetration of antiretrovirals is important when used as prevention to protect women from new infection and viral replication, but it is also critical in women living with HIV to minimize viral shedding and help protect their sexual partners. Female genital shedding of HIV has been shown in previous studies to be correlated with plasma viral load and is reduced by ART.[138-140] Furthermore, Kourtis *et al*. [141] found that higher efavirenz concentration in plasma was associated with lower risk of HIV genital shedding (however, the association was not significant for efavirenz concentration in cervicovaginal fluid and genital shedding). Though the relationship between systemic or local exposure of other antiretrovirals and genital viral shedding remains unexplored, we would reasonably assume that an optimal systemic/local exposure will suppress viral shedding and viral reservoir at the transmission site. We would also generally assume that when antiretrovirals are used as pre-exposure prophylaxis (PrEP), an optimal exposure in female genital tissues is critical in prevention of HIV acquisition from sexual transmission. This assumption is supported, for example, by the CAPRISA (i.e., Centre for the AIDS Program of Research in South Africa) 004 trial which is a randomized clinical trial accessing the effectiveness and safety of a 1% vaginal gel formulation of tenofovir, and suggests higher tenofovir concentration in the cervicovaginal fluid provides better protection against HIV infection.[142] Generally, for tenofovir and lamivudine, most of our study participants had tissue concentrations in FGTs close to or higher than the plasma concentrations, implying an optimal penetration for the antiviral effect; the highest penetration in vaginal tissue implies better protection at the common

inter-sex transmission site. However, effectiveness of oral tenofovir-based PrEP for cisgender women reported by clinical trials are inconsistent. For instance, the effectiveness for women in the serodiscordant couples (Partners PrEP (i.e., PrEP for the prevention of HIV-1 acquisition among East African heterosexual men and women in HIV-1 serodiscordant partnerships): 62% protection with TDF alone and 73% protection with TDF/FTC [71]) are much higher than other cisgender women groups (FEM-PrEP (Preexposure Prophylaxis Trial for HIV Prevention among African Women) [72] and VOICE (i.e., Vaginal and Oral Interventions to Control the Epidemic) trial[73]: discontinued for futility), likely confounded by non-adherence.[76] Therefore, further studies of exposure-efficacy relationship are needed and so are more alternative PrEP options for women.

There are several limitations to our study. First, we only measured total drug concentrations in tissues, which are inevitably higher than the free drug concentrations. For tenofovir and lamivudine attainment of expected therapeutic effect depends on the free drug portion that can diffuse into infected $CD4^+$ T-cells. Tenofovir and lamivudine are known to be 99% and 36% binding to plasma protein. As there are multiple binding components in tissues, such as phospholipids, interstitial albumin and lipoproteins,[143] the free drug concentrations are expected to be lower than the total concentration we measured. Second, estimation of AUC of penetration ratios, which may be a more relevant measure of relative penetration, was not possible due to the nature of using postmortem samples with limited sampling times available. Third, so far, target concentrations or cutoff values for TPR for these antiretrovirals has not been established to relate to efficacy of HIV suppression or prevention. Thus, a cutoff of 1 was chosen as

it could be intuitively interpreted as the “penetrating ability” based on the concentration in the circulating system. Finally, there were several outliers who had extremely high FGT concentrations. It could reflect the nature of post-mortem sampling such as the high variability in patient deterioration in their hospital course before death, variable dosing before death, and variable post-mortem storage conditions.

In conclusion, the current study measured concentrations and determined penetration ratios of tenofovir, lamivudine, efavirenz and fluconazole in postmortem ovarian, uterine, cervical, and vaginal tissues from a population of Ugandan women previously living with HIV/AIDs. The postmortem analysis provides a unique opportunity to evaluate antiretroviral exposure in submucosal tissues. At steady state, tenofovir and lamivudine had better penetration at the solid tissue compartments of the FGT, while penetration of efavirenz was relatively poorer. Fluconazole exposure was consistently less than plasma but still expected to reach FGT tissues in concentrations adequate to treat target pathogens. In addition, although it is often used as a FGT surrogate, we found that cervical tissue may not be able to represent the entire FGT when measuring penetration of anti-infective drugs.

CHAPTER 4 Characterizing Postmortem redistribution of Tenofovir, Lamivudine and Efavirenz in a Mouse Model

4.1 Introduction

In previous chapters, penetration of multiple antiretroviral drugs and an antifungal in human female genital tissues and/or brain tissues were explored with postmortem human tissues. Despite the convenience to assume human body is at static state after death, chemical and biological activities still go on postmortem, such as passive diffusion, blood movement, and putrefaction [86]. These activities become the driving forces of postmortem redistribution, referring to the process by which drugs or other substances in the body may move from one tissue to another or within tissues after death. A long list of substances has been reported to subject to postmortem redistribution by forensic toxicologists [116, 137, 144]. Substances included in the list are usually antidepressants, antipsychotics, benzodiazepines, cardiovascular drugs, amphetamines and opioids. To avoid the impact of postmortem redistribution, the protocol of our autopsy studies limited the time of autopsy sampling within 24 hours after death. Nonetheless, studies show that for some substances redistribution occurred in early-stage postmortem (range from 4.5- to 74- hour postmortem [145, 146]). In addition, postmortem distribution of antiretroviral (ARV) drugs is unknown since it has never been previously described in humans or animals. Substances with volume of distribution larger than 3 L/kg, that are lipophilic, and/or organic base have greater potential to undergo postmortem redistribution [86]. Based on these properties, among the ARVs we have

studied in previous postmortem analysis, lamivudine (pKa 14.3) and efavirenz (pKa 12.5 and Vd 4.5 L/kg) may subject to postmortem redistribution.

In this study, we used a mice model to quantitatively and qualitatively evaluate the postmortem redistribution of three ARVs (tenofovir, lamivudine and efavirenz) by comparing drug concentrations at a series of postmortem time points to concentrations at the time of death. In addition, the potential site-dependent postmortem redistribution [146] was also explored by investigating both brain and liver. We hypothesized that postmortem redistribution is different in these two tissues, since they are largely different in structure and composition (e.g., brain has 60% lipid content vs. 5-15% in liver; liver is highly blood perfused while the blood-brain-barrier reduced the perfusion of substances in blood into brain parenchyma).

4.2 Methods

4.2.1 Animal and study design

Animal experiments were conducted under approved protocol by the Virginia Commonwealth University institutional animal care and use committee (IACUC). ICR (Institute of Cancer Research) mice (Envigo, Dublin, VA, USA) were administered a daily intra-peritoneal injection at a dose of 60 mg/kg tenofovir disoproxil fumarate, 60 mg/kg lamivudine and 30 mg/kg efavirenz for 5 consecutive days. On the 5^{th} day of administration, all mice were sacrificed by cervical dislocation 2 hours after the last intra-peritoneal injection. Brain and liver of 30 mice (29 female and 1 male) were harvested in groups of 6 at right after sacrifice (0 hour), 2-, 6-, 12- and 24 hours post-sacrifice, which are the five postmortem time groups. We were only able to harvest whole blood samples

from the postmortem time 0 group mice since blood clot occurred soon after death. Plasma was separated from whole blood by EDTA. Samples were snap-frozen immediately after collection and kept in –80°C freezers until sample analysis.

4.2.2 Concentration determination with LC-MS/MS assay

Blood and tissue sample processing and condition settings of the assays for tenofovir, lamivudine and efavirenz were the same as described in section 2.2.3 in chapter 2. The lower limit of quantification (LLOQ) for the three compounds in mice tissues were 40 ng/g tissue. For concentrations below LLOQ (BLQ), the concentrations were assumed to be half of BLQ (20 ng/g tissue).

4.2.3 Data analysis

Tissue-to-plasma ratios (TPRs) were calculated at time 0 to show a relative concentration gradient between tissue and plasma and between tissues. Postmortem redistribution was explored with concentrations of each postmortem time groups. Summary statistics of median and IQR of concentrations at each time points were calculated. Difference among all time groups were tested with one-way ANOVA, and post-hoc comparisons between following postmortem time points (2-, 6-, 12- and 24-hour) and time of death (time 0) were done with t test (with p-value adjustments).

4.3 Results

4.3.1 Tissue penetration of tenofovir, lamivudine and efavirenz in mice brain and liver

Median (IQR) of TPRs for tenofovir, lamivudine and efavirenz in brain and liver are presented in Table 4-1. Efavirenz had the highest penetration (median 1.1) in brain, comparing to only 0.7% tenofovir and 3% lamivudine distributed into brain from plasma. In contrast, TPR of tenofovir was drastically higher in liver (median 36) compared to the other two ARVs (medians: lamivudine, 0.76; efavirenz, 2.4).

Table 4-1 Median (IQR) of tissue penetration ratios of tenofovir, lamivudine and efavirenz in mice brain, and liver (time 0).

	Tenofovir	Lamivudine	Efavirenz
Brain	0.007 (0.027, 0.04)	0.03 (0.027, 0.041)	1.11 (0.95, 1.42)
Liver	36.1 (16.2, 60.5)	0.80 (0.65, 1.00)	2.43 (2.14, 2.74)

4.3.2 Distribution of tenofovir, lamivudine and efavirenz in mice postmortem

Concentrations of the ARVs at time of death and a series of postmortem time points were utilized to investigate the potential of postmortem redistribution. In the brain, over a period of 24-hour postmortem, tenofovir and lamivudine had an overall ascending trend while efavirenz showed a descending trend. In the liver, the overall trend was the same for lamivudine and efavirenz as in brain, but not for tenofovir which decreased at the end (Figure 4-1). Overall, the variations of concentration (within the same time point

group) of the three drugs were large (%CV ranges from 27% for efavirenz in liver to 63% for tenofovir in brain). Notably, fold difference (or rate of change) was profound in the first two hours postmortem. The median (IQR) concentrations for each ARV, and rate of change at the following time points after death comparing to time of death (time 0) are shown in Table 4-2.

Adjusted p-values of comparisons between postmortem time points and the time of death are also shown in Figure 4-1. There is no statistical significance between postmortem time points and time of death for efavirenz in brain and tenofovir in both brain and liver. In contrast, concentration of lamivudine at 24- hour postmortem in both brain and liver were significantly higher than time 0, while concentration of efavirenz at all following postmortem time points were significantly lower than time 0.

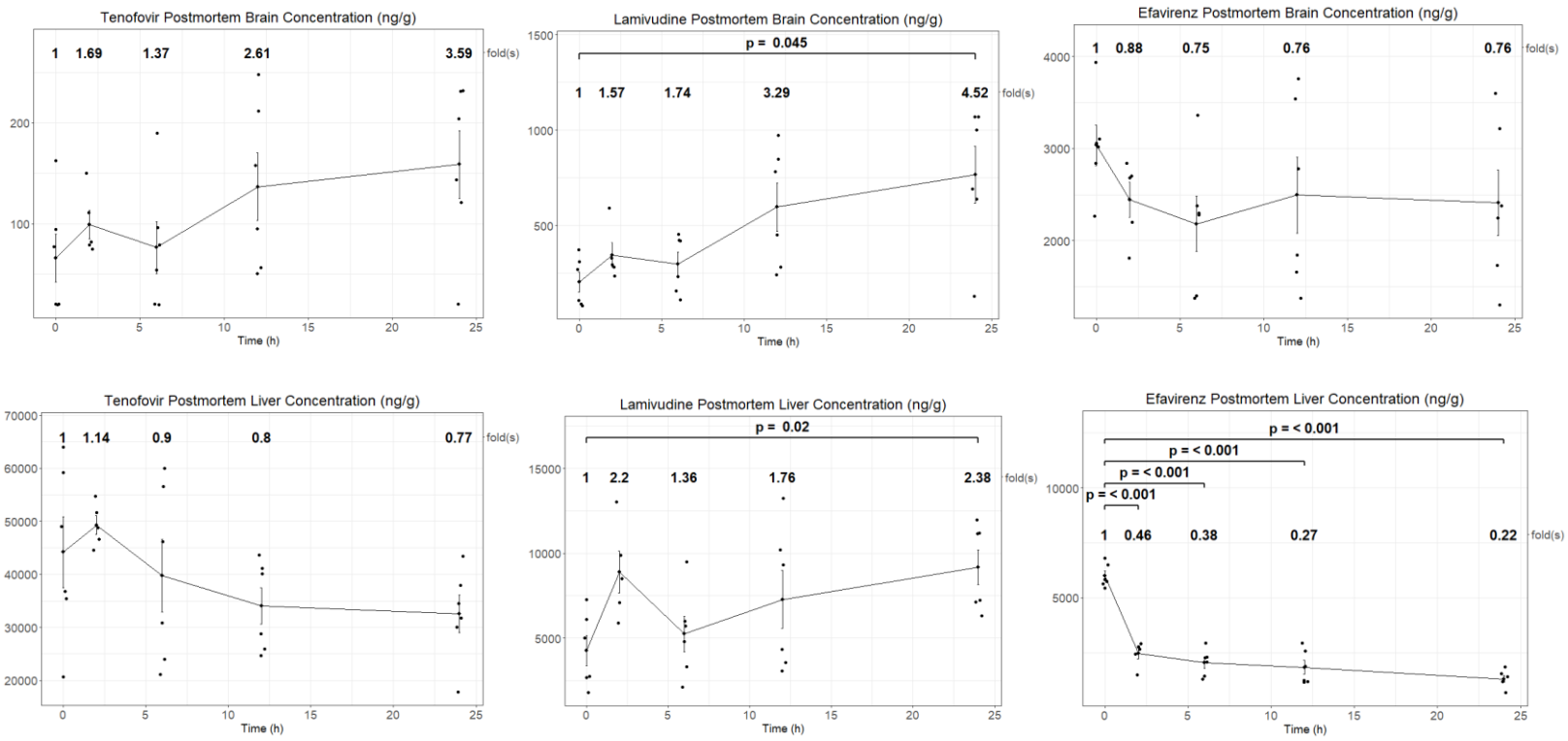

Figure 4-1 Concentrations of tenofovir, lamivudine and efavirenz in mice brain (upper panel) and liver (lower panel) at different time points postmortem. Values above each time point are the fold-change in concentrations from time 0.

Table 4-2 Summary of concentrations at a series of time postmortem in brain and liver. Rate of change is the ratio between median concentration of the four postmortem time points (2-, 6-, 12- and 24- hour) and the median concentration of time at death (time 0).

Postmortem time points, hour	**Tenofovir**		**Lamivudine**		**Efavirenz**	
	Median (IQR), ng/g	**Rate of change**	**Median (IQR), ng/g**	**Rate of change**	**Median (IQR), ng/g**	**Rate of change**
Brain						
0	48 (20, 90)	1.00	187 (92, 300)	1.00	3040 (2885, 3090)	1.00
2	82 (79, 111)	1.69	294 (280, 328)	1.57	2680 (2200, 2700)	0.88
6	66 (28, 92)	1.37	325 (174, 421)	1.74	2290 (1618, 2360)	0.75
12	126 (66, 198)	2.61	616 (324, 832)	3.29	2312 (1706, 3350)	0.76
24	174 (127, 225)	3.59	845 (651, 1051)	4.52	2310 (1856, 3010)	0.76
Liver						

0	42900 (35750, 56650)	1.00	3860 (2675, 5840)	1.00	5780 (5650, 6330)	1.00
2	48800 (46600, 51600)	1.14	8480 (7100, 9880)	2.20	2660 (2440, 2760)	0.46
6	38500 (25700, 54000)	0.90	5250 (3675, 5925)	1.36	2170 (1584, 2295)	0.38
12	34400 (26700, 40900)	0.80	6810 (3750, 9960)	1.76	1566 (1200, 2406)	0.27
24	33100 (30450, 37100)	0.77	9190 (7165, 11185)	2.38	1295 (1185, 1496)	0.22

4.4 Discussion

The overall trends of redistribution for lamivudine and efavirenz kept consistent in brain and liver, however, the directions are different with lamivudine increasing while efavirenz decreasing over the 24-hour postmortem time. Since efavirenz is a substrate of multiple metabolic enzymes including cytochromes P450s (P450s) and UDP-glucuronosyltransferases (UGTs) in human [121, 147] and in mice [148], the decrease concentration over time is likely due to ongoing metabolism in brain and liver, and as liver has more abundant expression [148], the decrease in liver is more profound than in brain. For tenofovir and lamivudine which are mainly eliminated unchanged in urine instead of by metabolic enzymes [149, 150], their direction of redistribution in a certain tissue is more likely driven by the surrounding concentration gradients. Therefore, the overall postmortem increase of lamivudine in brain and liver, and tenofovir in brain indicates lower concentrations/less distribution in the very tissue compared to surrounding tissues. In contrast, the overall decreasing trend of tenofovir concentration in liver could be due to its higher initial concentration at time of death compared to its surroundings, given the high tissue-to-plasma penetration ratio of tenofovir in mice liver, which was much higher than lamivudine.

Notably, the rates of change in the first two hours are more profound than any of the following times for each drug in each tissue compartment, which was possibly due to a transient “living” status of the mice after sacrifice, during which period there was enzyme-mediated metabolism and blood movement still going on. This is also why I did not force straight regression lines across the postmortem concentrations to derive a

postmortem rate of change, in addition to the fact that the tissue concentrations were contributed by different mice, and the change over time may be an artificial effect of between subject variability.

Overall, with the animal study, we confirmed the postmortem redistribution of antiretrovirals in the brain, however, the pattern and extent differed by drug which was likely driven by the physiochemical features of each compound, such as metabolic pathway and lipophilicity [86]. Therefore, in the previous chapter, the concentration of efavirenz we measured in human brain tissues may be underestimated, while the concentration of tenofovir and lamivudine may be overestimated. However, we are not able to apply the results qualitatively for the following reasons.

Of note, postmortem change of the tissue penetration ratios was not available in the animal study due to blood coagulation occurred soon after death. Without a penetration metric, although we have demonstrated drug redistribution in the postmortem brain, we remain uncertain whether or how the postmortem penetration ratios would change. Furthermore, we hesitate to extrapolate the results to human as the quantitative extrapolation would require a good understanding of the "postmortem allometric scaling" between preclinical species and human while postmortem changes are distinct between humans and animals, such as the rate of decomposition [151]. Additionally, disease related factors that confound the drug penetration in humans may not be reflected by the animal model. Besides above mentioned, there are other limitations in current study. First, we did not capture the postmortem change before the 2-hour postmortem time point, however, in retrospect, it is possible that a rapid change occurred earlier than 2-hour. Second, we gave mice ARVs intraperitoneally, which is a different route of

administration from human, as gravity and body position also impacts postmortem redistribution [94], it may lead to different distribution pattern from human.

In conclusion, in this study, we observed potential postmortem redistribution of tenofovir, lamivudine and efavirenz in a mice model, which displayed various trends that differed by drug, tissue and postmortem time point.

CHAPTER 5 Physiologically Based Pharmacokinetic Modeling of Tenofovir and Forgiveness Evaluation of Nonadherence

5.1 Introduction

Human Immunodeficiency Virus (HIV) is huge burden to global health, with an estimated 38.4 million people living with HIV (PWH) by the end of 2021 [1]. To prevent further infection and control the spread of the pandemic, people at risk of HIV infection are recommended to take pre-exposure prophylaxis (PrEP) [2]. Tenofovir is a nucleotide reverse transcriptase inhibitor (NRTI) widely prescribed as the backbone of antiretroviral therapy and one important component of two PrEP regimens [2-6]. Tenofovir disoproxil fumarate (TDF) is the ester prodrug formulated to increase the oral bioavailability of tenofovir. TDF undergoes rapid hydrolysis by esterase extensively existing in the human body and releases tenofovir [7]. Once inside the cell, tenofovir undergoes two steps of phosphorylation to form the active metabolite tenofovir diphosphate (TFVdp) which competes with the natural nucleotides and terminates the replication of HIV [7]. Compared to men who have sex with men (MSM) and transgender women, effectiveness of PrEP for heterosexual women is lower, which is largely attributed to poor adherence [8]. Besides, the relatively low exposure of TFVdp at the site of infection for women compared to MSM and transgender women is another possible reason for lower efficacy of PrEP [9, 10]. Although nonadherence is prevalent and inevitable for the oral daily PrEP [11, 12], it still showed protection for people at risk of HIV infection even in the presence of nonadherence [12]. In essence, what matters in HIV prevention is the drug exposure at the time of HIV exposure. In other words, even if PrEP users do not take their medication every day, as long as the concentrations of TFV or TFVdp at the transmission site and circulatory system are optimal, they are still protected from HIV. For

instance, in a study of PrEP in an MSM and transgender women group, a TFVdp concentration of 700 fmol/punch from dry blood spot was identified to be associated with high efficacy; a following dose-frequency-ranging study in healthy volunteers (participants received 33%, 67%, and 100% of daily dosing) found that the target TFVdp plasma concentration of 700 fmol/punch could be achieved with only 2-3 doses per week in individuals less than 110 kg. Some modeling efforts have been made to identify tenofovir target concentrations in plasma with clinical pharmacokinetic (PK)/pharmacodynamic (PD) data [12, 13]. However, there has not been a clinical study linked the PD (HIV prevention) given nonadherence and the PK at transmission site for cisgender women (concentration of TFVdp at FGT).

Physiologically based pharmacokinetic (PBPK) modeling is a computational modeling approach applied to aid and facilitate drug research and development. A PBPK model combines the physicochemical features of the drug and physiological properties of the population of interest, to simulate possible pharmacokinetic (PK) profiles of the target population. The simulations could inform formulation development, dose selection, regimen optimization, etc. There have been several tenofovir PBPK models developed previously, with the purposes of predicting tenofovir (administered as oral TDF) exposure in special populations (i.e., pregnant women [14], fetus [15], and the geriatric [16]), and predicting the tenofovir exposure change mediated by drug-drug interaction [17-19] (summarized in Table 5-1). However, there are inconsistent parameter values from different references used across different PBPK models, and some critical information was incorrectly used or not reported (Table 5-1, as comments shown in bracket). Besides, there has not been a PBPK model predicting tenofovir or TFVdp in the transmission site and evaluating the efficacy of PrEP in women at risk of HIV infection, especially in the scenario of nonadherence.

This study is aimed to characterize plasma PK of tenofovir with noncompartmental analysis and compartmental PK modeling; and to evaluate effectiveness of TDF based oral PrEP given nonadherence with PBPK modeling approach. The hypothesis is that less than 7 doses per week of TDF-based oral PrEP can also provide protection from HIV; and protection provided by the same amount of weekly dose differs by the missing dose interval.

Table 5-1 Summary of previous PBPK models for tenofovir. Parameters shown here are only for non-pregnant population.

PBPK Study	**De Sousa Mendes, 2015 (2 papers summarized in this column)** [14, 15]	**De Sousa Mendes, 2015** [16]	**Ball, 2017** [17]	**Liu, 2020** [18]	**Parvez, 2021** [19]	**Zhang, 2023** [20]	
Purpose	Maternal and fetal PK during pregnancy	Geriatric	DDI with S44121	DDI with probenecid	DDI with para-aminosalicylic acid	Maternal PK during pregnancy	
Modeling platform	Simcyp (V13R1)	Simcyp (V17R1)	Simcyp (V14.1)	Simcyp (V15)	Simcyp (V16)	PKSim	
Parameter values						TDF	TFV
MW (g/mol)	287	287	287	287	287	635.5	287
pKa	3.7-6.5	3.7-6.5	3.7-6.5	3.75	3.75	3.75	3.8
Log P	-2.21	-2.21	-2.21	1.25	1.25	2.1	-0.85

F	0.28 (pregnancy-maternal model). 0.18 (pregnancy-fetal model). [Both values were cited from VIREAD label. The latter one could be typo]	0.32 [Cited from Barditch-Crovo, 2001. Seems to be a value between fast and fed]	Fa (fraction absorbed): 0.28	Fa (fraction absorbed): 0.2	Fa [Not clear if this is fraction absorbed or bioavailability]: 0.73 [Cited from Rajoli, 2015[21], which was about intramuscular nanoformulation, so the absorption should not be the same with oral, and this value is not found in that paper]	-	-
ka (1/h)	0.56	1	0.56	1.03	1.03	-	-
Permeability	-	-	-	P_{app}=256×10^-6 cm/s (LLC-PK1)	-	P_{app}=13×10^-6 cm/s	P_{app}=0.41×10^-6 cm/s

fu	0.993	0.993	0.993	0.93	0.3	0.928	0.993
Main binding protein	albumin	albumin	-	-	-	albumin	albumin
B:P ratio	0.58	0.58	0.58	1 [Cited from VEMLIDY production information, which is tenofovir alafenamide, not TDF]	0.58	[Shown as "-"]	0.58
Kp method	Rodgers and Rowland	Rodgers and Rowland	Rodgers and Rowland	Method 2	-	Rodgers and Rowland	
V_{ss} (L/kg)	0.31 (Simcyp predicted)	4.87 (scaling factor of 17.88)		0.307	0.31 [There is also a V_d of 0.81 L/kg listed in the table,	-	

					not clear how it was used]		
Total CL (l/h)	14.2	16.2	-	-	-	-	-
CL_R (l/h)	10.6	13.12	-	-	11.3	GFR fraction=1; Tubular secretion=0.32; fR=0.73	0.066 (L/h/kg)
CL-secretion: uptake	OAT1	-	OAT1	OAT1, OAT3	OAT1, OAT3	-	-
CL_{int}	5.8 (µL/min/10^6 cells)	-	5.8 (µL/min/10^6 cells)	5.8 (OAT1) and 3.6 (OAT3) (µL/min/10^-6 cells)	5.8 (OAT1) and 1.2 (OAT3) (L/h)	-	-
CL-secretion: efflux	MRP4	-	MRP	MRP4	MRP4	-	-

CL_{int}	1 (μL/min/10^6 cells)	-	1	1 (μL/min/10^-6 cells)	1 (L/h) (Cited from De Sousa Mendes, 2015)	-	-
CL_{ad} (L/h)	3.6	3.1	3.6	-	3.6	-	-
Hepatic transport							
CL_{PD}_passive diffusion	4×10^-6 (mL/min/10^6 cells)	-	-	4×10^-5 (mL/min/10^6 cells)	-	-	-
$CL_{int,T}$	1.4 (μL/min/10^6 cells)	-	-	Sinusoidal uptake: 3.125 (mL/min/10^6 cells)	-	0.13 (unit not shown)	1.16 (unit not shown)

Abbreviations: MW: molecular weight, pKa: acid dissociation constant, log P: logarithm of n-octanol: buffer partition coefficient, Fa: fraction absorbed, Ka: first-order absorption rate constant, fu: ratio of unbound concentration to the total concentration of the drug in plasma, B:P ratio: blood-to-plasma partition ratio, P_{app}: apparent permeability; V_{ss}: steady state volume of distribution, Kp: tissue-to-plasma partition coefficient, Km: Michaelis-Menten constant, CL_R: renal clearance, fR: fraction excreted unchanged via kidney, $CL_{int,T}$: transporter-mediated intrinsic clearance, $CL_{PD,apical}$: passive diffusion clearance between renal cell and proximal tubule, $CL_{int,CYP2C9}$: CYP2C9-mediated intrinsic clearance, CL_{ad}: additional systemic clearance.

5.2 Methods

The datasets used for noncompartmental analysis (NCA), compartmental PK analysis and the PBPK development for the FGT compartment were kindly shared by Dr. Mackenzie Cottrell at University of Carolina at Chapel Hill. The datasets are a subset of PK data of the clinical study NCT01330199 [22].

Study design of NCT01330199 related to analysis of this chapter

Twenty-four healthy, premenopausal women were randomly assigned to three groups (n=8 per group), and received a single dose of 150 mg, 300 mg and 600 mg TDF, respectively. Blood samples of each volunteer were taken at baseline (pre-dose), and 0.5-, 1-, 2-, 3-, 4-, 6-, 9-, 12-, 18-, 24-, 36-, and 48-hour post-dose. Two vaginal tissues from different volunteers were also collected at each time point of 6-, 12-, 24- and 48-hour post-dose (eight vaginal tissues in total).

5.2.1 NCA and compartmental PK analysis of tenofovir (administered as oral TDF) in healthy women

Both NCA and compartmental PK analysis were conducted with the software PKPlus (V2.5, SimulationsPlus, Lancaster, CA, USA).

NCA

The NCA does not require assumption of compartmental structure for the model of PK. The area under the concentration- time curve (AUC) was calculated with the "linear up, log down" trapezoidal rule (i.e., linear trapezoidal method for increasing concentrations and log-linear trapezoidal method for decreasing concentrations). To be specific, for two given time points t1 and t2, and the respective concentrations C1 and C2, the AUC between t1 and t2 is calculated as equation (1) if $C2 \geq C1$, or as equation (2) if $C2 < C1$. At least three observation

data points were used to determine the terminal phase. Apparent clearance (CL/F) was calculated as dose divided by $AUC_{0\text{-}inf}$. Other PK parameters calculated for three doses of TDF including Cmax, Tmax, Clast, Cmin, Vz/F (volume of distribution during terminal phase) and terminal half-life T1/2. Vz/F and T1/2 are calculated with equations (3) and (4), in which λz is the terminal slope of the concentration on a natural-log scale. AUC and Cmax normalized by dose were used to test for nonlinearity by one-way ANOVA.

$$AUC = \frac{1}{2} \times (C_1 + C_2)(t_2 - t_1) \qquad (1)$$

$$AUC = \frac{C_2 - C_1}{lnC_2 - lnC_1}(t_2 - t_1) \qquad (2)$$

$$Vz/F = \frac{Dose}{AUC}\frac{1}{\lambda_Z} \qquad (3)$$

$$T_{1/2} = \frac{ln2}{\lambda_Z} \qquad (4)$$

Compartmental PK analysis

One-, two-, and three- compartmental models were fitted to the individual PK concentration data respectively. Apparent clearance of the central compartment (CL/F), first-order absorption constant (Ka), first-order transport constants between peripheral compartments and the central compartment (k12, k21, k13 and k31), (apparent) volumes of distribution of each compartment (Vc/F, V2 and V3) and T1/2 were reported. Visual inspection based on goodness-of-fit plots and Akaike Information Criteria (AIC) were used for model selection, and a structural model with the minimum AIC value was preferred.

5.2.2 PBPK modeling with GastroPlus

The tenofovir PBPK models were developed with the software GastroPlus (version 9.8.2, SimulationsPlus, Lancaster, CA, USA). The modeling workflow is shown in Figure 5-1. Briefly,

an intravenous tenofovir PBPK model was firstly developed and refined against observed clinical data from Deeks et al. [23], followed by the development and refinement of the oral model with the observations from Kim et al. [24]. Finally, the oral tenofovir model was utilized to predict PK profiles under nonadherence scenarios and to evaluate the forgiveness of different nonadherence.

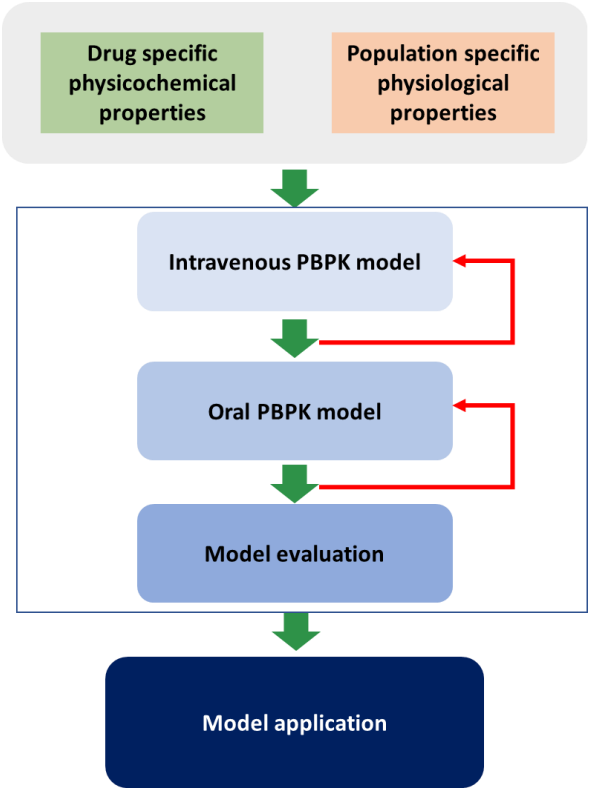

Figure 5-1 Modeling workflow.

Model parameterization

Drug dependent parameter values are shown in Table 5-2. The physiology of a typical 30-year-old American female, with a body weight of 60 kg and height of 162 cm was used in the model development, and the physiological parameter values such as tissue volumes and tissue blood flow rates are shown in Table 5-3 and schematic of the structural model is shown in Figure

5-2. An IV tenofovir PBPK model was first developed to determine parameter values for distribution and clearance. The clinical PK study of tenofovir given as IV infusion showed that renal clearance is about 68% to 80% of the total clearance [23], thus an additional clearance was assumed to be attributed to other systemic clearance mechanisms instead of hepatic since tenofovir is not a substrate of the hepatic metabolic enzymes [7]. Originally, the terminal elimination phase was not well captured with the partition coefficient values calculated by the default mechanistic methods which underpredicted the volume of distribution. Thus, three approaches were tested to deal with this issue: 1. Adding transporters to the liver and kidney compartments, as studies have suggested that OAT1, OAT3 and MRP4 might be involved in the excretion of tenofovir [27-32]; 2. Assuming some tissues are permeability-limited; 3. Adding scaling factors to the partition coefficients as suggested by Peters et al. [33]. The third approach was eventually applied with some adjustments for the best fit with the observed data. Briefly, the default mechanistic method (Lucacova (Rodgers-Single)) was used to calculate the original Kps, with a range of 0.14- 0.42. Further, as informed by several animal studies [34, 35] including ours (Chapter 4, Table 4-1), the variation of penetration ratios of tenofovir in different tissues were large (range: 0.01 (brain) to 40 (liver)). Thus, tissues were grouped into two according to how the original estimated Kp values compared to the penetration ratios in the animal studies: a ≤ 1 scaling factor was multiplied to the group of tissues with smaller Kps (i.e., lung, adipose, muscle, heart and skin), and a >1 scaling factor were multiplied to the group with larger Kps (i.e., kidney, liver, spleen, bone marrow and rest of body). Exceptions were the brain compartment and FGT compartment, for which the penetration ratios from our previous study (Chapter 2) and the NCT01330199 study were used. The combinations of Kp scaling factors tested were 0.25 & 4, 0.25 & 5, 0.5 & 5, 0.5 & 10 and 1 & 5, and the 0.5 & 10 combination was selected as the best fit to the observation data (Figure 5-3). The Kp values used in the final model are shown in Table 5-3. For the oral tenofovir model, the clearances and Kps from the IV model were carried over.

Since all the built-in absorption scaling factor (ASF) models in GastroPlus resulted in largely overestimated Tmax and over/underestimated bioavailability, a user-defined ASF model was optimized for the best fit to data [36].

To incorporate the TFVdp in the FGT compartment, some assumptions were made for simplicity: 1. TFVdp in the FGT is only converted from tenofovir in the FGT by one type of adenylate kinase; 2. TFVdp formed in FGT is only eliminated from the FGT (as opposed to from circulation or from crossing cell membranes). In addition, due to scarcity of kinetic information of the conversion of tenofovir to TFVdp by adenylate kinases, the value of the maximum rate constant (Vmax) of TFVdp formation and intrinsic clearance (CLint) of TFVdp were optimized by data fitting.

Table 5-2 Summary of drug dependent parameters for tenofovir PBPK models.

	Value	**Reference**
PBPK model	full	
MW (g/mol)	287	Drugbank
pKa	3.7 and 6.5	[14]
Log P	1.25	[18]
f_u	0.993	[14]
B:P ratio	0.58	[14]
Kp method	Lucacova (Rodgers-Single) with scaling factors of 0.5 and 10.	Optimized
Total CL (L/h)	14.22	[23]
CL_R (L/h)	9.66	[23]
CL_{ad} (L/h), systemic	4.56	[23]
P_{aff} (cm/s) (Caco-2)	0.29 × 10^−6	[25]
P_{eff} (cm/s × 10^-4) (human)	0.2089	GatroPlus converted from Caco-2 P_{aff}
TFVdp formation through adenylate kinases		

V_{max} (mg/s/mg enzyme)	0.9 × 10^-3	Data fitting
Km (mg/L)	861	[26]

Abbreviations: MW: molecular weight, pKa: acid dissociation constant, log P: logarithm of n-octanol: buffer partition coefficient, fu: ratio of unbound concentration to the total concentration of the drug in plasma, B:P ratio: blood-to-plasma partition ratio, P_{app}: apparent permeability; V_{ss}: steady state volume of distribution, Kp: tissue-to-plasma partition coefficient, Km: Michaelis-Menten constant, CL_R: renal clearance, CL_{ad}: additional systemic clearance.

Table 5-3 Physiological parameters of a typical 30-year-old woman, with a 162 cm height and 60 kg body weight that were used in the final PBPK model.

Organ	Organ volume (mL)	Organ blood flow (mL/s)	Kp
Lung	863	97	0.21
Liver	1303	22	2.7
Spleen	129	2.2	3.1
Gut	-	10	-
Adipose	26278	13	0.07
Muscle	14730	7.4	0.115
Heart	258	4.1	0.2
Brain	1356	12	0.01
Kidney	300	16	3.7
Skin	1962	4.9	0.22
Genital tract (ReproOrg)	77	0.27	0.6
Red bone marrow	1011	5.1	1.6
Yellow bone marrow	2665	1.3	1.4
Rest of body	2142	1.1	3.1
Artery	1330	87	-
Vein	2659	87	-

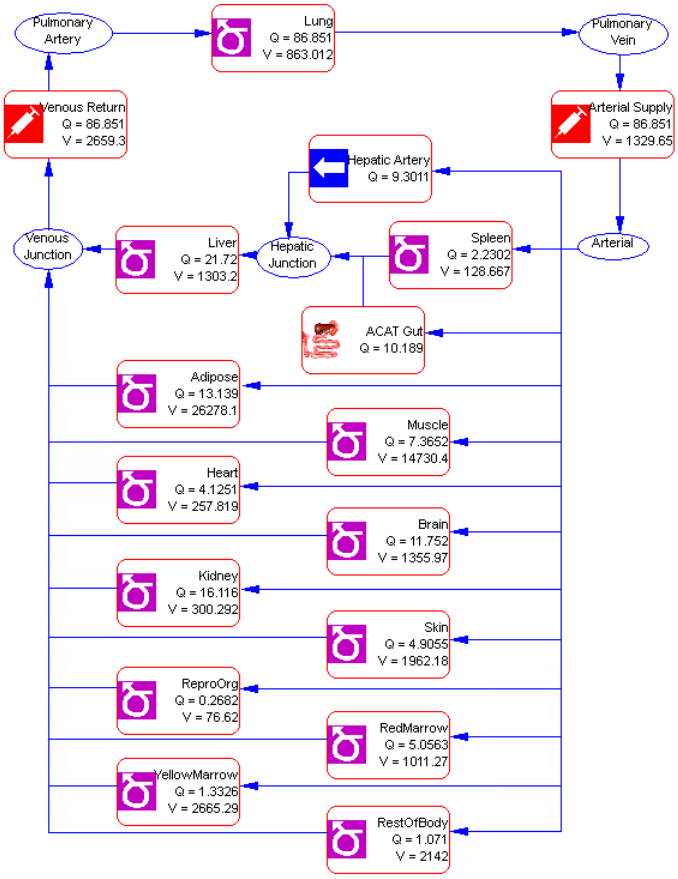

Figure 5-2 The structural model of tenofovir. Values in the boxes are physiological parameters of a typical 30-year-old American female (Snapshot from GastroPlus 9.8.2). Q: blood flow into the tissue; V: tissue volume.

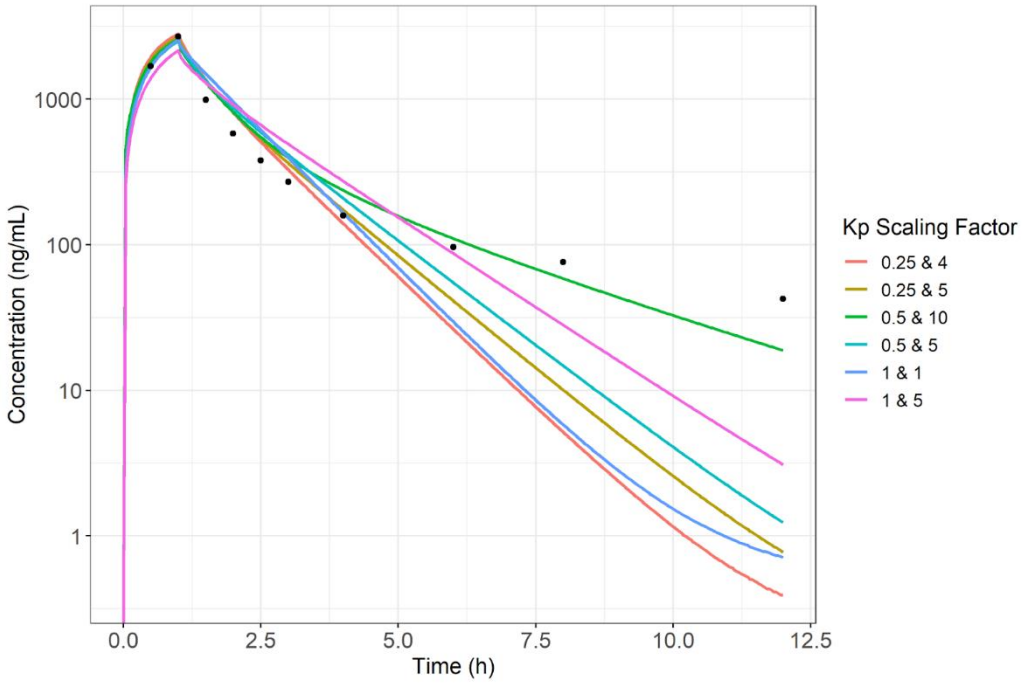

Figure 5-3 Optimization for Kp scaling factors. The black points are the observed concentrations from tenofovir IV infusion clinical study (Deeks 1998). The solid lines are the predicted tenofovir plasma concentrations after 1 mg/kg IV infusion with different sets of Kp scaling factors.

Model evaluation

The performance of the model was evaluated by comparing the predicted with the observed plasma PK data from clinical studies. The lineshapes of the average predicted plasma concentration were evaluated with both visual inspection and mean absolute percent error (MAPE) compared to clinical data (acceptance: MAPE<50%), and the precision of important PK parameters was evaluated with fold error (FE) of AUC, Cmax and Tmax (acceptance: within 0.5-2). MAPE and FE were calculated as equation (5) and (6), where C_{obs} and C_{pred} represent the observed and predicted concentrations and θ represents a particular PK parameter:

$$MAPE = \frac{1}{N}\sum_{N=1}^{n}\frac{|C_{obs} - C_{pred}|}{C_{obs}} \times 100\% \quad (5)$$

$$FE = \frac{\theta_{pred}}{\theta_{obs}} \quad (6)$$

Prediction of PK profiles for nonadherence to tenofovir

Eleven regimen plans with a series of nonadherence extent, from missing one dose per week to missing six doses per week (Table 5-4), were selected as representatives of nonadherence behaviors and used for simulation for 100 virtual female subjects. For 2-, 3-, 4- and 5- doses per week regimens, plan 1 represents the plans with longer nonadherence interval, while plan 2 represents the plans with shorter nonadherence interval. The PK profiles including tenofovir in plasma and FGT, and TFVdp in FGT were simulated for two weeks (336 hours). The second week was considered to reach steady state, of which the PK profiles were used to evaluate the forgiveness of nonadherence. In the evaluation, the simulated plasma tenofovir concentrations were compared to two target concentrations (0.81 ng/g for women at low-risk and 5.8 ng/g for women at high risk [12]), and the simulated TFVdp concentrations in FGT were compared with one target concentration (2.77 ng/g). The first two target concentrations for tenofovir in plasma were identified by Garcia-Cremades et al. with a population pharmacokinetic (PopPK)-pharmacodynamic (PD) analysis, as the trough concentrations for having a 50% reduction of HIV infection (or EC50) in the group of women at low and high risk of HIV infection, respectively [12]. The target concentration for TFVdp in FGT was an ex vivo EC50 identified by a cervical explant HIV challenging study (in-house data, unpublished). Two metrics were calculated for this evaluation by comparing the simulated concentrations and target concentrations: 1. time above target concentration during the second week (steady state); 2. the percentage of people above the target concentration for all the time during the second week.

Table 5-4 Nonadherence schedules. “X” represents that a 300 mg TDF is taken at the time point indicated in the first row, and the blanks represents missing doses.

	Dosing time (h)	**0**	**24**	**48**	**72**	**96**	**120**	**144**	**168**	**192**	**216**	**240**	**264**	**288**	**312**
1	**7 doses**	X	X	X	X	X	X	X	X	X	X	X	X	X	X
2	**6 doses**	X	X	X	X	X	X		X	X	X	X	X	X	
3	**5 doses - plan 1**	X	X	X	X	X			X	X	X	X	X		
4	**5 doses - plan 2**	X	X	X		X	X		X	X	X		X	X	
5	**4 doses - plan 1**	X	X	X	X				X	X	X	X			
6	**4 doses - plan 2**	X	X			X	X		X	X			X	X	
7	**3 doses - plan 1**	X	X	X					X	X	X				
8	**3 doses - plan 2**	X		X		X			X		X		X		
9	**2 doses - plan 1**	X		X					X		X				
10	**2 doses - plan 2**	X			X				X			X			
11	**1 dose**	X							X						

5.3 Results

5.3.1 NCA and compartmental models

The summary of NCA is shown in Table 5-5. Nonlinearity PK was shown for 600 mg TDF, as the AUC and Cmax of 600 mg was only about 150-160% (instead of 200%) of those of 300 mg; also indicated by ANOVA of dose-normalized AUC ($p=0.03$). Results of compartmental modeling are summarized in Table 5-5. A two-compartment model best described the PK profiles of tenofovir, as the two-compartmental model had the smallest AIC value (Table 5-6); and as the observed vs. predicted concentration plots shown in Figure 5-4, the two-compartmental model showed smaller dispersion than the one-compartmental model, while very similar to the three-compartmental model.

Table 5-5 Noncompartmental analysis of plasma tenofovir PK profiles of NCT01330199 (oral administration of tenofovir disoproxil fumarate 150, 300 and 600 mg). Mean (SD) is shown for the PK parameters.

Dose	Sample size	AUCinf (ng*h/mL)	AUClast (ng*h/mL)	Cmax (ng/mL)	Clast (ng/mL)	Tmax (h)	Thalf (h)	Vz/F (mL)	CL/F (mL/h)	AUCinf/Dose (ng*h/mL/mg)	Cmax/Dose (ng/mL/mg)
150 mg	8	1276 (153.6)	1104 (122.9)	119.8 (27.89)	6.72 (1.5)	1.5 (0.76)	17.63 (2.36)	3026 (560)	118.9 (12.79)	8.51 (1.02)	0.8 (0.19)
300 mg	8	2450 (812.4)	2107 (706.4)	258 (101.4)	12.09 (3.97)	1.19 (0.53)	19.46 (3.76)	3697 (1093)	132.9 (36.97)	8.17 (2.71)	0.86 (0.34)
600 mg	8	3616 (783.7)	3220 (680.2)	421.8 (122.2)	16.3 (4.80)	1.89 (0.36)	16.26 (3.16)	4047 (1287)	173.3 (39.89)	6.02 (1.32)	0.7 (0.2)

Table 5-6 Summary of compartmental modeling of tenofovir PK profiles from clinical study NCT01330199. Mean (SD) is shown for each parameter.

	AIC	CL (L/h)	Ka (1/h)	Vc (L)	K12 (1/h)	K21(1/h)	K13 (1/h)	K31(1/h)	T1/2 (h)
One-compartment	-21.22 (3.805)	120.8 (32.07)	716.8 (2585)	2016 (507.7)	-	-	-	-	11.65 (1.21)
Two-compartment	-31.8 (8.558)	138.9 (38.59)	194.4 (947.5)	754.1 (301.9)	0.56 (0.26)	0.18 (0.07)	-	-	17.87 (3.01)
Three-compartment	-28.2 (9.08)	134.8 (37.02)	1.04 (0.47)	704.5 (225.1)	0.38 (0.21)	0.20 (0.09)	0.28 (0.25)	0.18 (0.15)	24.03 (16.96)

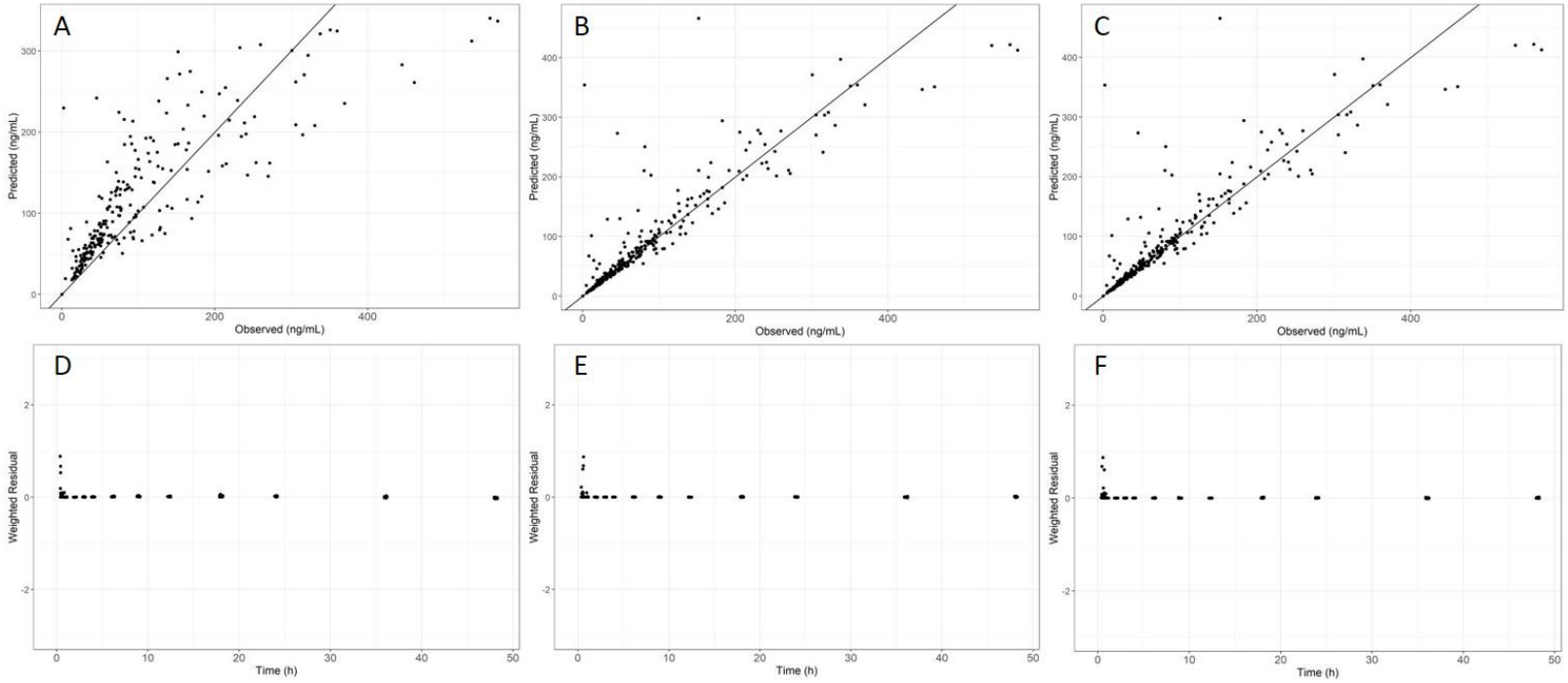

Figure 5-4 Goodness-of-fit plots of one- (A and D), two- (B and E) and three-compartmental (C and F) models for tenofovir. A-B are the observed vs. predicted plots, and the solid lines are the lines of unity. D-F are the plots of weighted residual vs. time.

5.3.2 Tenofovir PBPK model evaluation

Evaluation results of both IV and oral models are summarized in Table 5-7, and simulated PK profiles overlapped with the observed clinical data are shown in Figure 5-5. Predictions from both models were accurate by visual inspection, and the performance were acceptable since the FE values were not less than 0.5 or larger than 2 (range: 0.61 to 1.48), and the MAFE values were no larger than 36%, expect for the prediction for 600 mg TDF (MAPE=54%).

Table 5-7 Evaluation of tenofovir PBPK model performance with plasma PK profiles from clinical studies.

	Study	PK parameters	Observed	Predicted	Fold error	Mean absolute fold error
IV infusion	Deeks, 1998.	AUC_{last} (ng*h/mL)	4100	4600	1.12	32.0%
		C_{max} (ng/mL)	2700	2600	0.96	
		T_{max} (h)	-	-	-	
Oral	Kim, 2007.	AUC_{last} (ng*h/mL)	2231	2036	0.91	23.0%
		C_{max} (ng/mL)	245	257	1.05	
		T_{max} (h)	0.75	1	1.33	
	NCT01330199 - TDF 150 mg	AUC_{last} (ng*h/mL)	1104	1131	1.02	35.8%
		C_{max} (ng/mL)	120	138	1.15	
		T_{max} (h)	1.5	1.17	0.78	
	NCT01330199 - TDF 300 mg	AUC_{last} (ng*h/mL)	2107	2378	1.13	19.6%

		C_{max} (ng/mL)	258	286	1.11	
		T_{max} (h)	1.19	1.12	0.94	
	NCT01330199 - TDF 600 mg	AUC_{last} (ng*h/mL)	3320	4779	1.48	54.2%
		C_{max} (ng/mL)	422	563	1.33	
		T_{max} (h)	1.89	1.15	0.61	

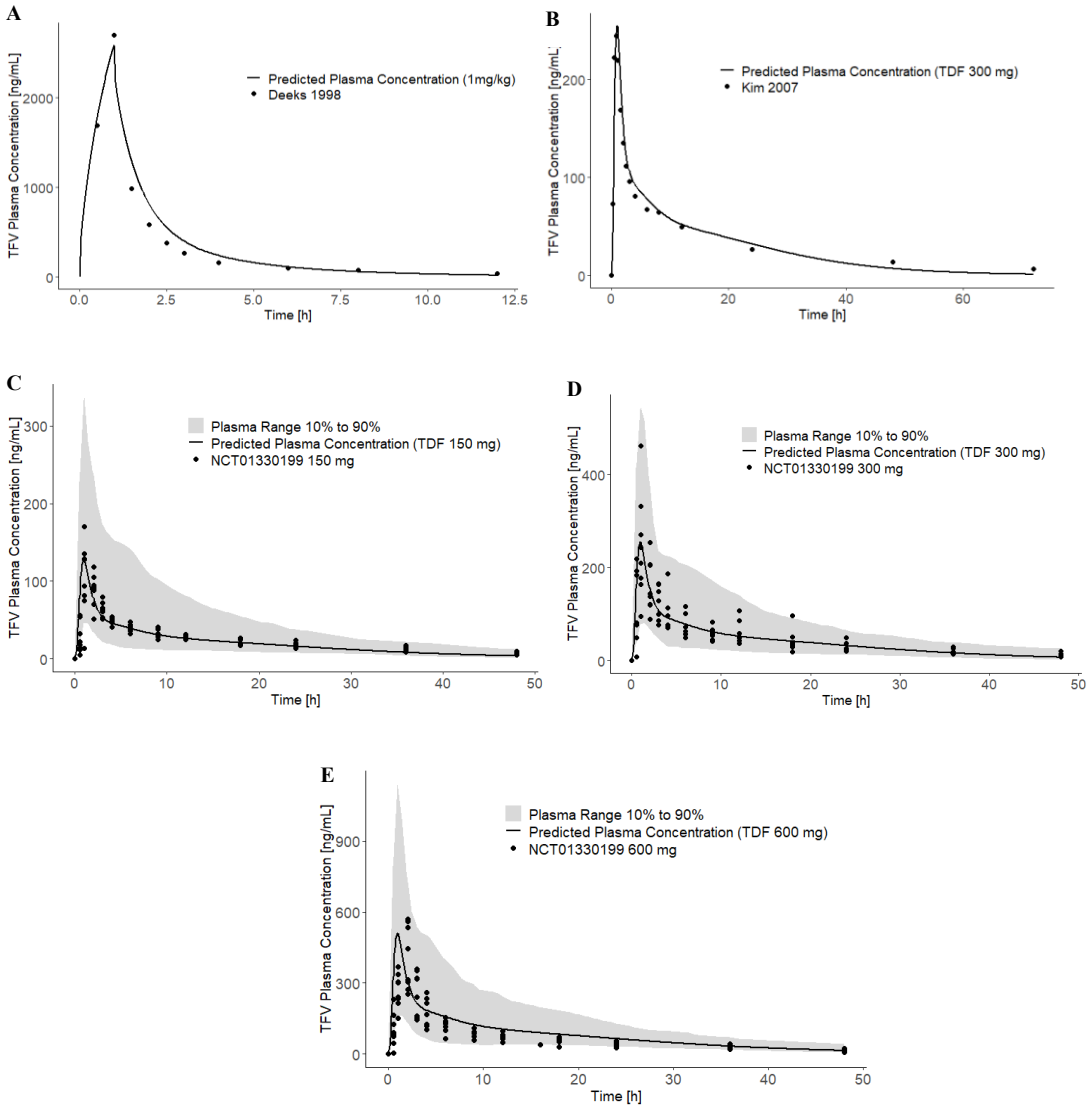

Figure 5-5 PK profiles of tenofovir after (A) IV infusion of 1 mg/kg, (B) 300 mg oral TDF, (C) 150 mg oral TDF, (D) 300 mg oral TDF, (E) 600 mg oral TDF. Solid black lines are the mean simulated plasma concentration. Black points in (A) and (B) are the mean observed plasma concentrations, while in (C), (D) and (E) are individual observed plasma concentrations. Grey bands are the 90% prediction interval of the simulation of 100 virtual subjects.

5.3.3 Prediction of tenofovir and TFVdp PK profiles under different nonadherence scenarios

Attainment of target concentrations of tenofovir in plasma and TFVdp in the FGT are summarized in Table 5-8 and Table 5-9, and the simulated PK profiles of 100 virtual female subjects are shown in Figure 5-6 and Figure 5-7. In the second week, for tenofovir in plasma (Table 5-8), median time above target ranged from 3.5 – 7 days when comparing the simulated population profiles to the low-risk target concentration, while the median time ranged from 2.2 – 7 days compared to the high-risk target; for TFVdp in FGT (Table 5-9), median time ranged from 2.3 – 7 days. Six of the dosing plans resulted in over half of women above the low-risk target, in contrast to only 3 plans had most women above the high-risk target; for TFVdp in FGT, the same 3 plans resulted in most women above the target. For plans with the same number of doses per week, the plans with dosing spread more evenly (plan 2) led to better results of target attainments than the plans with longer off-treatment intervals (plan 1).

Table 5-8 Summary of target attainment of tenofovir in plasma for serial dosing plans of nonadherence.

	Low - risk		High - risk	
Target C_{trough} concentration	0.8 ng/mL		5.1 ng/mL	
	Mean time above target (day)	% Of people above target	Mean time above target (day)	% Of people above target
7 doses	7.0	100	7.0	100
6 doses	7.0	100	7.0	83
5 doses - plan 1	7.0	72	6.5	26
5 doses - plan 2	7.0	98	7.0	78
4 doses - plan 1	6.5	34	5.3	4
4 doses - plan 2	7.0	68	6.4	29
3 doses - plan 1	5.6	23	4.5	1
3 doses - plan 2	7.0	78	6.4	21
2 doses - plan 1	5.8	24	4.4	1
2 doses - plan 2	6.6	35	4.6	3
1 dose	3.5	2	2.2	0

Table 5-9 Summary of target attainment of TFVdp in FGT for serial dosing plans of nonadherence.

Target concentration	Plan	Median time above target (day)	% Of people above target
Ex vivo EC50 – 2.77 ng/g	7 Doses	7.0	100
	6 Doses	7.0	85
	5 Doses Plan 1	6.5	26
	5 Doses Plan 2	7.0	79
	4 Doses Plan 1	5.4	5
	4 Doses Plan 2	6.5	28
	3 Doses Plan 1	4.5	1
	3 Doses Plan 2	6.4	23
	2 Doses Plan 1	4.5	2
	2 Doses Plan 2	4.7	4
	1 Dose	2.3	0

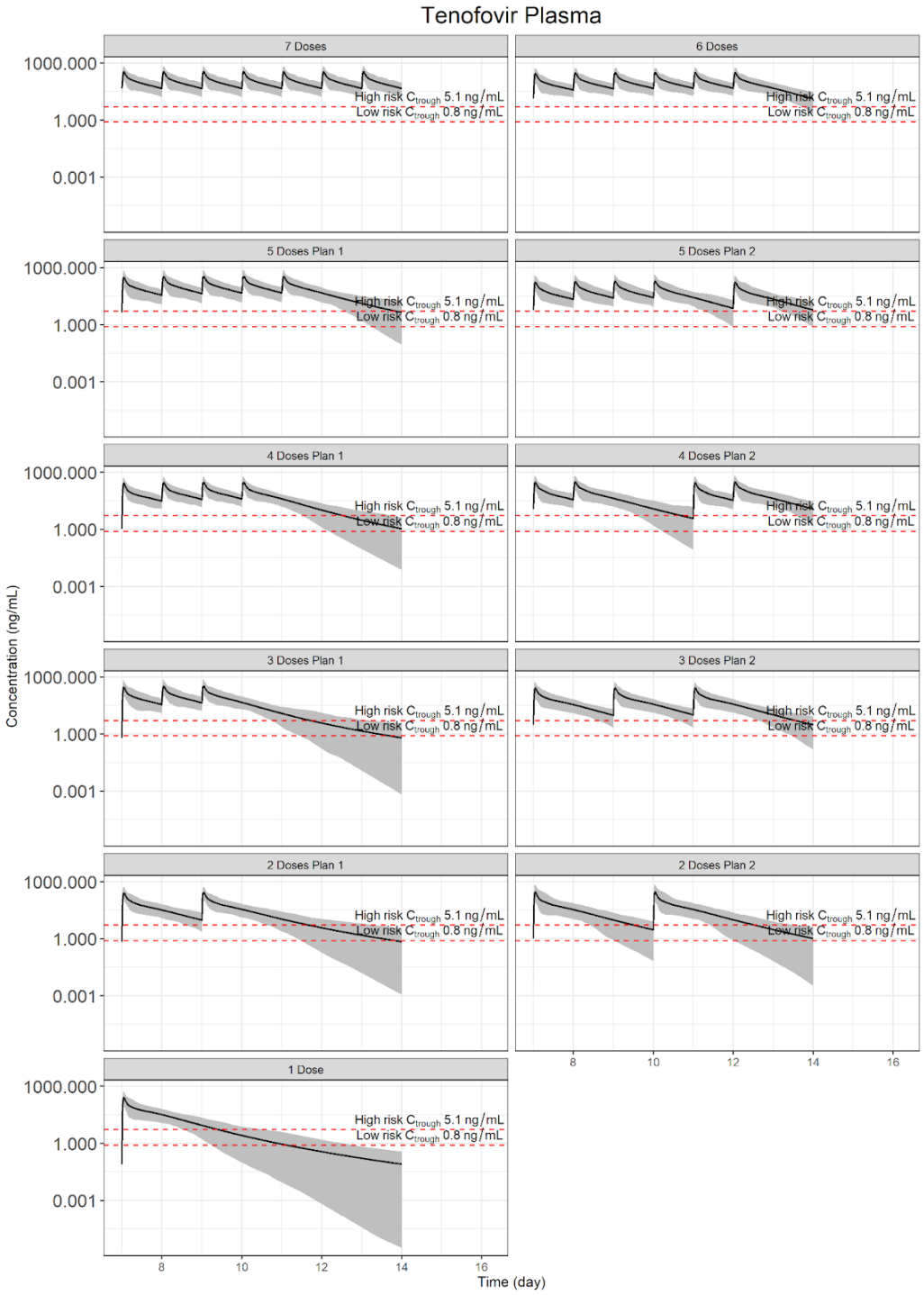

Figure 5-6 Simulation of tenofovir plasma PK profiles under different nonadherence scenarios. Solid black lines are the mean predicted plasma concentration. The grey band represents the 90% prediction interval.

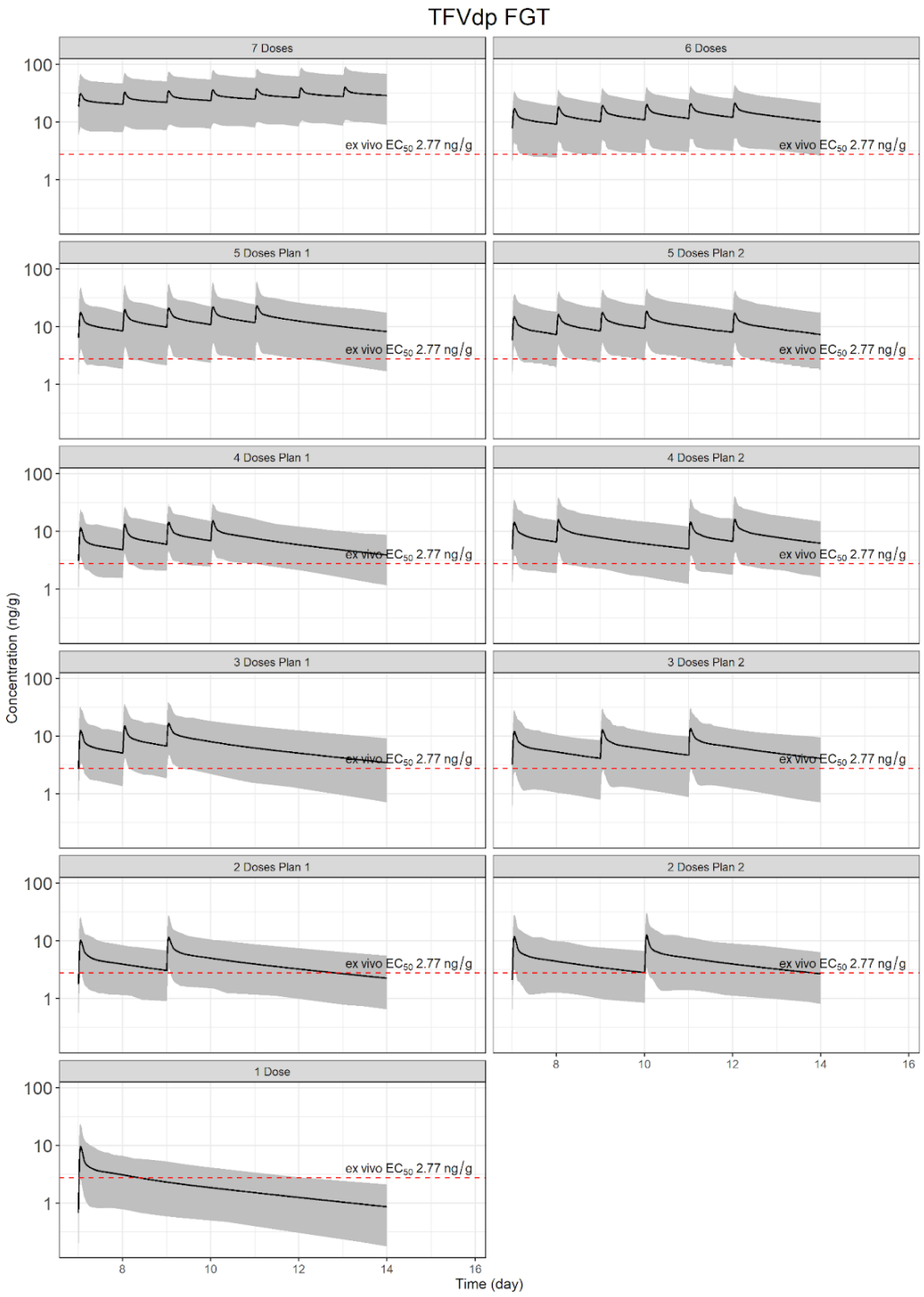

Figure 5-7 Simulation of TFVdp PK profiles in FGT under different nonadherence scenarios. Solid black lines are the mean predicted plasma concentration. The grey band represents the 90% prediction interval.

5.4 Discussion

In this study I first did an exercise of analysis of tenofovir PK from the study NCT01330199 with both NCA and compartmental modeling approach. The NCA revealed nonlinearity of TDF at 600mg, the 200% labeled dose, which could be due to a saturation process involved in the absorption. Similar PK results were published by Barditch-Crovo et al.[37], although they did not acknowledge the nonlinearity. The compartmental models informed the development of distribution related parameters in the PBPK modeling. Later, the tenofovir PBPK models developed in this study were able to quantitatively predict tenofovir PK profiles in plasma, and both tenofovir and TFVdp's PK profiles in the female genital tissues. Based on efficacy targets demonstrated by previous PopPK analysis [12] and our ex vivo PKPD study, the model can be used to predict and compare "forgiveness" of nonadherence patterns.

Nonadherence is prevalent for the daily oral TDF/FTC for PrEP, as revealed by the SHIPP study with dry-blood-spot testing, in the third months on PrEP, only 51% of the study population remained fully adherent and the full adherence rate kept declining [11]. However, results of studies that measured adherence also showd that PrEP still exhibited protective effects even with nonadherence [13]. Some questions remain unanswered: 1. To what extent or how many missing doses is forgivable? 2. With the same number of missing doses, is there a schedule more forgivable than others? There have been some efforts to explore the correlation between tenofovir exposure in plasma and HIV protection, and target concentrations were proposed [12, 38]. By pooling the average plasma concentration data from six PrEP randomized clinical trials (RCTs) including cisgender women and men (the HIV negative partners in the HIV serodiscordant couples), MSM and transgender women, and fitting an Emax model, Hendrix estimated the median tenofovir plasma concentration associated with 90% protection of HIV infection (EC90) as 105-110 ng/mL [13]. Garcia-Cremades et al. pooled individual-level data from three PrEP RCTs and estimated the

plasma concentrations associated with 50% and 90% protection (EC50 and EC90) with a PopPK/PD analysis, and further stratified by sex, risk (low or moderate-to-high, referred to as "low" or "high" in the current study for simplicity) and formulation [12]. The EC50s were estimated from the PKPD model, while the EC90s were extrapolated from the EC50s [12]. Thus, the EC50 associated trough concentrations (Ctrough) were selected as the target used for evaluation in the current study. Meanwhile, our tenofovir PBPK model is the first to delineate PK profiles of both tenofovir and its active metabolite in the FGT, which is enabled by the paired plasma tenofovir, FGT tenofovir and FGT TFVdp measured in the NCT01330199 clinical trial. The ex vivo EC50 of TFVdp was used as the target since there has not been an in vivo EC50 identified by clinical study. The simulations for nonadherence with our tenofovir PBPK model provide some reference to the two questions we asked earlier: 1. For most women (>50%) to keep having tenofovir exposure above the target, depending on their risk level, 5-7 doses/week for women at low risk, and 6-7 doses/week for women at high risk is recommended to ensure efficacy; 2. In the scenario missing multiple doses is inevitable and the individual is able to plan ahead and separate the missing doses (instead of having a rather long PrEP interruption), 3-4 doses/week and 5 doses/week could also protect most low-risk women and high-risk women, respectively. The target attainment metrics of TFVdp in FGT is consistent with those of tenofovir in plasma for women at high risk, which makes sense since in the ex vivo model, the cervical explant was challenged with an HIV titer that ensured the infection if no intervention (incubation with antiretroviral drugs prior to challenge) took place, which can be considered as "high risk". However, the evaluation for forgiveness is highly related to the accuracy of the target concentrations and risk level and is subject to change when other target concentrations are available. Given that in reality nonadherence to daily oral PrEP is prevalent in women, RCTs need to be designed to explore the feasibility of the on-demand oral PrEP or regimen schedules with "pill vacation".

There are still some gaps left in the study. 1. The enzyme kinetics involved in the conversion of tenofovir to TFVdp were unknown, thus the values of parameters such as Vmax, Km and protein expression in the FGT were validated with clinical data, which warranted kinetic studies in the future; 2. Several transporters are known to be involved in the disposition of tenofovir [27-32], however, because adding transporters in the PBPK model did not improve the lineshape of the terminal phase, they were not retained in the final model. This also implies other underlying mechanisms that could contribute to the distribution of tenofovir. For example, as indicated by the animal studies [34, 35], tissues like the liver and kidney had drastically larger penetration ratios. These tissues may trap more tenofovir in earlier time and then serve as the "drug bank" slowly releasing the drug later. In addition, since TFVdp can dephosphorylate back to tenofovir [39], it is possible that the TFVdp is another source of supply that slows down the elimination of tenofovir; 3. The mechanism of nonlinearity was unclear and not incorporated into the PBPK model. This led to the overprediction of tenofovir administered as 600 mg TDF compared to observation data, as the MAPE was larger than 50%. This issue is not significant for now since 600 mg TDF is not prescribed for women, but future investigation is needed, for example, to study the feasibility of an on-demand oral PrEP with a loading dose of 600 mg TDF for women.

In conclusion, I characterized the PK profiles of tenofovir with noncompartmental analysis and compartmental modeling approaches; and developed a full-body tenofovir PBPK model which enables the prediction of tenofovir and TFVdp in the FGT, the HIV transmission site for women, in addition to the prediction of tenofovir in the circulatory system. The application of this model provided reference for increasing protection of PrEP given inevitable nonadherence.

CHAPTER 6 Summary, Limitations, and Opportunities

Great successes have been achieved with antiretroviral drugs in the treatment and prevention of HIV as we enter the fifth decade of the HIV epidemic, but major challenges are still confronting us with the HIV reservoirs and low adherence of PrEP, especially in women [76]. These challenges have hampered the antiretroviral drugs to become the cure for people living with HIV or to exert 100% protection for people at risk of HIV infection. Investigation of the antiretroviral drug distributions in tissues is one key approach to improve the current treatment and prevention strategy, however, research in tissues is largely limited by the accessibility of collecting and analyzing those tissue samples in humans. The **main objective of my dissertation** is to investigate distribution of antiretroviral drugs in the difficult-to-access tissues, the brain and the female genital tissues, and to predict exposure of the most commonly prescribed antiretroviral drug, tenofovir, in the circulatory system and female genital tissues, with a physiologically based pharmacokinetic (PBPK) modeling approach.

The postmortem study we conducted in Uganda enables characterization of the currently known most robust tissue pharmacology data presented in chapter 2 and chapter 3 in this thesis. Improving our understanding of the penetration of antiretroviral drugs into the CNS and determining the optimal exposure and treatment regimen is critical to improving therapy for HIV, and to balance between protecting the CNS from HIV persistence and from drug-induced neurotoxicity. In chapter 2, we characterized the penetration of four antiretroviral drugs, dolutegravir, tenofovir, lamivudine and efavirenz in 13 brain regions, including CSF, the most commonly used biospecimen as surrogate of

the entire CNS. Our findings suggested the compartmentalization of antiretroviral drug penetration in CNS as marked by the significant regional differences in relative tissue penetration for three of the four antiretroviral drugs (dolutegravir was the exception), with ratios between the regions of the highest drug penetration and the lowest drug penetration for all four antiretroviral drugs were about 2-fold. Furthermore, CSF was not always representative of the entire CNS. For lamivudine, concentrations in two of the cortical regions, the frontal lobe and the occipital lobe, were significantly less than the CSF. For tenofovir, concentration in CSF was not strongly correlated with the average concentration across other 12 solid brain tissues (referred as "composite brain" in chapter 2). Furthermore, we identified several demographic and clinical characteristics that predicted significantly higher CSF or composite brain penetration, namely being female (higher dolutegravir CSF penetration ratios), no concomitant use of rifampin (higher tenofovir composite brain penetration ratios), and testing for positive of *Cryptococcus* (higher lamivudine CSF penetration ratios). We hope these findings will inspire similar studies in the future to explore exposure and penetration differences across brain regions for other antiretroviral drugs and provide reference to strategical selection of the antiretroviral combination and dose optimization based on characteristics of an individual patient that balance between efficacy and safety.

Achieving optimal exposure of antiretroviral drugs in the female genital tissues is critical for suppressing HIV reservoirs for women living with HIV, and for protecting women at risk of HIV from sexual transmission. As previous studies focus on the lower female genital tissues (cervix and vagina), exposure data of antiretroviral drugs in the upper genital tissues (uterus and ovary) was obscure [78, 83-85, 131-133]. In chapter 3, we

characterized the penetration of three antiretroviral drugs (i.e., tenofovir, lamivudine and efavirenz) and an antifungal drug (fluconazole) in ovarian, uterine, cervical and vaginal tissues. Similar to our finding in the CNS (chapter 2), compartmentalization of drug penetration in the female genital tract was observed: the penetration ratios of the four drugs were significantly higher in the vaginal tissues than the cervical tissues, and the regional differences were more pronounced for tenofovir and lamivudine as the median drug penetration ratios in the vaginal tissues were 50% more than in the cervical tissues, while for efavirenz and fluconazole, the difference in median drug penetration ratio between the region of highest penetration and that of the lowest penetration were 27% and 2%, respectively. The regional difference might create an environment for evolutionary selection in HIV mutations and lead to development of HIV resistance in the less penetrating tissues.

Limitations of studies described in chapter 2 and chapter 3 are closely related to their postmortem nature. First, although being the most robust postmortem data collection, sample sizes of the brain data for dolutegravir and efavirenz were relatively small due to difficulties in collecting all compartmentalized tissue samples from each decedent, which restrained the power of some statistical analysis. Second, our participants were at an advanced stage of diseases that involved increased permeability of blood-brain-barrier and decreased renal function, which might confound our measurement of penetration. Thus, cautions need to be employed when extrapolating the current results to a general HIV population. Third, as the purpose of achieving optimal tissue concentration of antiretroviral drugs is to eliminate HIV in the tissue, the HIV viral load in tissue is the primary endpoint that directly reflects the adequacy of use and exposure of the

antiretroviral drugs (i.e., understanding of concentration (pharmacokinetics (PK)) is just a bridge to approach to the drug effect (pharmacodynamics (PD)), instead of the ultimate goal). But in the context of postmortem research, since the HIV RNA has low stability and could go through rapid degradation after death, common PCR assays were assumed to be not sensitive enough to give us reliable measurements of postmortem tissues (obtained after different case-dependent postmortem intervals, which ranged from 2-32 hour in our study, that contributes to additional variability); thus, the current postmortem study did not measure viral load. If both rapid autopsy (within 6 hours after death) and highly sensitive PCR are available in the future, the viral load of HIV RNA in the tissue should be measured and linked to the drug PK.

Postmortem redistribution is an inevitable issue involved in any postmortem analysis. Although the protocol of our Uganda study had limited the time of autopsy to be within 24 hours after death, postmortem redistribution is not unlikely [145, 146]. In chapter 4, we quantitatively assessed the potential for postmortem redistribution of tenofovir, lamivudine and efavirenz using a mouse model. The postmortem concentration profiles exhibited trends that differed by drug, tissue type and postmortem time point. We proposed some hypothesis of the mechanism of the postmortem that are not exhaustive but warrants further study with more tissues involved: 1. for drugs that are substrates of metabolic enzymes, the enzyme-mediated elimination will drive a descending trend within a certain period of time (while some viability is still remained for the enzymes); 2. for drugs that are not substrates of metabolic enzymes, their overall trend of redistribution is subject to the concentration gradient around the tissue. One limitation of this study is that we could not observe and compare a “true postmortem” effect as each mouse can

only be sacrificed once and their tissues can only contribute to one time point as opposed to observing the drug redistribution postmortem of each mouse over time, and their contributions introduce inter-mouse variability. A separate group of mice with drug monitored by an imaging technology could be included in a future study to fill this gap. Our findings may have implications for previous postmortem human studies if postmortem redistribution of antiretroviral drugs in humans is also not negligible. For example, the values of tissue-to-plasma ratios may not be the same as those of subjects who alive since the rates of postmortem redistribution for tissue and plasma could be different. However, with all these limitations presented, currently the postmortem analysis is still the only approach to extensively sample various tissue compartments from different participants at a minimal risk.

Finally, in chapter 5, I took a step further by combining our knowledge of exposure of tenofovir in the circulatory system and the female genital tissues, and the model-estimated pharmacodynamic targets, to predict "forgiveness" of nonadherence to PrEP with PBPK modeling. The simulation results implied a possibility of increasing adherence by "being nonadherent (but wisely)", as some of the dosing plans with scattered missingness had better target achievements. More detail regarding the enzyme kinetics involved in the formation of the active metabolite tenofovir diphosphate is needed. Moreover, while developing the PBPK models, we had attempted to separate the female genital tract into two compartments as informed by chapter 3 that, tenofovir penetration in the vaginal tissues were higher than the other three female genital tissues and the model had been developed. However, the simulation did not succeed due to an internal error with the population simulator of the GastroPlus software (version 9.8.2 and

9.8.3), which can be resolved with upgraded software in the future. The full-body PBPK modeling is a "zoomed-in" PK modeling approach compared to the classic compartmental PK modeling which assumes the human body is just composed of one, two or three compartment(s). Unlike population PK modeling, the simulations based on PBPK modeling is capable of incorporating interindividual variability from multiple levels (e.g., amount of dose intake, pH in the gastrointestinal tract, tissue volume and blood flow, enzyme/transporter protein expression, etc.), as long as the PK process of interest is parametrized in the model; and the benefit of this is that the simulation is more likely to delineate the heterogeneity of the population. Although PBPK modeling is a powerful tool to predict PK in special populations, as we are looking forward to a future with precision/individual medicine, we need more comprehensive information of human biology and drug PK from individuals instead of a summary from a population. We are limited by the contemporary analytical technology, most of which are invasive, expensive, or time/labor consuming. However, some imaging technologies have shown promising potentials in filling this gap, for example positron emission tomography (PET), single-photon emission CT (SPECT) and magnetic resonance imaging (MRI) [152]. As these technologies advance, they can inform the PBPK modeling to predict drug PK accurately for a specific individual.

In conclusion, my research provides a rare glimpse into the activities and distribution of antiretroviral drugs in commonly difficult-to-access tissues, namely the CNS and the female genital tissues, utilizing postmortem analysis techniques. My findings show that different regions within organs, such as the CNS and the female genital tract, exhibit significantly different degrees of penetration to antiretroviral drugs; and commonly used

surrogates, such as cerebrospinal fluid for the CNS and cervical tissue and cervicovaginal fluid for the female genital tract, are not adequate in representing their respective systems. My results also show that distribution mechanisms of antiretroviral drugs are still active after death and emphasize minimizing the postmortem time interval between death and tissue collection for future postmortem studies. Lastly, I demonstrated the development of an antiretroviral drug PBPK model and the usefulness of such a model in simulating and predicting the use of PrEP to inform future studies and clinical trials. Each aspect of this research contributes to our current understanding of how antiretroviral drugs interact with different compartmentalized tissues within the biological systems; and my investigation further underlines the importance of future studies and clinical trials on advancing our comprehension of the pharmacology and mechanisms of the antiretroviral drugs in these tissues to overcome the bottlenecks in defeating HIV.

References

1. Lozano R, Naghavi M, Foreman K et al. Global and regional mortality from 235 causes of death for 20 age groups in 1990 and 2010: a systematic analysis for the Global Burden of Disease Study 2010. *Lancet* 2012; **380**: 2095-128.
2. Murray CJL, Lopez AD. Alternative projections of mortality and disability by cause 1990-2020: Global burden of disease study. *Lancet* 1997; **349**: 1498-504.
3. WHO. Newsroom: The top 10 causes of death. 2020.
4. WHO. The global health observatory: HIV. 2023.
5. Fettig J, Swaminathan M, Murrill CS et al. Global Epidemiology of HIV. *Infectious Disease Clinics of North America* 2014; **28**: 323-+.
6. Simon V, Ho DD, Karim QA. HIV/AIDS epidemiology, pathogenesis, prevention, and treatment. *Lancet* 2006; **368**: 489-504.
7. Moir S, Chun TW, Fauci AS. Pathogenic Mechanisms of HIV Disease. *Annual Review of Pathology: Mechanisms of Disease, Vol 6* 2011; **6**: 223-48.
8. Levy JA. PATHOGENESIS OF HUMAN-IMMUNODEFICIENCY-VIRUS INFECTION. *Annals of the New York Academy of Sciences* 1989; **567**: 58-68.
9. Le LT, Spudich SS. HIV-Associated Neurologic Disorders and Central Nervous System Opportunistic Infections in HIV. *Seminars in Neurology* 2016; **36**: 373-81.
10. Tan IL, Smith BR, von Geldern G et al. HIV-associated opportunistic infections of the CNS. *Lancet Neurology* 2012; **11**: 605-17.
11. Javadi S, Menias CO, Karbasian N et al. HIV-related Malignancies and Mimics: Imaging Findings and Management. *Radiographics* 2018; **38**: 2051-68.
12. Dlamini Z, Mbele M, Makhafola TJ et al. HIV-Associated Cancer Biomarkers: A Requirement for Early Diagnosis. *International Journal of Molecular Sciences* 2021; **22**.
13. WHO. Latest HIV estimates and update on COVID-19 disruptions. 2022.
14. Amblard F, Patel D, Michailidis E et al. HIV nucleoside reverse transcriptase inhibitors. *European Journal of Medicinal Chemistry* 2022; **240**.
15. Xiao TS, Cai YF, Chen B. HIV-1 Entry and Membrane Fusion Inhibitors. *Viruses-Basel* 2021; **13**.
16. Zhang C, Xie Q, Wan CC et al. Recent Advances inn Small-Molecule HIV-1 Inntegrase Inhibitors. *Current Medicinal Chemistry* 2021; **28**: 4910-34.
17. Voshavar C. Protease Inhibitors for the Treatment of HIV/AIDS: Recent Advances and Future Challenges. *Current Topics in Medicinal Chemistry* 2019; **19**: 1571-98.
18. DHHS. Guidelines for the Use of Antiretroviral Agents in Adults and Adolescents with HIV. 2022.
19. DHHS. Guidelines for the Use of Antiretroviral Agents in Pediatric HIV Infection. 2023.
20. DHHS. Recommendations for the Use of Antiretroviral Drugs During Pregnancy and Interventions to Reduce Perinatal HIV Transmission in the United States. 2023.
21. WHO. Consolidated Guidelines on HIV Prevention, Testing, Treatment, Service Delivery and Monitoring: Recommendations for a Public Health Approach. 2021.

22. Lau CY, Adan MA, Maldarelli F. Why the HIV Reservoir Never Runs Dry: Clonal Expansion and the Characteristics of HIV-Infected Cells Challenge Strategies to Cure and Control HIV Infection. *Viruses-Basel* 2021; **13**.
23. Chaillon A, Gianella S, Dellicour S et al. HIV persists throughout deep tissues with repopulation from multiple anatomical sources. *Journal of Clinical Investigation* 2020; **130**: 1699-712.
24. Dahl V, Peterson J, Spudich S et al. Single-copy assay quantification of HIV-1 RNA in paired cerebrospinal fluid and plasma samples from elite controllers. *Aids* 2013; **27**: 1145-9.
25. Joseph SB, Kincer LP, Bowman NM et al. Human Immunodeficiency Virus Type 1 RNA Detected in the Central Nervous System (CNS) After Years of Suppressive Antiretroviral Therapy Can Originate from a Replicating CNS Reservoir or Clonally Expanded Cells. *Clinical Infectious Diseases* 2019; **69**: 1345-52.
26. Lorenzo-Redondo R, Fryer HR, Bedford T et al. Persistent HIV-1 replication maintains the tissue reservoir during therapy. *Nature* 2016; **530**: 51-+.
27. Beckford-Vera DR, Flavell RR, Seo Y et al. First-in-human immunoPET imaging of HIV-1 infection using Zr-89-labeled VRC01 broadly neutralizing antibody. *Nature Communications* 2022; **13**.
28. Guadalupe M, Reay E, Sankaran S et al. Severe CD4(+) T-cell depletion in gut lymphoid tissue during primary human immunodeficiency virus type 1 infection and substantial delay in restoration following highly active antiretroviral therapy. *Journal of Virology* 2003; **77**: 11708-17.
29. Mabvakure BM, Lambson BE, Ramdayal K et al. Evidence for both Intermittent and Persistent Compartmentalization of HIV-1 in the Female Genital Tract. *Journal of Virology* 2019; **93**.
30. Riggs PK, Chaillon A, Jiang GC et al. Lessons for Understanding Central Nervous System HIV Reservoirs from the Last Gift Program. *Current Hiv/Aids Reports* 2022; **19**: 566-79.
31. Mzingwane ML, Tiemessen CT. Mechanisms of HIV persistence in HIV reservoirs. *Reviews in Medical Virology* 2017; **27**.
32. Schnell G, Price RW, Swanstrom R et al. Compartmentalization and Clonal Amplification of HIV-1 Variants in the Cerebrospinal Fluid during Primary Infection. *Journal of Virology* 2010; **84**: 2395-407.
33. Sturdevant CB, Joseph SB, Schnell G et al. Compartmentalized Replication of R5 T Cell-Tropic HIV-1 in the Central Nervous System Early in the Course of Infection. *Plos Pathogens* 2015; **11**.
34. Oliveira MF, Chaillon A, Nakazawa M et al. Early Antiretroviral Therapy Is Associated with Lower HIV DNA Molecular Diversity and Lower Inflammation in Cerebrospinal Fluid but Does Not Prevent the Establishment of Compartmentalized HIV DNA Populations. *Plos Pathogens* 2017; **13**.
35. Lamers SL, Rose R, Maidji E et al. HIV DNA Is Frequently Present within Pathologic Tissues Evaluated at Autopsy from Combined Antiretroviral Therapy-Treated Patients with Undetectable Viral Loads. *Journal of Virology* 2016; **90**: 8968-83.
36. Tso FY, Kang GB, Kwon EH et al. Brain is a potential sanctuary for subtype C HIV-1 irrespective of ART treatment outcome. *Plos One* 2018; **13**.

37. Gisslen M, Keating SM, Spudich S et al. Compartmentalization of cerebrospinal fluid inflammation across the spectrum of untreated HIV-1 infection, central nervous system injury and viral suppression. *Plos One* 2021; **16**.
38. Akiyama H, Jalloh S, Park S et al. Expression of HIV-1 Intron-Containing RNA in Microglia Induces Inflammatory Responses. *Journal of Virology* 2021; **95**.
39. Spudich S, Robertson KR, Bosch RJ et al. Persistent HIV-infected cells in cerebrospinal fluid are associated with poorer neurocognitive performance. *Journal of Clinical Investigation* 2019; **129**: 3339-46.
40. Strain MC, Letendre S, Pillai SK et al. Genetic composition of human immunodeficiency virus type 1 in cerebrospinal fluid and blood without treatment and during failing antiretroviral therapy. *Journal of Virology* 2005; **79**: 1772-88.
41. Smit TK, Brew BJ, Tourtellotte W et al. Independent evolution of human immunodeficiency virus (HIV) drug resistance mutations in diverse areas of the brain in HIV-infected patients, with and without dementia, on antiretroviral treatment. *Journal of Virology* 2004; **78**: 10133-48.
42. Salemi M, Lamers SL, Yu S et al. Phylodynamic analysis of human immunodeficiency virus type 1 in distinct brain compartments provides a model for the neuropathogenesis of AIDS. *Journal of Virology* 2005; **79**: 11343-52.
43. Lamers SL, Salemi M, Galligan DC et al. Human immunodeficiency virus-1 evolutionary patterns associated with pathogenic processes in the brain. *Journal of Neurovirology* 2010; **16**: 230-41.
44. Salemi M, Rife B. Phylogenetics and Phyloanatomy of HIV/SIV Intra-Host Compartments and Reservoirs: The Key Role of the Central Nervous System. *Current Hiv Research* 2016; **14**: 110-20.
45. Cusini A, Vernazza PL, Yerly S et al. Higher CNS Penetration-Effectiveness of Long-term Combination Antiretroviral Therapy Is Associated With Better HIV-1 Viral Suppression in Cerebrospinal Fluid. *Jaids-Journal of Acquired Immune Deficiency Syndromes* 2013; **62**: 28-35.
46. Cysique LA, Vaida F, Letendre S et al. Dynamics of cognitive change in impaired HIV-positive patients initiating antiretroviral therapy. *Neurology* 2009; **73**: 342-8.
47. Letendre S, Marquie-Beck J, Capparelli E et al. Validation of the CNS penetration-effectiveness rank for quantifying antiretroviral penetration into the central nervous system. *Archives of Neurology* 2008; **65**: 65-70.
48. Carvalhal A, Gill MJ, Letendre SL et al. Central nervous system penetration effectiveness of antiretroviral drugs and neuropsychological impairment in the Ontario HIV Treatment Network Cohort Study. *Journal of Neurovirology* 2016; **22**: 349-57.
49. Gates TM, Cysique LA, Siefried KJ et al. Maraviroc-intensified combined antiretroviral therapy improves cognition in virally suppressed HIV-associated neurocognitive disorder. *Aids* 2016; **30**: 591-600.
50. Vassallo M, Durant J, Biscay V et al. Can high central nervous system penetrating antiretroviral regimens protect against the onset of HIV-associated neurocognitive disorders? *Aids* 2014; **28**: 493-501.
51. Hakkers CS, Hermans AM, van Maarseveen EM et al. High efavirenz levels but not neurofilament light plasma levels are associated with poor neurocognitive functioning in asymptomatic HIV patients. *Journal of Neurovirology* 2020; **26**: 572-80.

52. Gutierrez-Valencia A, Viciana P, Palacios R et al. Stepped-Dose Versus Full-Dose Efavirenz for HIV Infection and Neuropsychiatric Adverse Events A Randomized Trial. *Annals of Internal Medicine* 2009; **151**: 149-W34.
53. Mukonzo JK, Okwera A, Nakasujja N et al. Influence of efavirenz pharmacokinetics and pharmacogenetics on neuropsychological disorders in Ugandan HIV-positive patients with or without tuberculosis: a prospective cohort study. *Bmc Infectious Diseases* 2013; **13**.
54. Srinivas N, Rosen EP, Gilliland WM et al. Antiretroviral concentrations and surrogate measures of efficacy in the brain tissue and CSF of preclinical species. *Xenobiotica* 2019; **49**: 1192-201.
55. Demuth M, Czub S, Sauer U et al. Relationship between viral load in blood, cerebrospinal fluid, brain tissue and isolated microglia with neurological disease in macaques infected with different strains of SIV. *Journal of Neurovirology* 2000; **6**: 187-201.
56. Calcagno A, Bonora S, Simiele M et al. Tenofovir and emtricitabine cerebrospinal fluid-to-plasma ratios correlate to the extent of blood-brainbarrier damage. *Aids* 2011; **25**: 1437-9.
57. Best BM, Letendre SL, Koopmans P et al. Low Cerebrospinal Fluid Concentrations of the Nucleotide HIV Reverse Transcriptase Inhibitor, Tenofovir. *Jaids-Journal of Acquired Immune Deficiency Syndromes* 2012; **59**: 376-81.
58. Lahiri CD, Reed-Walker K, Sheth AN et al. Cerebrospinal fluid concentrations of tenofovir and emtricitabine in the setting of HIV-1 protease inhibitor-based regimens. *Journal of Clinical Pharmacology* 2016; **56**: 492-6.
59. Van den Hof M, Blokhuis C, Cohen S et al. CNS penetration of ART in HIV-infected children. *Journal of Antimicrobial Chemotherapy* 2018; **73**: 484-9.
60. Nicol MR, Pastick KA, Taylor J et al. Cerebrospinal Fluid and Brain Tissue Penetration of Tenofovir, Lamivudine, and Efavirenz in Postmortem Tissues with Cryptococcal Meningitis. *Clin Transl Sci* 2019; **12**: 445-9.
61. Ferrara M, Bumpus NN, Ma Q et al. Antiretroviral drug concentrations in brain tissue of adult decedents. *Aids* 2020; **34**: 1907-14.
62. Letendre SL, Mills AM, Tashima KT et al. ING116070: A Study of the Pharmacokinetics and Antiviral Activity of Dolutegravir in Cerebrospinal Fluid in HIV-1-Infected, Antiretroviral Therapy-Naive Subjects. *Clinical Infectious Diseases* 2014; **59**: 1032-7.
63. Gelé T, Chéret A, Castro Gordon A et al. Cerebrospinal fluid exposure to bictegravir/emtricitabine/tenofovir in HIV-1-infected patients with CNS impairment. *The Journal of antimicrobial chemotherapy* 2021.
64. Calcagno A, Moltó J, Borghetti A et al. Older Age is Associated with Higher Dolutegravir Exposure in Plasma and Cerebrospinal Fluid of People Living with HIV. *Clinical pharmacokinetics* 2021; **60**: 103-9.
65. Tashima KT, Caliendo AM, Ahmad M et al. Cerebrospinal fluid human immunodeficiency virus type 1 (HIV-1) suppression and efavirenz drug concentrations in HIV-1-infected patients receiving combination therapy. *Journal of Infectious Diseases* 1999; **180**: 862-4.

66. Antinori A, Perno CF, Giancola ML et al. Efficacy of cerebrospinal fluid (CSF)-penetrating antiretroviral drugs against HIV in the neurological compartment: Different patterns of phenotypic resistance in CSF and plasma. *Clinical Infectious Diseases* 2005; **41**: 1787-93.
67. Best BM, Koopmans PP, Letendre SL et al. Efavirenz concentrations in CSF exceed IC50 for wild-type HIV. *Journal of Antimicrobial Chemotherapy* 2011; **66**: 354-7.
68. Nightingale S, Chau TTH, Fisher M et al. Efavirenz and Metabolites in Cerebrospinal Fluid: Relationship with CYP2B6 c.516G -> T Genotype and Perturbed Blood-Brain Barrier Due to Tuberculous Meningitis. *Antimicrobial Agents and Chemotherapy* 2016; **60**: 4511-8.
69. Delille CA, Pruett ST, Marconi VC et al. Effect of protein binding on unbound atazanavir and darunavir cerebrospinal fluid concentrations. *Journal of Clinical Pharmacology* 2014; **54**: 1063-71.
70. UNAIDS: Global HIV & AIDS statistics — Fact sheet, https://www.unaids.org/en/resources/fact-sheet (accessed Nov 2021).
71. Baeten JM, Donnell D, Ndase P et al. Antiretroviral Prophylaxis for HIV Prevention in Heterosexual Men and Women. *New England Journal of Medicine* 2012; **367**: 399-410.
72. Van Damme L, Corneli A, Ahmed K et al. Preexposure Prophylaxis for HIV Infection among African Women. *New England Journal of Medicine* 2012; **367**: 411-22.
73. Marrazzo JM, Ramjee G, Richardson BA et al. Tenofovir-Based Preexposure Prophylaxis for HIV Infection among African Women. *New England Journal of Medicine* 2015; **372**: 509-18.
74. Grant RM, Lama JR, Anderson PL et al. Preexposure Chemoprophylaxis for HIV Prevention in Men Who Have Sex with Men. *New England Journal of Medicine* 2010; **363**: 2587-99.
75. Molina JM, Capitant C, Spire B et al. On-Demand Preexposure Prophylaxis in Men at High Risk for HIV-1 Infection. *New England Journal of Medicine* 2015; **373**: 2237-46.
76. Hodges-Mameletzis I, Fonner VA, Dalal S et al. Pre-Exposure Prophylaxis for HIV Prevention in Women: Current Status and Future Directions. *Drugs* 2019; **79**: 1263-76.
77. Louissaint NA, Cao YJ, Skipper PL et al. Single Dose Pharmacokinetics of Oral Tenofovir in Plasma, Peripheral Blood Mononuclear Cells, Colonic Tissue, and Vaginal Tissue. *AIDS Res Hum Retroviruses* 2013; **29**: 1443-50.
78. Patterson KB, Prince HA, Kraft E et al. Penetration of Tenofovir and Emtricitabine in Mucosal Tissues: Implications for Prevention of HIV-1 Transmission. *Sci Transl Med* 2011; **3**.
79. Stieh DJ, Maric D, Kelley ZL et al. Vaginal Challenge with an SIV-Based Dual Reporter System Reveals That Infection Can Occur throughout the Upper and Lower Female Reproductive Tract. *PLoS Pathog* 2014; **10**: e1004440.
80. Herrera C, Lwanga J, Lee M et al. Pharmacokinetic/pharmacodynamic investigation of raltegravir with or without lamivudine in the context of HIV-1 pre-exposure prophylaxis (PrEP). *J Antimicrob Chemother* 2021; **76**: 2129-36.

81. Thurman AR, Schwartz JL, Cottrell ML et al. Safety and Pharmacokinetics of a Tenofovir Alafenamide Fumarate-Emtricitabine based Oral Antiretroviral Regimen for Prevention of HIV Acquisition in Women: A Randomized Controlled Trial. *Eclinicalmedicine* 2021; **36**: 100893.
82. Hendrix CW, Chen BA, Guddera V et al. MTN-001: Randomized Pharmacokinetic Cross-Over Study Comparing Tenofovir Vaginal Gel and Oral Tablets in Vaginal Tissue and Other Compartments. *Plos One* 2013; **8**.
83. Kwara A, DeLong A, Rezk N et al. Antiretroviral drug concentrations and HIV RNA in the genital tract of HIV-infected women receiving long-term highly active antiretroviral therapy. *Clin Infect Dis* 2008; **46**: 719-25.
84. Dumond JB, Yeh RF, Patterson KB et al. Antiretroviral drug exposure in the female genital tract: implications for oral pre- and post-exposure prophylaxis. *AIDS* 2007; **21**: 1899-907.
85. Rahangdale L, De Paris K, Kashuba ADM et al. Immunologic, Virologic, and Pharmacologic Characterization of the Female Upper Genital Tract in HIV-Infected Women. *J Acquir Immune Defic Syndr* 2015; **68**: 420-4.
86. Yarema MC, Becker CE. Key concepts in postmortem drug redistribution. *Clin Toxicol (Phila)* 2005; **43**: 235-41.
87. Kamphuis AEM, Borra LCP, van der Hulst R et al. Postmortem redistribution of morphine in humans: Important variables that might be influencing the central blood/peripheral blood ratio. *Forensic Science International* 2021; **329**.
88. Gerostamoulos D, Beyer J, Staikos V et al. The effect of the postmortem interval on the redistribution of drugs: a comparison of mortuary admission and autopsy blood specimens. *Forensic Science Medicine and Pathology* 2012; **8**: 373-9.
89. Olson KN, Luckenbill K, Thompson J et al. Postmortem Redistribution of Fentanyl in Blood. *American Journal of Clinical Pathology* 2010; **133**: 447-53.
90. Saar E, Beyer J, Gerostamoulos D et al. The time-dependant post-mortem redistribution of antipsychotic drugs. *Forensic Science International* 2012; **222**: 223-7.
91. Krinsky CS, Lathrop SL, Zumwalt R. An Examination of the Postmortem Redistribution of Fentanyl and Interlaboratory Variability. *Journal of Forensic Sciences* 2014; **59**: 1275-9.
92. Gleba J, Kim J. A Mechanism-Based Forensic Investigation into the Postmortem Redistribution of Morphine. *Journal of Analytical Toxicology* 2020; **44**: 256-62.
93. J H, P K, T K et al. Post-mortem Redistribution of Alprazolam in Rats. *Prague medical report* 2020; **121**.
94. Dryburgh E, Honeybun L, Sturrock K et al. Using mu X-Ray CT to observe postmortem diffusion from the stomach in a rat model. *Forensic Science International* 2020; **312**.
95. Sager JE, Yu JJ, Ragueneau-Majlessi I et al. Physiologically Based Pharmacokinetic (PBPK) Modeling and Simulation Approaches: A Systematic Review of Published Models, Applications, and Model Verification. *Drug Metabolism and Disposition* 2015; **43**: 1823-37.
96. Jones HM, Rowland-Yeo K. Basic Concepts in Physiologically Based Pharmacokinetic Modeling in Drug Discovery and Development. *Cpt-Pharmacometrics & Systems Pharmacology* 2013; **2**.

97. Kuepfer L, Niederalt C, Wendl T et al. Applied Concepts in PBPK Modeling: How to Build a PBPK/PD Model. *Cpt-Pharmacometrics & Systems Pharmacology* 2016; **5**: 516-31.
98. Mendes MD, Hirt D, Urien S et al. Physiologically-based pharmacokinetic modeling of renally excreted antiretroviral drugs in pregnant women. *British Journal of Clinical Pharmacology* 2015; **80**: 1031-41.
99. Liu XMI, Momper JD, Rakhmanina N et al. Physiologically Based Pharmacokinetic Models to Predict Maternal Pharmacokinetics and Fetal Exposure to Emtricitabine and Acyclovir. *Journal of Clinical Pharmacology* 2020; **60**: 240-55.
100. Mendes MD, Hirt D, Vinot C et al. Prediction of human fetal pharmacokinetics using ex vivo human placenta perfusion studies and physiologically based models. *British Journal of Clinical Pharmacology* 2016; **81**: 646-57.
101. Mendes MD, Chetty M. Are Standard Doses of Renally-Excreted Antiretrovirals in Older Patients Appropriate: A PBPK Study Comparing Exposures in the Elderly Population With Those in Renal Impairment. *Drugs in R&D* 2019; **19**: 339-50.
102. Ball K, Jamier T, Parmentier Y et al. Prediction of renal transporter-mediated drug-drug interactions for a drug which is an OAT substrate and inhibitor using PBPK modelling. *European Journal of Pharmaceutical Sciences* 2017; **106**: 122-32.
103. Liu SN, Desta Z, Gufford BT. Probenecid-Boosted Tenofovir: A Physiologically-Based Pharmacokinetic Model-Informed Strategy for On-Demand HIV Preexposure Prophylaxis. *Cpt-Pharmacometrics & Systems Pharmacology* 2020; **9**: 40-7.
104. Schnell G, Joseph S, Spudich S et al. HIV-1 Replication in the Central Nervous System Occurs in Two Distinct Cell Types. *Plos Pathogens* 2011; **7**.
105. Tong CYW, Costelloe S, Hubb J et al. Deep Sequencing of HIV-1 in Cerebrospinal Fluid. *Clinical Infectious Diseases* 2015; **61**: 1022-5.
106. Gianella S, Pond SLK, Oliveira MF et al. Compartmentalized HIV rebound in the central nervous system after interruption of antiretroviral therapy. *Virus Evolution* 2016; **2**.
107. Dahl V, Gisslen M, Hagberg L et al. An Example of Genetically Distinct HIV Type 1 Variants in Cerebrospinal Fluid and Plasma During Suppressive Therapy. *Journal of Infectious Diseases* 2014; **209**: 1618-22.
108. Beguelin C, Vazquez M, Bertschi M et al. Viral Escape in the Central Nervous System with Multidrug-Resistant Human Immunodeficiency Virus-1. *Open Forum Infectious Diseases* 2016; **3**.
109. Gatanaga H, Oka S, Ida S et al. Active HIV-1 redistribution and replication in the brain with HIV encephalitis. *Archives of Virology* 1999; **144**: 29-43.
110. Lustig G, Cele S, Karim F et al. T cell derived HIV-1 is present in the CSF in the face of suppressive antiretroviral therapy. *Plos Pathogens* 2021; **17**.
111. Cysique LA, Brew BJ. Prevalence of non-confounded HIV-associated neurocognitive impairment in the context of plasma HIV RNA suppression. *Journal of Neurovirology* 2011; **17**: 176-83.
112. Robertson KR, Smurzynski M, Parsons TD et al. The prevalence and incidence of neurocognitive impairment in the HAART era. *Aids* 2007; **21**: 1915-21.
113. Lanman T, Letendre S, Ma Q et al. CNS Neurotoxicity of Antiretrovirals. *Journal of Neuroimmune Pharmacology* 2021; **16**: 130-43.

114. Hung KM, Chen PC, Hsieh HC et al. Mitochondrial defects arise from nucleoside/nucleotide reverse transcriptase inhibitors in neurons: Potential contribution to HIV-associated neurocognitive disorders. *Biochimica Et Biophysica Acta-Molecular Basis of Disease* 2017; **1863**: 406-13.
115. EACS. Guidelines for the management of people living with HIV in Europe (V11.1). 2022.
116. Mantinieks D, Gerostamoulos D, Glowacki L et al. Postmortem Drug Redistribution: A Compilation of Postmortem/Antemortem Drug Concentration Ratios. *Journal of Analytical Toxicology* 2021; **45**: 368-77.
117. Wang F, Namuju OC, Pastick KA et al. A post-mortem analysis of tenofovir, lamivudine, efavirenz and fluconazole penetration in female genital tissues. *Journal of Antimicrobial Chemotherapy* 2022; **77**: 3180-6.
118. TIVICAY (dolutegravir) Tablets Label.
119. VIREAD (tenofovir disoproxil fumarate) tablets and powder label.
120. EPIVIR (lamivudine) tablets and solution label.
121. Sustiva (efavirenz) tablets label.
122. Calcagno A, Cusato J, Simiele M et al. High interpatient variability of raltegravir CSF concentrations in HIV-positive patients: a pharmacogenetic analysis. *Journal of Antimicrobial Chemotherapy* 2014; **69**: 241-5.
123. Morris ME, Rodriguez-Cruz V, Felmlee MA. SLC and ABC Transporters: Expression, Localization, and Species Differences at the Blood-Brain and the Blood-Cerebrospinal Fluid Barriers. *Aaps Journal* 2017; **19**: 1317-31.
124. Gele T, Furlan V, Taburet AM et al. Dolutegravir Cerebrospinal Fluid Diffusion in HIV-1-Infected Patients with Central Nervous System Impairment. *Open Forum Infectious Diseases* 2019; **6**.
125. Brinker T, Stopa E, Morrison J et al. A new look at cerebrospinal fluid circulation. *Fluids and Barriers of the Cns* 2014; **11**.
126. Tang MW, Shafer RW. HIV-1 Antiretroviral Resistance: Scientific Principles and Clinical Applications. *Drugs* 2012; **72**: E1-E25.
127. Boffito M, Waters L, Cahn P et al. Perspectives on the Barrier to Resistance for Dolutegravir plus Lamivudine, a Two-Drug Antiretroviral Therapy for HIV-1 Infection. *Aids Research and Human Retroviruses* 2020; **36**: 13-8.
128. Brenner BG, Wainberg MA. Clinical benefit of dolutegravir in HIV-1 management related to the high genetic barrier to drug resistance. *Virus Research* 2017; **239**: 1-9.
129. Martinez-Cajas JL, Wainberg MA. Protease inhibitor resistance in HIV-infected patients: Molecular and clinical perspectives. *Antiviral Research* 2007; **76**: 203-21.
130. Toy EC, Scerpella EG, Riggs JW. TUBOOVARIAN ABSCESS ASSOCIATED WITH CANDIDA-GLABRATA IN A WOMAN WITH AN INTRAUTERINE-DEVICE - A CASE-REPORT. *J Reprod Med* 1995; **40**: 223-5.
131. Dumond JB, Nicol MR, Kendrick RN et al. Pharmacokinetic Modelling of Efavirenz, Atazanavir, Lamivudine and Tenofovir in the Female Genital Tract of HIV-Infected Pre-Menopausal Women. *Clin Pharmacokinet* 2012; **51**: 809-22.
132. Mikamo H, Kawazoe K, Sato Y et al. Penetration of oral fluconazole into gynecological tissues. *Antimicrob Agents Chemother* 1999; **43**: 148-51.

133. Houang ET, Chappatte O, Byrne D et al. Fluconazole levels in plasma and vaginal secretions of patients after a 150-milligram single oral dose and rate of eradication of infection in vaginal candidiasis. *Antimicrob Agents Chemother* 1990; **34**: 909-10.
134. FDA. Bioanalytical Method Validation Guidance for Industry. 2018.
135. Yeh RF, Rezk NL, Kashuba ADM et al. Genital Tract, Cord Blood, and Amniotic Fluid Exposures of Seven Antiretroviral Drugs during and after Pregnancy in Human Immunodeficiency Virus Type 1-Infected Women. *Antimicrob Agents Chemother* 2009; **53**: 2367-74.
136. Owen EJ, Gibson GA, Buckman SA. Pharmacokinetics and Pharmacodynamics of Antimicrobials in Critically Ill Patients. *Surg Infect (Larchmt)* 2018; **19**: 155-62.
137. Leikin JB, Watson WA. Post-mortem toxicology: What the dead can and cannot tell us. *J Toxicol Clin Toxicol* 2003; **41**: 47-56.
138. Vettore MV, Schechter M, Melo MF et al. Genital HIV-1 viral load is correlated with blood plasma HIV-1 viral load in Brazilian women and is reduced by antiretroviral therapy. *J Infect* 2006; **52**: 290-3.
139. Nelson JAE, De Paris K, Ramirez C et al. Female genital tract shedding of HIV-1 is rare in women with suppressed HIV-1 in plasma. *Aids* 2020; **34**: 39-46.
140. Launay O, Tod M, Tschope I et al. Residual HIV-1 RNA and HIV-1 DNA production in the genital tract reservoir of women treated with HAART: the prospective ANRS EP24 GYNODYN study. *Antivir Ther* 2011; **16**: 843-52.
141. Kourtis AP, Wiener J, Hurst S et al. HIV Shedding in the Female Genital Tract of Women on ART and Progestin Contraception: Extended Follow-up Results of a Randomized Clinical Trial. *Jaids-Journal of Acquired Immune Deficiency Syndromes* 2019; **81**: 163-5.
142. Kashuba ADM, Gengiah TN, Werner L et al. Genital Tenofovir Concentrations Correlate With Protection Against HIV Infection in the CAPRISA 004 Trial: Importance of Adherence for Microbicide Effectiveness. *J Acquir Immune Defic Syndr* 2015; **69**: 264-9.
143. Rodgers T, Rowland M. Mechanistic approaches to volume of distribution predictions: Understanding the processes. *Pharm Res* 2007; **24**: 918-33.
144. Barnhart FE BH, Rossum KM. Postmortem Drug Redistribution. Forensic Sci Rev. , 2001; 101-29.
145. Moriya F, Hashimoto Y. Redistribution of basic drugs into cardiac blood from surrounding tissues during early-stages postmortem. *Journal of Forensic Sciences* 1999; **44**: 10-6.
146. Brockbals L, Staeheli SN, Gascho D et al. Time- and Site-Dependent Postmortem Redistribution of Antidepressants and Neuroleptics in Blood and Alternative Matrices. *Journal of Analytical Toxicology* 2021; **45**: 356-67.
147. Naidoo P, Chetty VV, Chetty M. Impact of CYP polymorphisms, ethnicity and sex differences in metabolism on dosing strategies: the case of efavirenz. *European Journal of Clinical Pharmacology* 2014; **70**: 379-89.
148. AM W, BC O, NN B. Biotransformation of Efavirenz and Proteomic Analysis of Cytochrome P450s and UDP-Glucuronosyltransferases in Mouse, Macaque, and Human Brain-Derived In Vitro Systems. *Drug metabolism and disposition: the biological fate of chemicals* 2023; **51**.

149. Tenofovir Disoproxil Fumarate (Viread) Package Insert.
150. Epivir (lamivudine) Tablets, Package Insert.
151. Brooks JW. Postmortem Changes in Animal Carcasses and Estimation of the Postmortem Interval. *Veterinary Pathology* 2016; **53**: 929-40.
152. Guo YY, Chu XY, Parrott NJ et al. Advancing Predictions of Tissue and Intracellular Drug Concentrations Using In Vitro, Imaging and Physiologically Based Pharmacokinetic Modeling Approaches. *Clinical Pharmacology & Therapeutics* 2018; **104**: 865-89.